ANALYSIS AND DESIGN OF A CAPILLARY DRIVEN BLOOD PLASMA SEPARATION MICROFLUIDIC DEVICE

Thesis by

Hojjat Madadi

In Partial Fulfillment of the Requirements for the Degree of

Doctor of Philosophy

Universitat Politècnica de Catalunya

Terrassa, Barcelona, Spain

2013

ANALYSIS AND DESIGN OF A CAPILLARY DRIVEN BLOOD PLASMA SEPARATION MICROFLUIDIC DEVICE

Hojjat Madadi

A dissertation submitted for the degree of Doctor of Philosophy

Supervisor: Dr. Jasmina Casals

Universitat Politecnica de Catalunya

Department of Mechanical Engineering

November 2013

Abstract

Recently, the emergence of lab-on-a-chip devices has seen in a variety of applications especially in clinical analysis and diagnostics. In particular the lack of suitable microdevices for separation of plasma from whole blood is a barrier to achieve a reliable lab on a chip (LOC) blood test. In order to address this issue, a novel self-driven high throughput blood plasma separator microchip is introduced as a first step to a miniaturized blood analysis. PDMS (Polydimethylsiloxane) is utilized as the base material for the microdevice fabrication to ensure the biocompatibility, the disposability (single-use to avoid contamination) and the low cost of the system for the mass-manufacturing. One of the characteristic features of the presented microdevice is that it needs to work just by capillary pressure eliminating the need of external sources. The requested capillary pressure to drive blood through the microdevice is derived via PDMS modification by analyzing different surfactants, which are mixed with pre-cured PDMS to achieve a stable hydrophilic character. Furthermore, a diamond microchannel integrated micropillar (dMIMP) pump with high throughput and with a resistance flow 35.5% lower than a circular based micropillar pump (cMIMP) has been developed. For this purpose, the pressure drop and flow resistance of a laminar flow through low aspect ratio MIMPs with different shapes and geometrical parameters are experimentally, numerically and analytically determined. In order to characterize the fabricated microcapillary pumps in PDMS, a novel and simple fabrication technique is introduced to overcome the PDMS deformation under high-pressure operation. The presented fabrication technique combines the use of stiff PDMS (10:2, the ratio between polymer base and cross liking agent) and a thin coating layer of the UV curable thiolene resin as supporter (Norland Optical Adhesive 63) on the fabricated PDMS microchannel. Finally, using all the achieved results in the material property and microcapillary pump design in the last steps, a novel self-driven high throughput microfluidic chip for blood plasma separation is designed and fabricated. The presented microdevice can successfully separate more than $0.1\mu L$ of plasma from a whole human fresh blood drop ($5\mu L$) without the need of external forces with high efficiency (more than 90%) and reasonable time (3 to 5 minutes). The achieved plasma volume ($0.1\ \mu L$) in $10\ \mu m$-depth collected channels of the presented self-driven microdevice paves the path to integrate this microfluidic circuit in a portable medical point-of-care-testing (POCT) for doing different blood analysis.

Acknowledgments

The best outcome from these four past years is finding my best friend and wife. I married the best person out there for me. There are no words to convey how much I love her. **Mahzad** has been a true and great supporter and has unconditionally loved me during my good and bad times. These past several years have not been an easy route, both academically and personally. I truly thank Mahzad for sticking by my side, even when I was irritable and depressed. I feel that we both learned a lot about life and strengthened our commitment during this time for making a wonderful future.

I dedicate this thesis to

my father 'Mohammad Hossein Madadi' and my mother 'Gerami Damadi'

for their constant support and unconditional love.

List of Papers

This thesis comprises a survey and the following papers:

Paper I

Hojjat Madadi, Jasmina Casals-Terré "Long-term behavior of nonionic surfactant-added PDMS for self-driven microchips" Microsystem Technologies, January 2013, Volume 19, Issue 1, pp 143-150.

Parts of this paper were also presented at:
Hojjat Madadi, Jasmina Casals-Terré "Study the Effects of Different Surfactants on hydrophilicity of Polydimethylsiloxane (PDMS)" ASME 2012, 11th Biennial Conference on Engineering Systems Design and Analysis, Volume 4, ESDA2012-82399, pp. 233-236.

Paper II

Hojjat Madadi, Mahdi Mohammadi, Jasmina Casals Terré, Roberto Castilla López, "A novel fabrication technique to minimize PDMS-microchannels deformation under high-pressure operation" Electrophoresis, Published online October 2013, DOI:10.1002/elps.201300340.

Paper III

Hojjat Madadi, Jasmina Casals Terré, Roberto Castilla López, M. Sureda Anfres, "High throughput microcapillary pump with efficient integrated low aspect ratio micropillars" Microfluidics and Nanofluidics, Accepted November 2013, In press.

Paper IV

Hojjat Madadi, Jasmina Casals-Terré "Validation of a novel high throughput self-driven microfluidic device for blood plasma separation" Manuscript submitted for publication.

Patent

Hojjat Madadi, Jasmina Casals-Terré "A self driven microfluidic device for separating liquid from a liquid including deformable particles", No. P201331666, Patent Pending.

Contents

I.   INTRODUCTION

Nowadays, considerable progress has been made in the field of microfluidics especially for chemical, biological, and biomedical applications. The biggest application of microfluidics has always been in the development of lab-on-a-chip systems. The advantages are: fewer probes, less reagents use, portability and more analysis on a smaller space. Actually, Point-of-care products show the greatest potential for this technology. The economic situation and efficiency standards of the health care industry sector have increased the interest of the researchers in the development of point-of care tests. This not only increases convenience, but also expedites results of the test. A standard example of a point-of-care device is a handheld blood-glucose monitor for diabetic patients [1]. The majority of attempts done by researchers in these years are focused on developing a point-of-care microchip for blood plasma separation, although there are many problems such as high efficiency without clogging or hemolysis (the rupture or destruction of red blood cells) in this approach.

The aim of this research is developing a microfluidic chip which with just a single drop of blood could separate plasma from whole blood without the need of external forces with high efficiency and reasonable time (minutes at most). This would be the first step towards the realization of single use, self-blood test which now takes multiple technicians' hours to do.

The possibility to use microfluidics in blood tests would increase the precision of the results, because the same patient could do the test to himself and would decrease costs. Such rapid and cheap tests requiring only a drop of blood should allow doctors to monitor the patients more frequently, enabling earlier detection of diseases. The new diagnostics tools should also be more accurate, with less manipulation errors and fastest processing. Traditional blood samples sit for hours or even days before the measurement processes are completed, allowing plenty of time for them to degrade. The proposed research project starts evaluating the different approaches used to separate plasma from whole blood using microfluidics. From the analysis of the current state of art, two main fields of study are pointed out: the use of neat fabrication techniques to overcome the hydrophobic behavior of currently used materials and the improvement of the separation efficiency by working on novel designs.

II. WHOLE HUMAN BLOOD

Blood is used in many clinical trials to detect a broad range of illnesses. But normally in order to do the tests, researchers previously separate the different elements of blood (See Fig.1): erythrocytes (red blood cells-RBC), leukocytes (white blood cells-WBC) and thrombocytes (platelets) from the plasma (serum and fibrin). Normally, RBC has a diameter between 3 and 8 um and its main characteristic is the level of hemoglobin that assists the transport of respiratory gases. WBC has a diameter between 8 and 12 um which the cells responsible to avoid infections and diseases. The other main components in blood are platelets which have a diameter between 2.65 to 2.9 μm and they aggregate to form clots. All these particles are suspended in plasma, which is 92% water and is yellow colored. Besides water, plasma also contains small particles (between 1 and 3 microns in diameter) that are mainly, serum albumin, clotting factors, hormones, carbon dioxide, proteins, electrolytes and immunoglobin. According to Kokoris [2], normal blood constituents are 45% RBC, 1% WBC, 0.5% platelets and the rest is plasma. Researchers such as Faivre have characterized the rheological behavior of blood, estimating a density of 1060kg/m3 and a viscosity of 0.02 Pa.s [3].
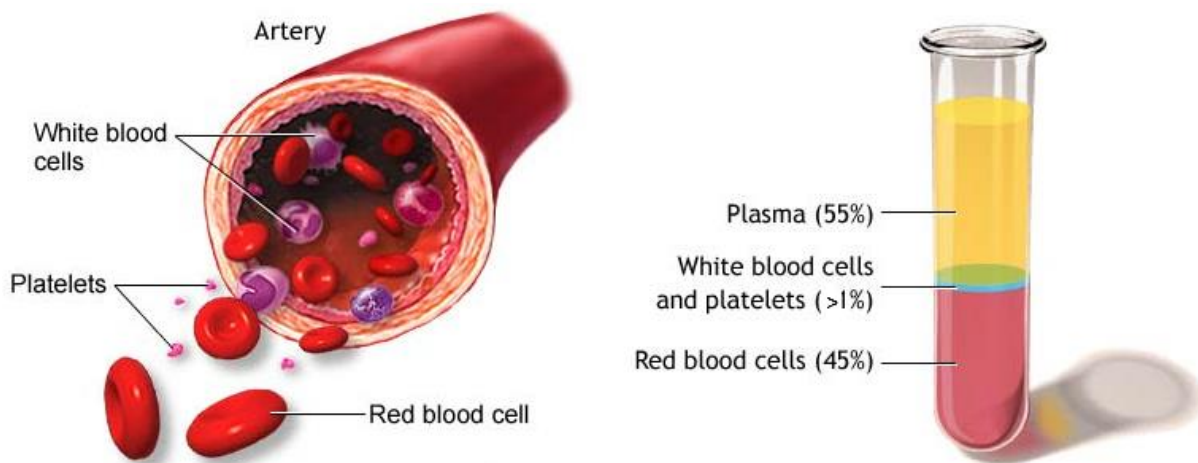
Figure 1.Blood composition. Health all refer, ADAM.

III. BACKGROUND

Many pathologies and physiological conditions can be diagnosed through the analysis of blood. In order to fulfill these analysis most researchers, scientist and doctors use centrifugation to separate plasma from blood. But this technique requires a clinical laboratory. In order to minimize error, reduce the time from blood collection and provide faster and yet less expensive and comprehensive results, "lab-on-a-chip" type of devices are attractive for blood plasma separation and analysis. This review describes different methods and some recent works for blood plasma separation by using micro technologies (See Fig.2).
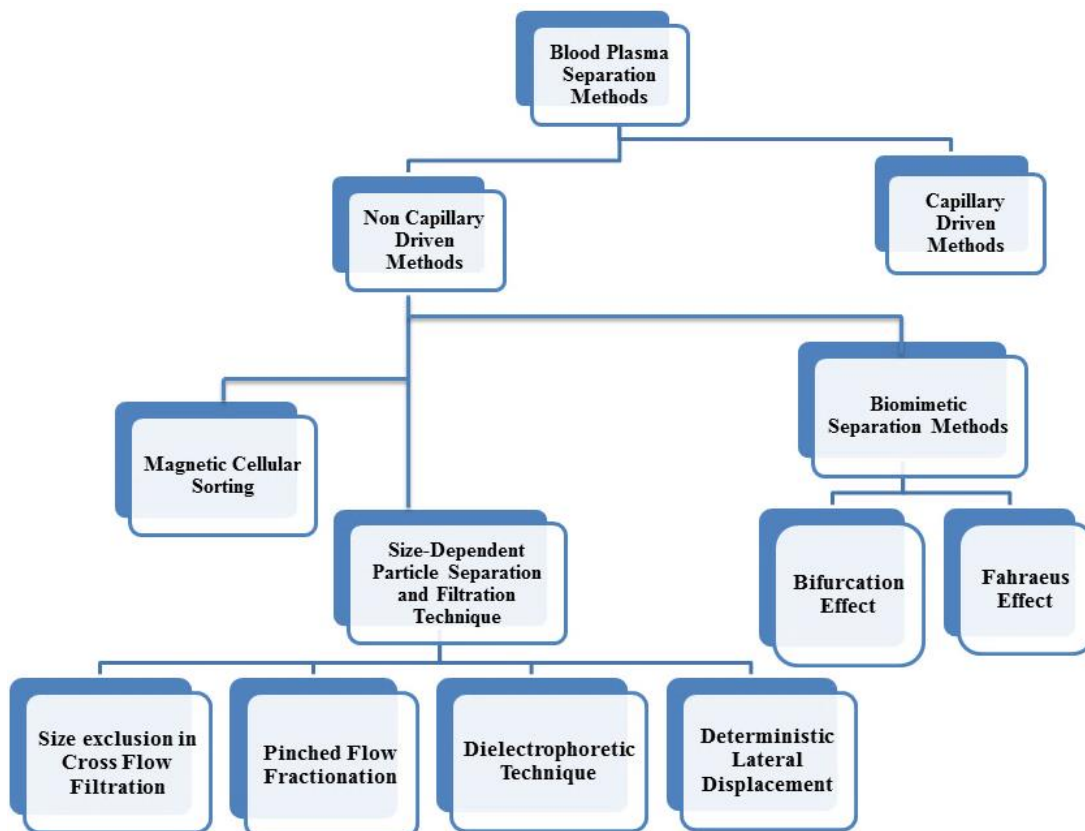
Figure 2. Diagram of blood plasma separation methods

1. NON CAPILLARY DRIVEN METHODS

1.1. MAGNETIC CELLULAR SORTING

Magnetic sorting of cells is particularly interesting in the case of separation of red blood cells from plasma because the cells contain hemoglobin molecules, which hold iron that has a magnetic behavior. By using this property its path can be modified in presence of a magnetic field offering the possibility to separate RBC from the other non-magnetic particles such as WBC or platelets. The magnetic cell sorter device can be miniaturized and used in applications in which a small volume of blood is required. Magnetic cellular sorting has traditionally been done using magnetic beads attached to the cells and then separates them from a pool of cells under a magnetic field. This method requires the design of a continuous flow system that should take into account the behavior of the magnetic particles under the effect of various forces such as magnetism, hydrodynamic drag and gravity.

Using a preliminary design for a particle separation device, Pamme and Manz demonstrated that it is possible to continuously separate particles on-chip, using free flow magnetophoresis [4]. Ingles et al. described a method for magnetic cell separation in microfluidic structures [5]. In their design, by placing the cellular flow under the influence of microfabricated magnetic strips at a constant angle of 9.6 degrees, a large deflection was created upon the magnetically labeled leukocyte cells from the rest of blood cell population.

In the last work using this technique, Furlani presented a method for the direct and continuous separation of red and white blood cells from plasma at the micro scale [6]. In whole blood, white blood cells (WBCs) behave as diamagnetic micro particles, while red blood cells (RBCs) exhibit diamagnetic or paramagnetic behavior depending on the oxygenation of their hemoglobin. The magnetic functionality was provided by an array of integrated soft magnetic elements, which were embedded transverse and adjacent to the microchannel (Fig. 3). A bias field was used to magnetize the elements, and once magnetized a magnetic force was applied on the blood cells as they flow through the microchannel. Specifically, the magnetized elements repel WBCs and attract deoxygenated RBCs (Fig. 3c).
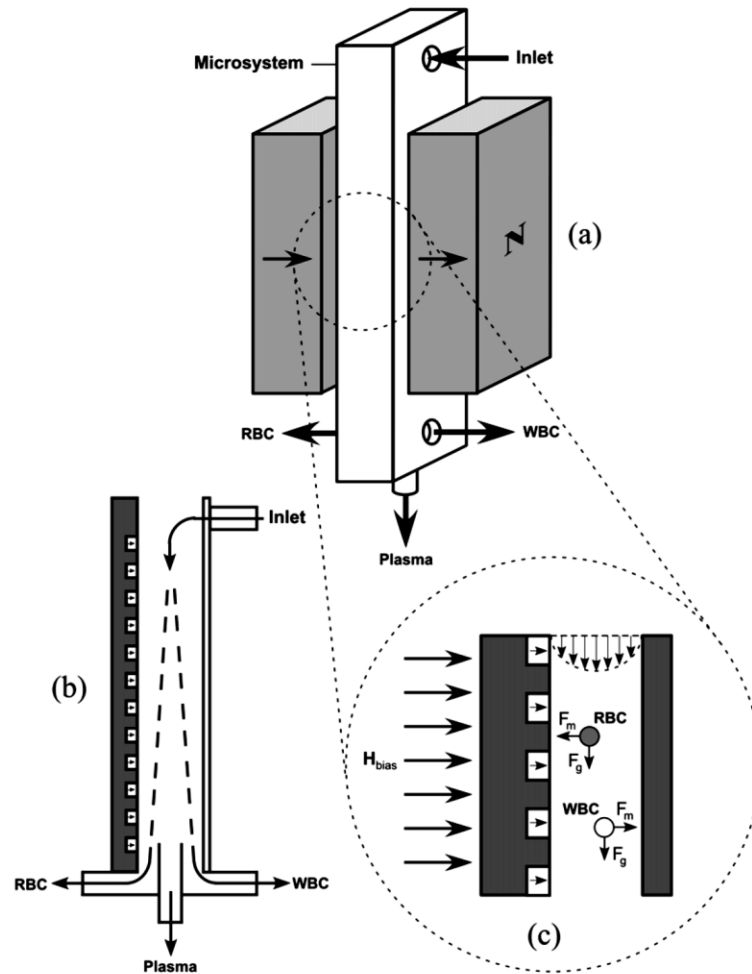
Figure 3.Schematic of magnetophoretic microsystem design by Furlani **[6]**

They investigated the cell separation as a function of the magnetic elements size and distances between them. As a consequence, the cell separation occurred over a shorter distance (faster) when increasing the size and spacing of the magnetic elements relative to the dimensions of the channel.

Although the magnetic cell sorter provides a powerful method for highly efficient cell separation, the magnetic fields are harmful for mammalian cells. High-intensity, static magnetic fields can cause disruption in cells and low-frequency magnetic fields can inhibit cell growth and proliferation.

1.2. SIZE-DEPENDENT PARTICLE SEPARATION AND FILTRATION TECHNIQUES

1.2.1. SIZE EXCLUSION IN CROSS-FLOW FILTRATION

Size-dependent particle separation (essentially filtration) is the simplest way of separating cells from plasma. Firstly this method had a severe clogging problem because in the first researches they used dead end filtration, for example Moorthy et al. presented a device to filtrate the cells greater than 3μm, however the device was easily clogged [7]. The cross-flow filtration mode could bypass the clogging related to dead-end filtration to some extent, increasing the efficiency of the separation and the filter life. In this filtration method, the flow of the particles is directed at a grazing angle to the surface of the filter. The flow near the filter can be strong enough to cause advection of cells and thus prevent clogging of the filter.
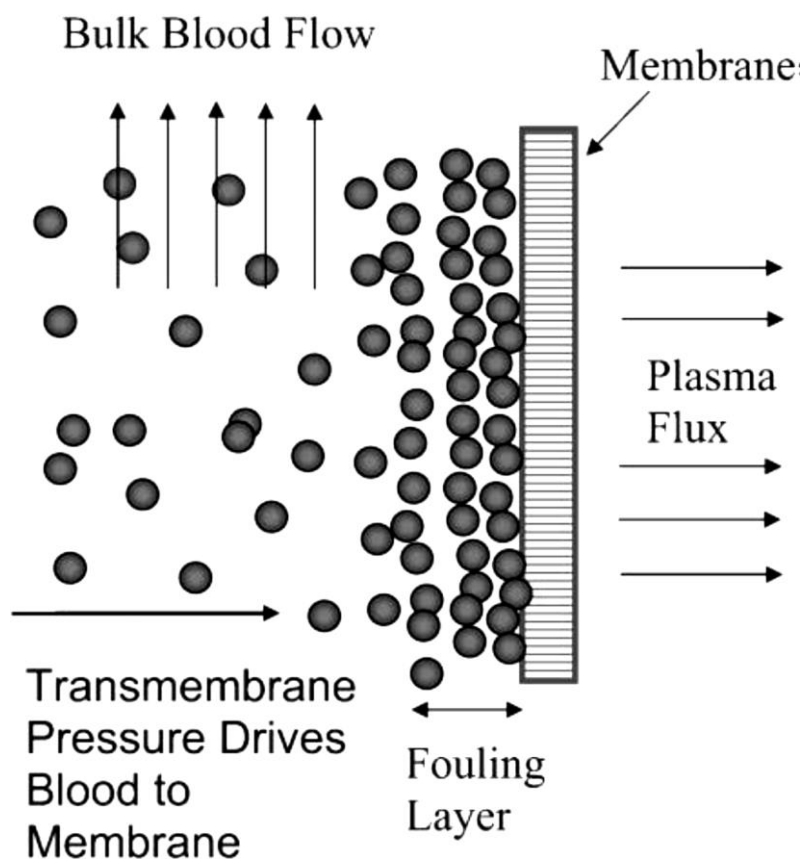
Figure 4. Mechanism of microporous membrane filtration **[8]**

Plasmapheresis researchers identified hematocrit, transmembrane pressure, and wall shear rate as the key operating variables controlling plasma filter flux during blood separation with

microporous membranes (See Fig.4). In these separations, higher levels of hematocrit increase filter fouling and reduce flux. Transmembrane pressure initially causes a rapid increase in flux but quickly reaches a pressure-independent equilibrium due to the accumulation of red blood cells at the filter face. In this pressure independent range, wall shear rate is the primary modulator of plasma flux, with greater levels of shear rate increasing plasma flux. Shear rate affects flux by modulating the thickness of the red cell fouling layer at the filter face through transport effects such as shear-enhanced diffusion.

Recently, Arata Aota et al developed a plasma separation method based on a microchip with a Cyclopore filter (a hydrophilic porous membrane) which utilizes the axial migration of blood cells observed in blood vessels [9]. Figure 5 illustrates the axial migration caused by viscous lift force and cross-flow filtration in this device.
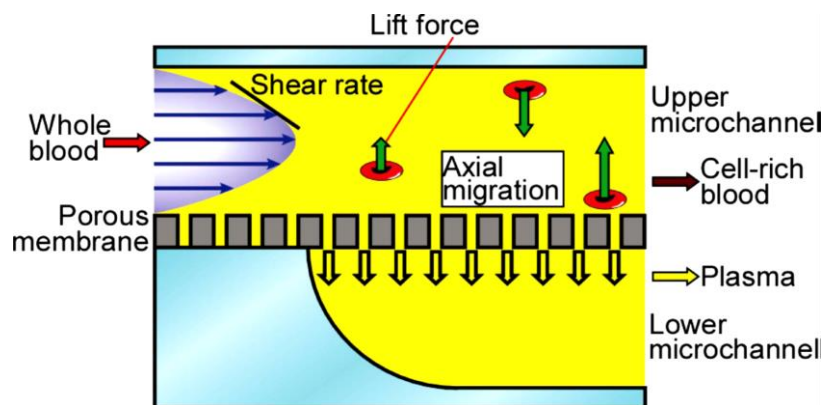
Figure 5. Principle of the plasma separation device utilizing axial migration by Arota Aota **[9]**

Even though this method was capable to separate 3µl plasma from 200 µl of whole blood without hemolysis, the dead-volume of this design is high to be utilized as a point-of-care device.

1.2.2. PINCHED-FLOW FRACTIONATION

When the particle and the channel diameter are of the same size scale Pinched-Flow fractionation is an effective method for continuous, size-dependent particle separation. In this

method the particles behavior is not similar to particles with low Reynolds number which follow fluid streamline base on Stokes' drug rule, in fact the particles concentrate in fluid streamline but remain close to the channel walls and in the last step when the particles come out from the constricted area of the channels the particles get separated from each other perpendicularly to the flow direction according to their sizes. In the last researches in this field, Rodriguez-Villareal et al. presented a microfluidic device that combined a pinched-flow constriction to separate plasma from whole blood with comparatively high flow rate [10].
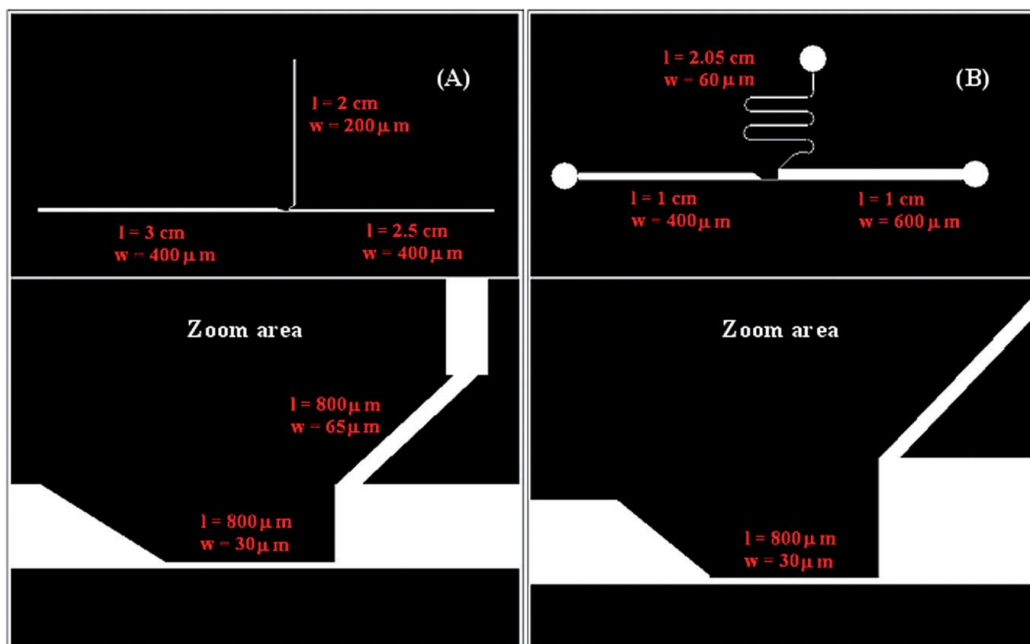
Figure 6.Plasma separation device by using pinched flow fractionation **[10]**

The device contains one main channel that injected the blood sample into the chip and a constricted channel was used to increase both the velocity and the shear rate as the velocity in the constricted channel was approximately 13.36 times higher than in the inlet/outlet channel (see Figure 6). It was also shown that by using the constricted channel, the cell-free area adjacent to the channel wall in the larger outlet channel enhanced as shown in Figure 7. Although no hemolytic effects were observed at relatively high sample flow rates of up to 200μl/min, this might be ascribed to the fact that the residence time of the cells inside the channel and exposure to the damaging wall shear stress is minimized at high flow rates.
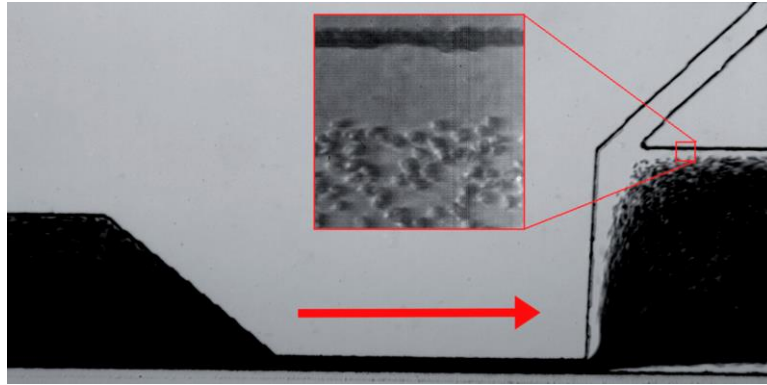
Figure 7. Arrow shows the flow direction, a cell-free area appears after the constricted channel which can be seen in the selected zoom area **[10]**

In this study the effects of temperature and the velocity of the flow rate on the blood separation were also investigated and as a result it is was demonstrated that when the temperature increased from 25 ºC to 50 ºC, there was a 250% increase in the cell-free area thickness. Moreover, a direct relationship between the cell-free area and the velocity of the flow rate was found.

1.2.3. DIELECTROPHORETIC TECHNIQUES

Nowadays, the variety of micro-electromechanical systems (MEMS) into areas such as biology and chemistry has increased. There are two types of electric field-based manipulation due to the properties of the particles to be sorted. Electrophoresis, a very well-known technique to separate different kinds of charged particles, which is based on the movement of charged particles in a uniform electric field. Detailed review of electrophoresis can be found in a recent literature review [11]. Dielectrophoresis is described by Pohl in 1978 as 'the translational motion of neutral matter caused by polarization effects in a non-uniform electric field' [12]. According to this, polarizable particles such as mammalian cells experience the dielectric force when subjected to a non-uniform electric field. The particles migrate to higher-field-strength region (positive dielectophoresis) or lower-field-strength region (negative dielectrophoresis) depending on their geometry, the frequency of the electric field and permittivity of the suspending medium and independently of their charge. So, a particular field can manipulate particles with great selectivity. Chang and Cho proposed a continuous, size-dependent particle separator by using dielectrophoretic technique to separate red blood

cells (5.4 ± 1.3 μm diameter) and white blood cells (8.1 ± 1.5 μm diameter) with a separation purity over 99% (See Fig.8) [13].
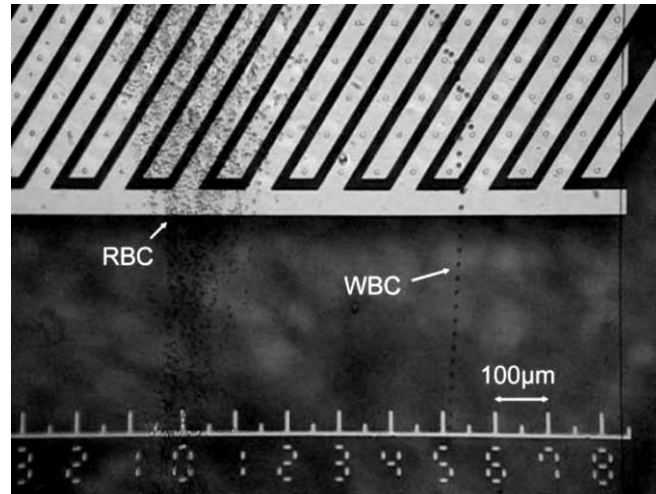
Figure 8.Separation of red blood cells (RBCs) and white blood cells (WBCs) with 10 Vrms sinusoidal wave (500kHz) and net flow rate of 0.11 μm/min **[13]**

In spite of all the outstanding advantages of dielectrophoretic techniques over conventional methods for plasma separation, it has some problems associated with hydrolysis and thermal convection or drawbacks such as cell damage due to the high electric field in the region of positive dielectrophoresis [14].

1.2.4. DETERMINISTIC LATERAL DISPLACEMENT

Deterministic hydrodynamics is another interesting physical phenomenon based on size particle separation. This technique was proposed by Huang et al. [15]. In this method, the particle fluid mixture flows through an array of micro-posts, in which each row is slightly shifted laterally by a distance respect to the row above it, as it is shown in Figure 9.
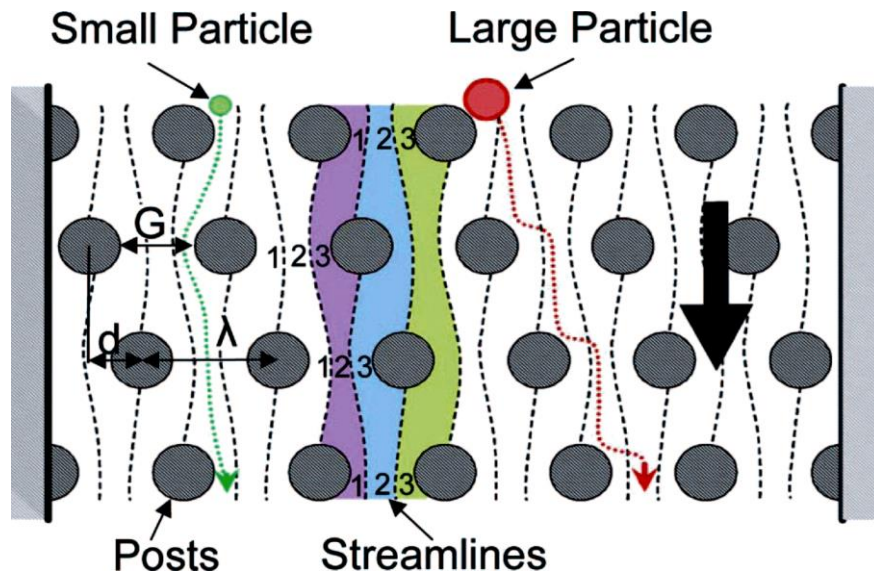
Figure 9. Schematic illustrating the separation by deterministic lateral displacement **[16]**

The asymmetric bifurcation of laminar flow around microposts leads the particle to choose their paths deterministically on the basis of their size. While large particles flow straight, small particles will have a zigzag displacement path. The particles can be collected separately after a number of rows. This method was effectively utilized for the separation of white and red blood cells [17]. Later, because of a high risk of clogging due to the numbers of posts utilized and the narrow gaps between them, Huang and their research group optimized the device including additional regions alongside the active sorting arrays [16]. Although this method is cost effective and can separate in parallel a large number of different sized particles, the handling and fabrication of the device is critical to its proper functioning.

1.3. BIOMIMETIC SEPARATION METHODS

Flow characteristics of blood flow in microcirculatory vessels are similar to that in microchannels. In the last decade, lots of attempts have been done to create a novel microfluidic device by using the same phenomena seen in vivo microhemodynamics. One of the interesting in vivo phenomena is the formation of a cell-free layer adjacent to the microvessel wall. This phenomenon along with the other biomimetic aspects makes a path to invent mechanism for blood plasma separation from whole blood.

13

1.3.1. BIFURCATION EFFECT

This method is based on the principle that when particles flow through a bifurcating area of a capillary, they have a tendency to travel into the vessel with the higher flow rate, leaving very few cells flowing into the lower-flow-rate vessel. In fact higher pressure gradient causes the cells to be drawn into the higher flow rate channel although asymmetric distribution of shear forces is another factor that produces a torque on the cell and finally a pull towards the faster flow rate channel.
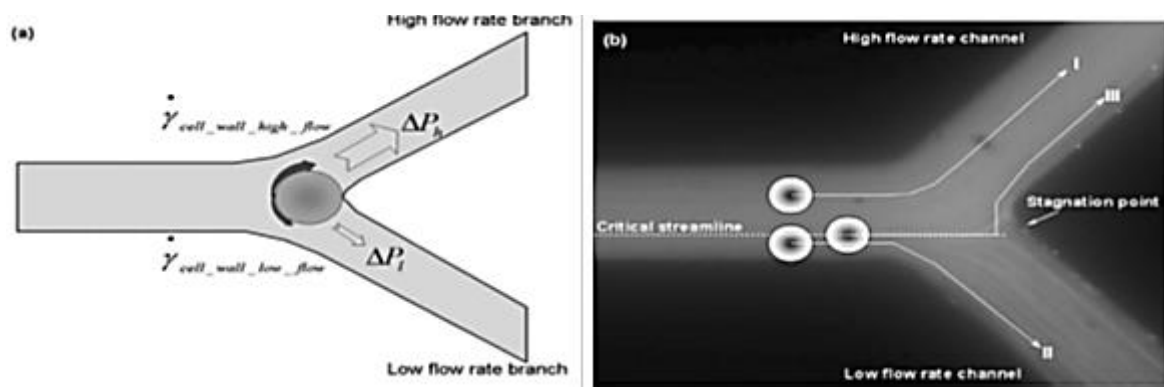
Figure 10.Schematic of the Zweifach–Fung effect [18]

As it is shown in the Fig. 10 when the centroid of a particle (I) is beyond the critical streamline, this particle will travel into the high flow rate channel and a particle (II) whose centroid is within the critical streamline will travel into the low flow rate channel while if a center of a particle (III) is on the critical streamline, due to the Bifurcation law it will travel into the high flow rate channel. In one of the prominent works in this field Yang et al. [18] fabricated a blood-plasma separation device by using this effect to separate blood cells from plasma. As it is shown in the Fig. 11 the blood was infused at a flow rate of 10 µl/h by a syringe pump. In order to quantify the efficiency of the system they used image processing to determine the total volume of plasma separated from whole blood. They tested the device at a variety of inlet hematocrit levels and only few blood cells flowed into the plasma outlet while there was not any clogging or hemolysis of cells during the experiments.
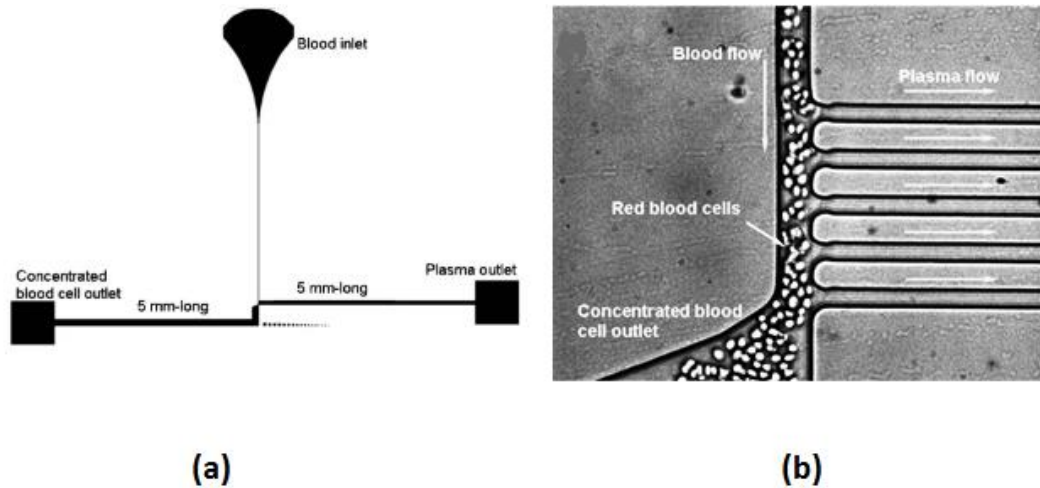
Figure 11.(a) Schematic diagram of a microfluidic blood plasma separation device (b) Photograph of the blood plasma separation region after infusing defibrinated sheep blood **[18]**

Using this approach Yang achieved almost a 100% of particle separation regardless of the inlet hematocrit levels although the flow rate was very low. This low flow rate could cause increase clogging problems at the bifurcation.

1.3.2. FAHRAEUS EFFECT

Fahraeus effect discovered by Robin Fahraeus is a very important phenomenon in the blood flow in microfluidic devices. According to this concept, the average concentration of red blood cells in human blood decreases as the diameter of the tube in which it is flowing decreases. Due to the small tube size (Diameter less than 500μm), the resistance of blood to flow will be decreased leading to the tendency of red blood cells to migrate toward the centerline of the tube and therefore a cell-free plasma layer is created next to the tube wall. In the recent years, some attempts were done to utilize this effect to separate plasma from whole blood. Faivre et al. [19] utilized this phenomenon to design a microdevice for extracting plasma from whole blood as it is shown in the Fig. 12.
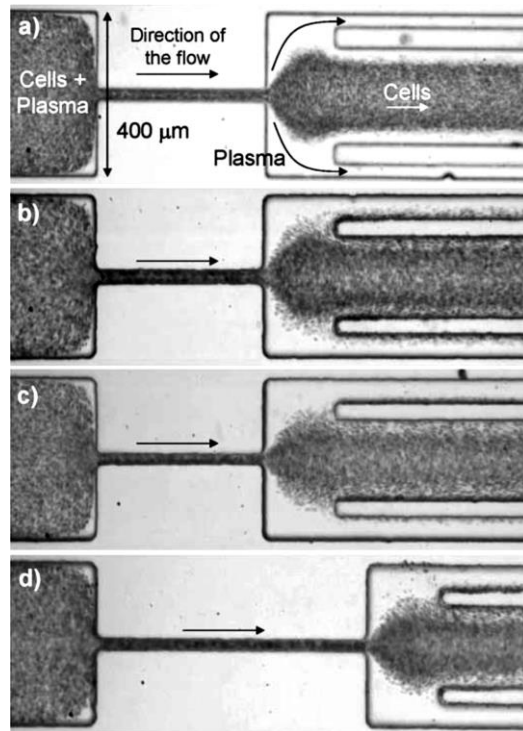
Figure 12.A microfluidic design for separating plasma from whole blood by Faivre et al. **[19]**

2. CAPILLARY DRIVEN METHODS

Although in the last decade many attempts have been done to improve the microfluidic device for blood plasma separation, there are only few works carried out to design a device without externally applied forces.

In 2005, Crowley and Pizziconi reported that plasma separation from whole blood is possible in a cross-flow micro-device in which the flow is driven by capillary forces [8]. The generic microfilter design consisted of an input reservoir, a narrow filtration channel with a transverse flow microfilter, a plasma outlet channel to collect filtered plasma, and a wider expanded channel connected in series with the filtration channel (Fig 13).

The filter was fabricated using a series of rectangular openings, ''pores'', placed on both sides of the filtration channel. This transverse flow microfilter operate entirely upon capillary action and was used to effectively isolate 14-45 Nano liter volumes of plasma from a single drop of blood. The duration of capillary operation was significantly extended through the use of an innovative microfluidic layout employing a narrow filtration channel connected in series with a larger expanded flow Channel. The obtained results of this work showed that

there is a significant potential for the development of capillary driven microflow devices that have advantages over the traditional methods of plasma separation. Various effect such as using a pulsatile flow to reduce clogging of the filter, are reported to enhance the efficiency of the microfiltration devices [20]. This type of device based on the microfiltration technique operated for at least 1 hour and extracted 8% of plasma volume at an average rate of 0.65 µL/ min.
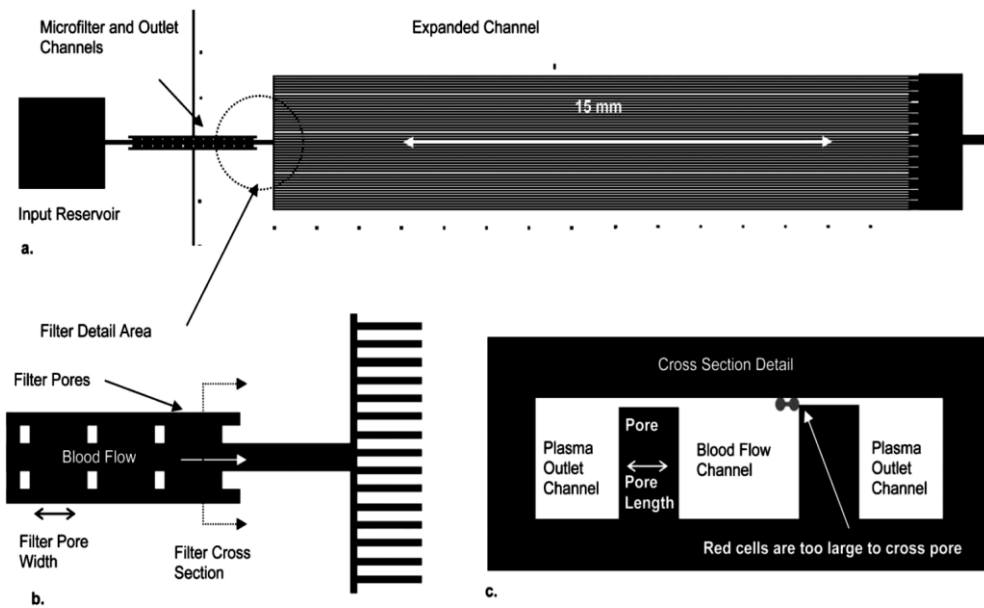
Figure 13.Microfilter device design and detail: (a) top view of generic device design with narrow and expanded channels, (b) filter detail area showing filter pores and expanded channel layout, (c) microfilter cross section **[8]**

Tyler Nathaniel Hinkle in 2008 proposed a design of a microfluidic device that separates plasma from a blood model without external pumping or other external forces [21]. In the design of this device they mixed the theories of microfluidics with the theories of standard filtration techniques. Figure 14 shows the schematics of the separation device.
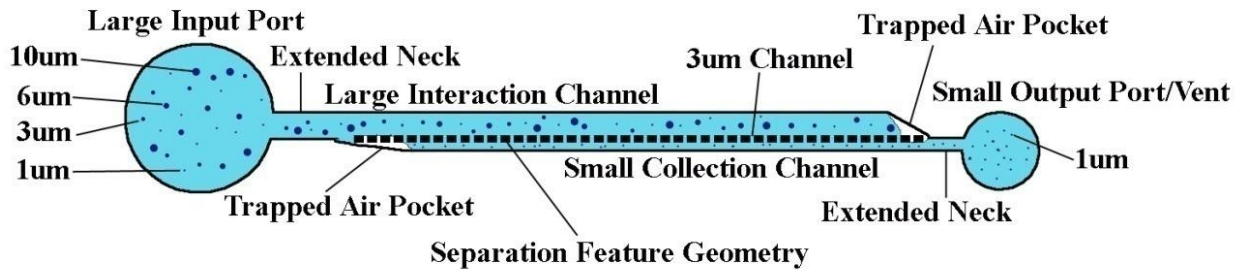
Figure 14. Schematic of the design of separation device and separating process [21]

The separated output comprises the suspended particles with diameter smaller than 3µm. To separate the plasma using the capillary force in the microfluidic channels, the surface of the microfluidic device requires strong hydrophilicity. Because of the hydrophobic nature of the PDMS used in the standard microfluidic fabrication technique, they developed a plasma-free hydrophilic surface treatment to overcome this problem and as a result they were able be to reduce of contact angle down to 53 degrees.

The experiments done by Hinkle showed that the separation process was successful even if only a few of the separation channels were open. The quantification and efficiency of the device was studied and as expected by increasing the bead size the efficiency increased. Although this research have shown desirable results of separation for this application, all the experiments were done using polystyrene beads and as a result they did not face blood cell phenomena such as clogging or hemolysis of cells in the separation technique. In addition, they did not consider the deformability of red cells as a big issue in the microdevice dimensioning.

A different capillary microfluidic device for blood plasma separation is presented by Chang Kim and his colleagues [22]. PDMS was used as the base material to fabricate the microdevice in this research, the nonionic surfactant Silwett L-77 was utilized to modify the hydrophobicity of PDMS. The plasma extraction device was designed to have a main blood channel with a planner cross flow filter to extract plasma from whole blood (See Figure.15).
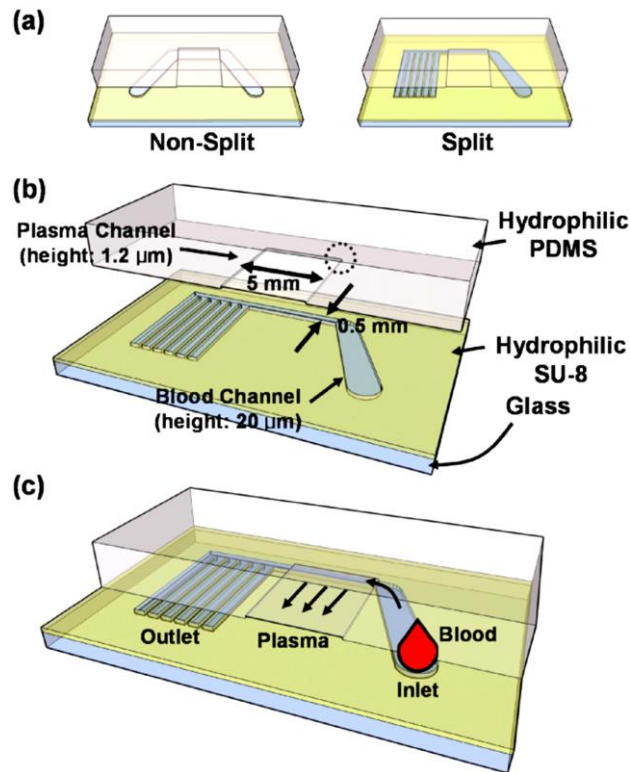
Figure 15. Schematic diagrams of the plasma extraction device. (a) Two types of blood channel structure (b) before and (c) after assembly **[22]**

As it is shown in Figure 15 (a), they improved the device by using split microchannels to promote flow and prevent the clogging of the entrance of the plasma channels. Although this microdevice confirmed the feasibility to use surfactant-added PDMS for building a capillary driven microdevie, the volume of the extracted plasma was very small in the order of 20 nL.

Recently, Hiramoaki Sakamoto and their colleagues proposed a PMMA microfluidic device for blood plasma separation that it is driven only by capillary action [23]. The design of this device contains an array of 2-μm-deep and 2-μm-wide PMMA channels as shown in Figure 16.
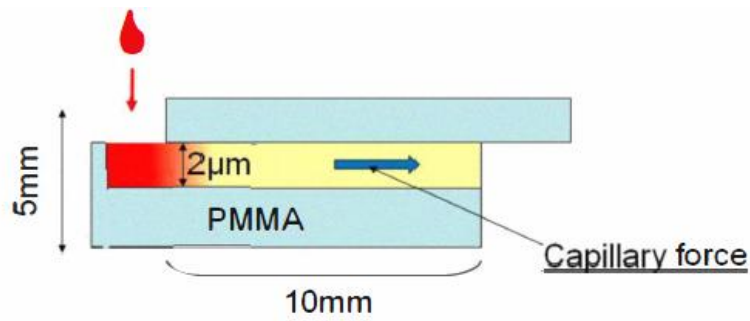
Figure 16.Schematic illustration of microfluidic device design **[23]**

In this research, the embossed PMMA sample was bonded to another PMMA plate using the surface activation method to create a very firm bonding. They utilized hot embossing and thermal bonding to fabricate the microfluidic device. To improve the wettability of the PMMA, firstly they performed O_2 plasma irradiation to obtain polar functional groups containing oxygen onto the surface and an applied Poly-L-Lysine coating that it actived the amino groups for promoting cell adhesion. The fabricated PMMA microchannels filtered a drop of blood in about 3 min with an efficiency of almost 100% and volumes of about 150 nL of blood plasma were isolated during this time. In spite of all the advantages of this design, clogging in the entrance of microchannel array is a challenge for using this approach.

3. REVIEW OF THE TECHNIQUES FOR BLOOD PLASMA SEPARATION

Some of the mentioned techniques require externally applied driving forces that need external equipment which is not desirable if we are designing a single use point-of-care test. Although external driving forces cannot be used, the principle of operation could be general and feasible to separate successfully plasma from whole blood with few modifications. Table 2 summarizes the different approaches researchers have been used to build plasma separation lab-on-chip devices and point out their particular characteristics.

Table 1. Summary of different microfluidic separation strategy

Guiding principle for separation	Magnetic cellular sorting	Size exclusion	Pinched flow fractionation	Zweifach-Fung effect-based separation	Capillary Action
Author, Year	Furlani (2007	Crowley and Pizziconi (2005)	Rodriguez-villareal (2010)	Yang (2006)	Sakamoto (2012)
Sample flow rate	500 particles/s	0.65 µL/min	200 µL/min	3-4 µL/min	1.67 µL/min
Separation efficiency	98%	99%	95%-97%	99%-100%	100%
Driving force	Gravitational and magnetic forces	Capillary action	Syringe pump	Syringe pump	Capillary action
Hydrophilicity	Not reported	Nature of Silicon dioxide	Not reported	Not reported	Oxygen plasma and Poly-L-Lysine
External equipment	Yes	No	Yes	Yes	No
General Remarks	Standard technique, difficult to miniaturized, Adverse biological effect	Simple and easy to manufacture, Problem with clogging	Low efficiency compared with other techniques	Flow based separation, Problem with clogging	High-throughput with no external forces

IV.   RESEARCH OBJECTIVE AND APPROACH

The thesis aims to address the lack of self-driven high throughput blood plasma separator microchips for blood analysis. The presented microsystem which is based on hydrodynamic principles has a high throughput and high efficiency and resulted in the application for a patent [24]. One of the characteristic features of the microdevice is to work automatically just by capillary pressure which eliminates the need of external sources. The requested capillary pressure to drive the microdevice is depended on the material hydrophilicity and surface tension. Moreover, the material of the system was chosen carefully to ensure the biocompatibility, the disposability (single-use to avoid contamination) and the low cost of the system for the mass-manufacturing.

On this basis, the research project focused in four main steps to produce a capillary driven microfluidic chip which with just a single drop of blood could separate plasma from whole blood without the need of external forces with high efficiency and reasonable time (minutes at most).

- Analyzing the different methods of blood plasma separation to achieve a high-throughput with high efficiency separation microdevice design
- Analyzing methods of PDMS (base material in microfabrication method) modification to achieve a stable hydrophilic character for providing the self-functionality of the microdevice
- Analysis and characterization of a high throughput microcapillary pump using microchannel integrated micropillar (MIMP) as an effective way to increase the volume of extracted plasma in the final microfluidic device.
- Analysis and characterization of the fabricated blood plasma separation microdevice based on the achieved hydrophilic material and high efficiency micropump/filter.

The research approach in this process is depicted in Figure 17.
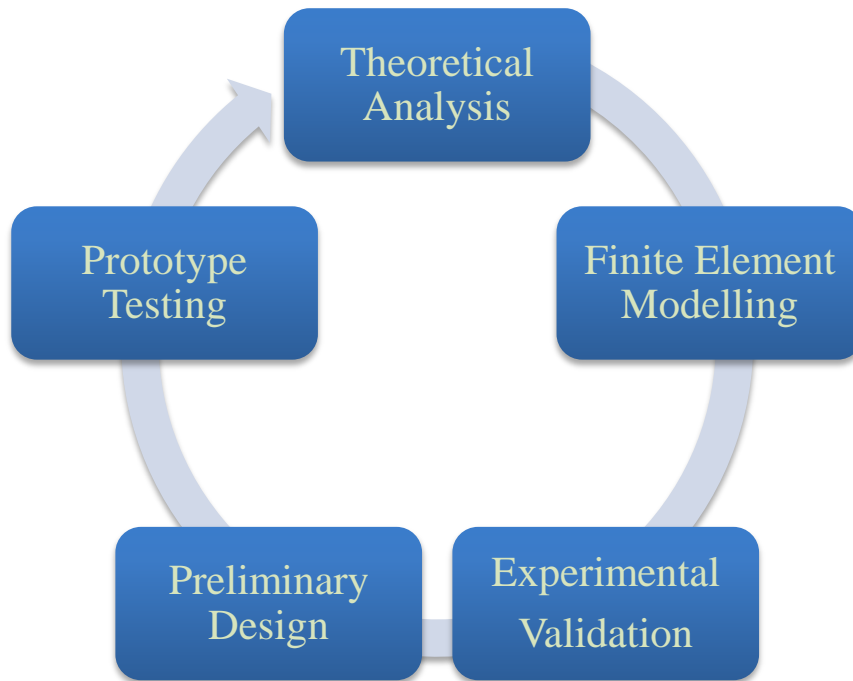
Figure 17. The illustration of research strategy

The validation of the blood plasma separation microdevice can be carried out using analytical modeling or simulation. The computer simulation not only reduces the microdevice development cost but also increases its throughput by defining the microchannels dimensions that are most effective in the operation of a self-driven microdevice. The Ansys workbench can be used to simulate the microchannel resistance flow and to validate the hypothesis done during the analytical modelling process. The microfabrication technology enables the creation of initial prototypes. In this thesis, a conventional photolithography process as a rapid and cost-effective technique associated with a wet chemical method was used to fabricate the microdevice. As the final goal of this thesis is the design and fabrication a self-driven microdevice, the performance of the microdevice was verified using just a droplet of fresh human blood (~5µm) in the microdevice inlet. Since the sample volume is very low a finger stick was utilized blood extraction during every test. The blood was driven in the microdevice by the capillary force due to the hydrophilicity of the material (defined in Paper I) while the efficiency and volume of the extracted plasma was investigated for every microdevice design (Paper IV).

V.   MATERIAL

Some of the presented designs in the literature needed external forces to move the fluid due to the hydrophobicity of materials (such as PDMS or PMMA) used in the manufacturing process. In fact, the intended design can be successfully applied to a portable point-of-care microdevice if the chosen material is hydrophilic or the hydrophobic behavior of the material is solved. For the fabrication of microfluidic device, Polydimethylsiloxane (PDMS) was chosen as one of the most common materials used for the flow delivery in the microfluidics chips, since it is clear, inert, non-toxic and non-flammable. Its inexpensiveness, straightforward fabrication and biological compatibility have made it a favorite material in the exploratory stages of the bio-microfluidic devices. One of the most important issue that we have faced in our experiments is related the hydrophobicity nature of PDMS. Untreated PDMS surface is hydrophobic, with a contact angle of approximately 108° [25] that prevents the movement of blood in the microdevice automatically. In fact the hydrophobicity of PDMS is due to the presence of methyl groups in its structure as it is shown in the Figure 18.
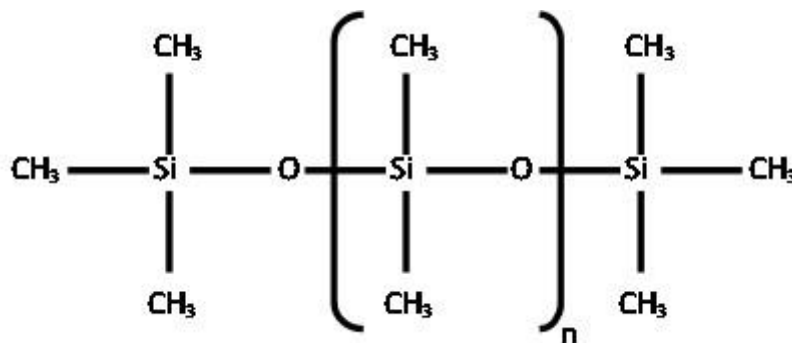
Figure 18. PDMS chemical structure containing methyl groups that make it hydrophobic

However, the Si-CH3 methyl groups can be converted to Si-OH silanol groups by using an oxygen plasma treatment that it makes the PDMS surface temporarily hydrophilic. But this strategy is undesirable for point-of-care devices due to the required long shelf lives of at least 6-12 months.

There are several techniques to achieve a hydrophilic behavior of PDMS (See Fig.19), but most of them face the problem of hydrophobic recovery after a short period of time while most commercial microdevices require long storage and distribution times.
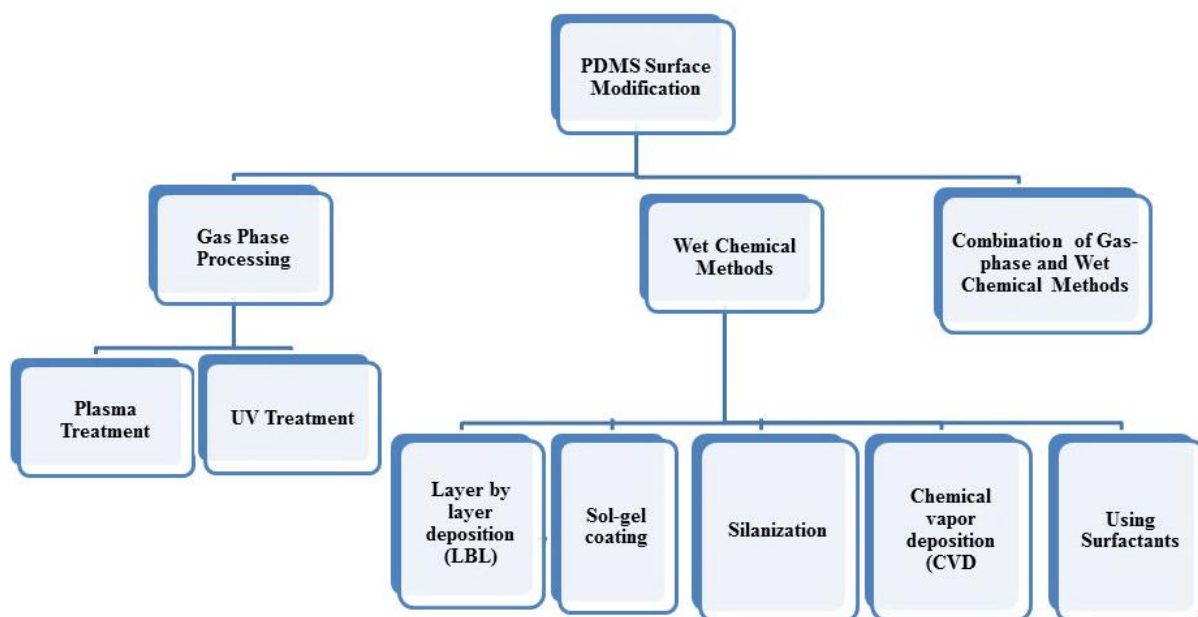
Figure 19.Summary of different technique for PDMS surface modification

The use of surfactant-added PDMS provides a novel method to overcome the hydrophobicity and to control the hydrophobic recovery over a long period of time. There are many different types of surfactants and not a deep methodology to choose one in terms of efficiency, clearance and duration of the hydrophilic behavior. Therefore in the first step toward making microdevice, three non-ionic surfactants with different critical micelle concentration and chemical composition: Triton X-100, Brij 35 and Tween 20 were compared in paper I. In this work, short and long-term studies were done using 5µL deionized water droplet on the surface of the prepared surfactant-added PDMS to find the ideal surfactant for fabrication the intended microdevice.

As it is shown in figure 20, all the surfactants showed a significant decrease of the contact angle during 600 s.
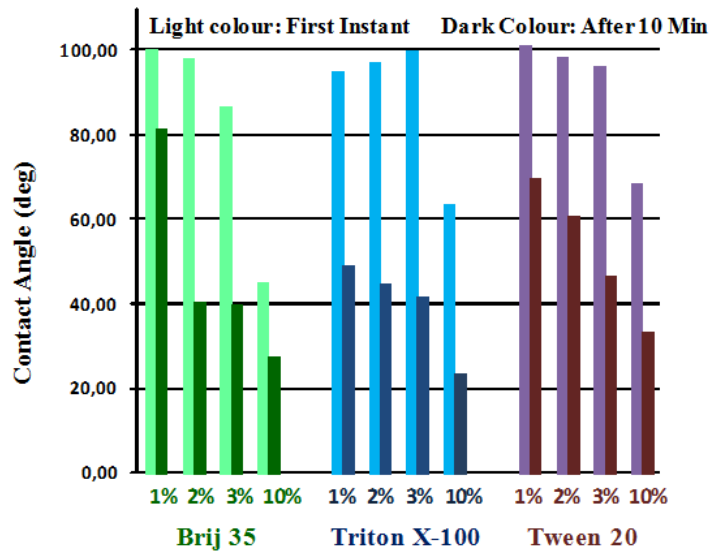
Figure 20. Variation of contact angle of water droplet on the surface of modified PDMS with different surfactant concentration

If the clearness is not an issue, a 10 % of Triton X-100 provides the fast and the highest reduction in contact angle up to 23º. If transparency is needed 3 % of Brij 35-added PDMS is the most effective surfactant with a reduction of the contact angle up to 40º. On the other hand, the hydrophobic recovery of surfactant-added samples were tested for 2 months and the stability of the samples contact angle after 2 months was similar to the one achieved at beginning and it was concluded that the interaction with an aqueous solution or high humidity are the only factors that could contribute to recover the hydrophobicity. Finally, the validation of surfactant-added PDMS for microfabrication of capillary driven single use devices was demonstrated by manufacturing a bifurcation microchannel with a cross section of 1.5 mm × 50 μm in the main channel and 1 mm × 50 μm in the branches with 3 cm in length.

According to these results, the use of PDMS with Brij 35 provides a good potential for building capillary driven devices without the need of tedious preprocessing techniques.

VI. MICROCAPILLARY PUMP DESIGN

Generally microfluidic circuits consist of two main parts: the pumping system (internal or external) and the circuit itself (chambers and fluidic resistance), see Fig. 21a.

In capillary driven circuits the pump plays a major role in the device performance. The MIMP (Microchannel Integrated Micropillars) capillary pump is an array of micropillars, which can be designed to program the flow rate of the liquid in the circuit. The efficiency of the MIMP capillary pump depends on the contact angles of the filling liquid with the microchannel wall that is an intrinsic property of the material (which is studied in paper I) and the characteristic dimensions of MIMP that directly relate to the MIMP flow resistance.

Microchannel integrated micropillars (MIMP) structure is a strong candidate for microcapillary pumps to transport a precise volume in Lab-on-a-Chip designs since pillar structures make a significant effect on the capillary flow by increasing the surface/volume ratio. Even though MIMP microcapillary pumps do not require an external energy source for fluid transportation, interesting property in healthcare and drug discovery applications, there are few works that characterize the capillary pump performance through the study of the different pillar shapes and their characteristic dimensions.
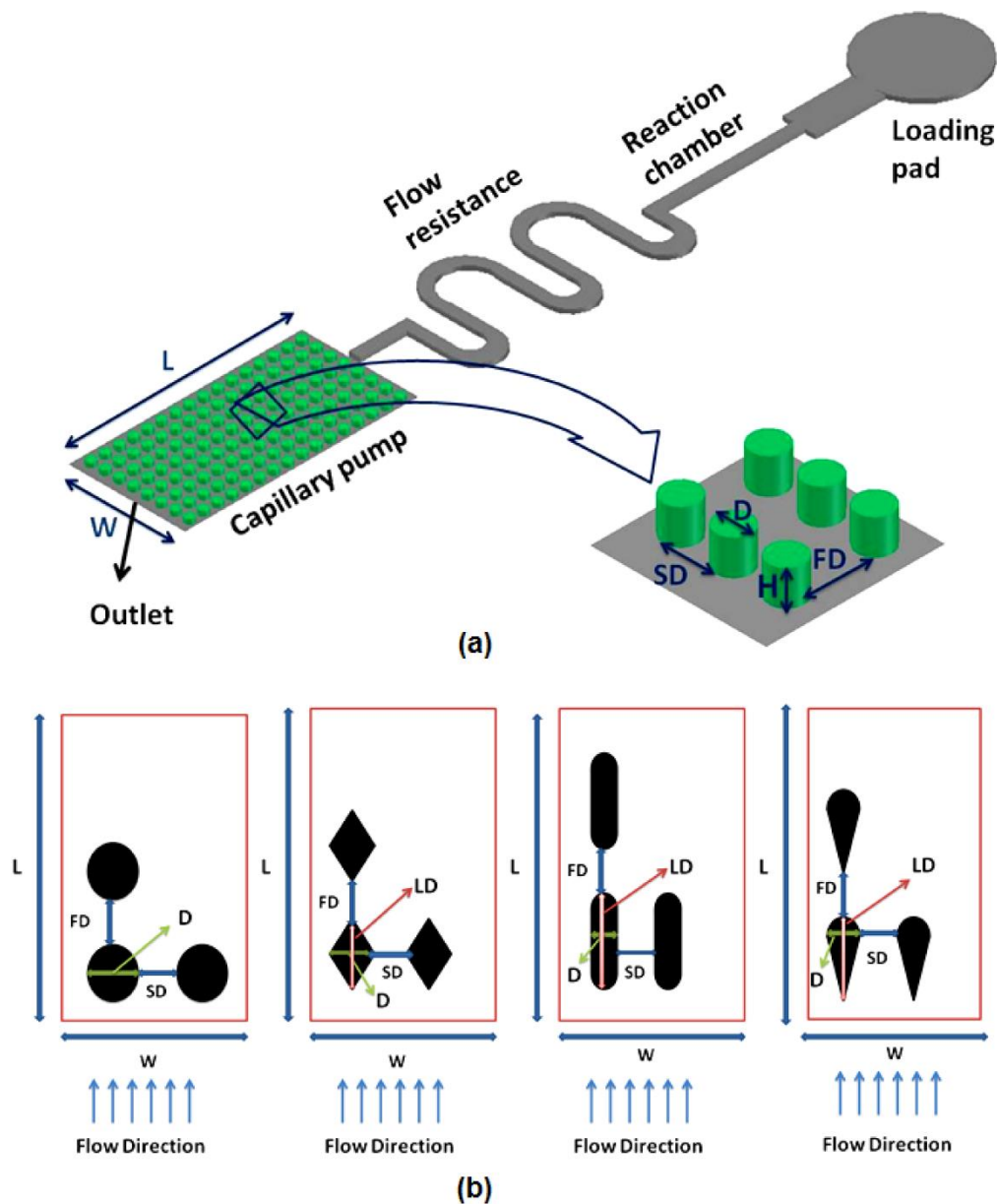
Figure 21. Schematics of a microfluidic circuit using a circular MIMP capillary pump b) The different pillar shapes (Circle, Diamond, Elongated, pine) and geometrical parameters (D: Diameter, LD: Large Diameter, SD: Side distance between pillars, FD: Forward distance between pillars) which can affect the flow resistance in MIMPs.

On this basis, understanding the effect of geometrical parameters of microchannels with integrated micropillars (MIMP) (see figure 21b) was investigated (paper III) not only to improve and optimize the design of microcapillary pumps for different passive microfluidic applications but also in particular to maximize the throughput in the presented blood plasma separation microdevice.

In order to study the hydrodynamic effect of different MIMP shapes with low aspect ratio (H/D ranged from 0.06 to 0.2), several PDMS MIMP channel were fabricated.

In spite of many advantages of PDMS and its broad use in biological laboratories, it has some drawbacks like hydrophobicity and its low elastic modulus, which causes a significant issue for high-pressure operation [26]. In terms of PDMS hydrophobicity, the previous work has been done on the surface modification of PDMS (paper I) but in the literature few studies have discussed the importance of PDMS channel deformation in microfluidics. The low elastic modulus of PDMS offers some advantages like easy replica molding without damage to features. However, this property has shown to generate a large variation of microchannel geometry and have broad impacts in microfluidic device performance [27].

Hence, in the second step of our work (paper II) to overcome the PDMS deformation under high pressure operation, a novel fabrication technique was introduced which combines the use of stiff PDMS (10:2, the ratio between polymer base and cross liking agent) and a thin coating layer of the UV curable thiolene resin as supporter (Norland Optical Adhesive 63) to fabricate PDMS microchannels.

The major advantages of this method are: simple and inexpensive fabrication, which does not need a complicated process. The verification of the presented technique was tested by considering microchannel integrated micropillars (MIMP) as a complex geometry (which is used in the characterization of microcapillary pumping device (Paper III)) under high pressure operation.

The variation of side distance between pillars in the microchannel-integrated micropillar was studied under high-pressure operation in two different arrays of samples: conventional fabricated samples and glass-stiff PDMS-NOA samples. As it is shown in figure 22, for the NOA coated samples, the variation of the gap-distance between posts is less than 1% for the pressures up to 60 kPa and less than 5% for the pressures up to 130 kPa. Several MIMP channels were fabricated showing a deformation up to 70% less than the same samples fabricated with standard PDMS.
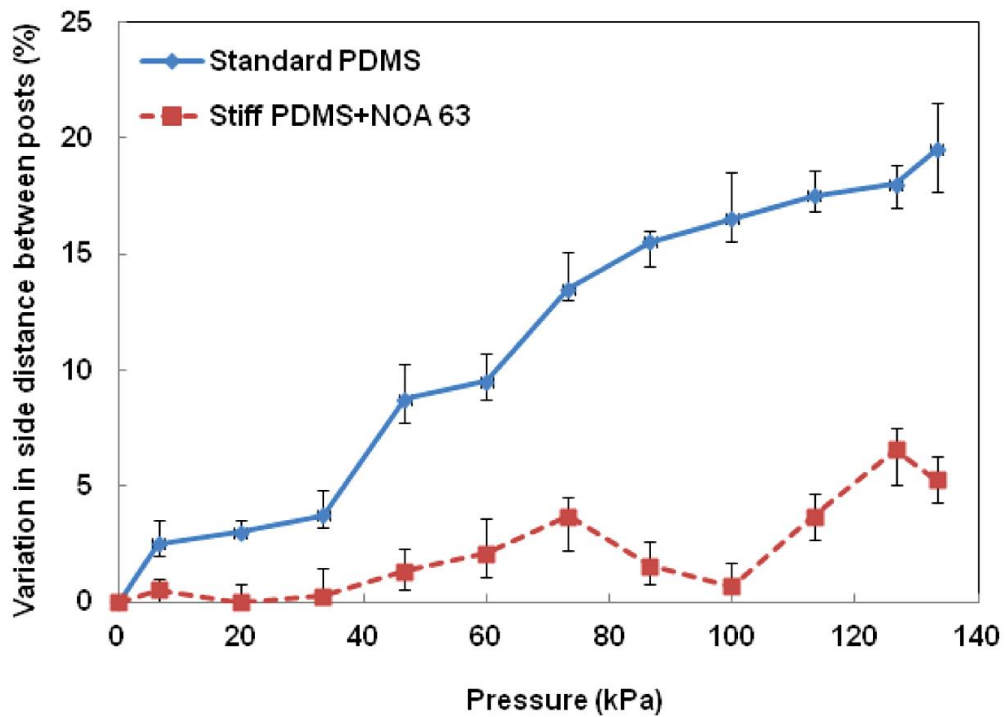
Figure 22. Comparison between change in side distance between posts at different pressures for (a) Standard PDMS (b) Stiff PDMS with NOA coating layer

By solving the PDMS drawback due to its low elastic module, the path was paved to characterize the MIMP capillary pump. Therefore, in the next step (paper III), a diamond microchannel integrated micropillar (dMIMP) pump with high throughput and with a resistance flow 35.5% lower than a circular based micropillar pump (cMIMP) has been developed. For this purpose, the pressure drop and flow resistance of a laminar flow through low aspect ratio MIMP with different shapes and geometrical parameters (See figure 21b) were experimentally, numerically and analytically determined. Several samples of PDMS MIMP channels have been fabricated using a modified soft lithography process which is explained earlier to prevent the PDMS deformation under high-pressure operation. Flow through the fabricated samples has been numerically solved and experimentally measured, with an agreement higher than 90%. The results have been used to validate the derived analytical formulation to determine the flow resistance in this type of channels, a fast approach to obtain the resistance flow in the design stage of microdevices. As it is shown in Figure 23, while the maximum flow resistance is achieved in elongated pillar MIMPs, the pine pillar MIMPs present comparable resistance flow to diamond pillar MIMPs being in both cases the minimum value of all considered shapes.

Figure 23. Variation of a) Pressure drop versus flow rate b) Flow resistance versus the Reynolds number

The analysis of the obtained results indicate that although porosity can be a determinant parameter to predict the resistance flow of MIMP, other geometrical parameters like, side distance between pillars or pillar shape, play a major role in this scenario. In the last part of this step, a high throughput optimized diamond MIMP pump has been designed, tested and validated as a capillary pump, showing that it can provide a flow rate 73% higher than a circular MIMP pump.

VII. VALIDATION OF THE MICRODEVICE

Using all the achieved results in the material property and microcapillary pump design in the last steps, a novel self-driven high throughput microfluidic chip for blood plasma separation is designed and fabricated in this work (paper IV). The design of microdevice is based on the hydrodynamic behavior of red blood cells in the PDMS channel as the up part while the blood plasma is separated through cross flow filtration MIMP glass channel in the down part of the microdevice as it is shown in Fig. 24.
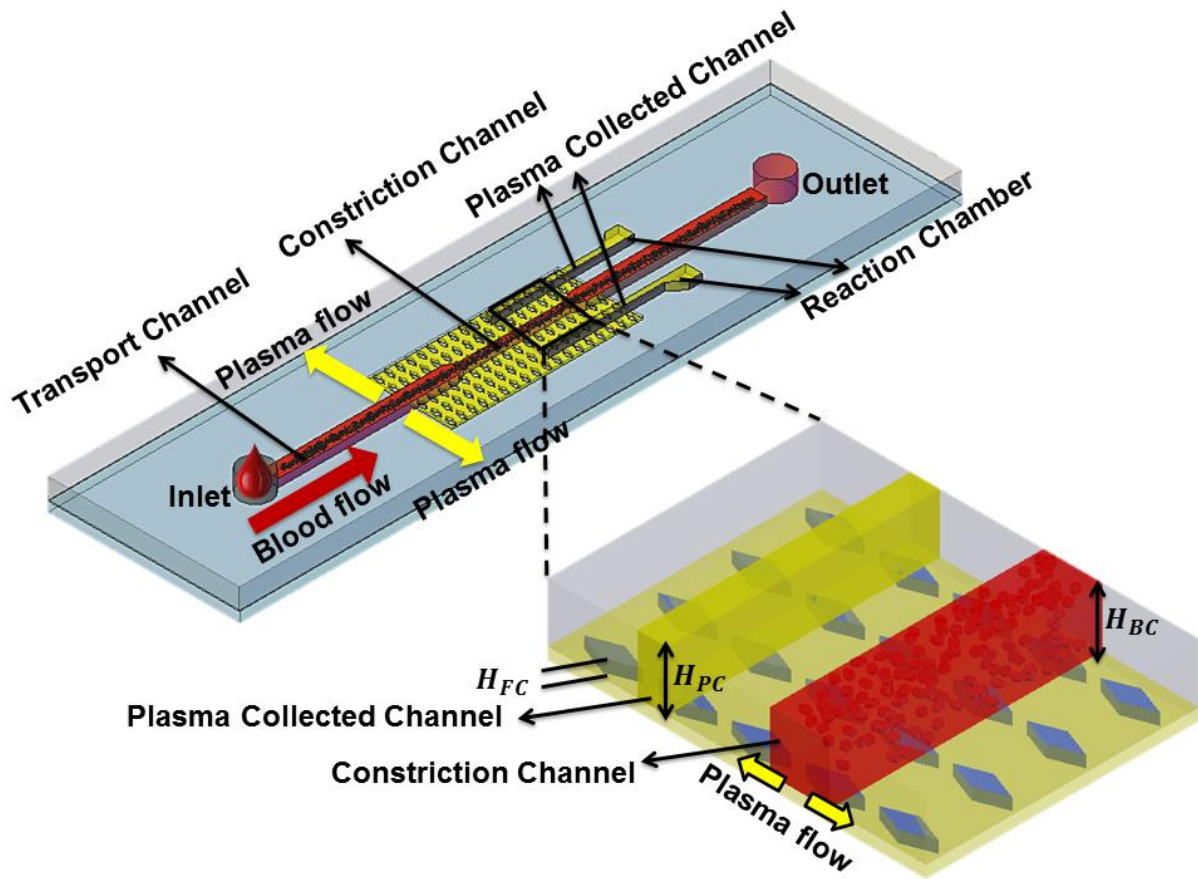
Figure 24. Schematic diagram of the blood plasma separation microdevice

The up part comprises a main blood channel (for transmission of the supplied whole blood) and plasma collected channel which is fabricated in PDMS using conventional photolithography. At a branch point of the transport channel a separation area is connected by an out of plane side channel for extracting the blood plasma. The separation side channel includes an arrangement of diamond microposts to decrease the flow resistance as well as increasing the capillary force according to the results of paper III. Because of the deformability of human red blood cells, the down part depth of the device (H_{FC}) is designed to be less than 2 μm to filter the red blood cells and it is fabricated based on a glass wet chemical process.

The presented microdevice has several advantages over the mentioned devices in the literature for blood plasma separation. This microdevice is self-driven which means that the capillary forces for the liquid transport in the microchannels is achieved due to the hydrophilicity of modified PDMS with nonionic surfactant (Brij 35 or Silwet L-77). This hydrophilicity is sufficient to separate 0.1μL of blood plasma from 5μL drop of the real fresh

blood. The microdevice is fabricated on PDMS and glass as the common materials in the microfabrication process with a simple and inexpensive method. The outstanding feature of the presented microdevice is provided by the both in plane and out of plane microchannel designs based on various hydrodynamic principles to postpone the entrance clogging in the separation border area and accordingly increase the separation efficiency. Besides the separated blood plasma is collected in the 10-µm-depth-PDMS-collected channel, which opens the possibility to integrate a reaction chamber for blood testing.

The microdevice performance for human whole blood plasma separation is shown in Figure 25. This design collected 0.09 µL of blood plasma from 5µL blood drop. According to the results, the plasma-collected channel was filled between 3 to 5 minutes with separation efficiency more than 98%. It is however, interesting to note that the filling time and efficiency of the straight channel design approved the increasing separation speed due to the perpendicularity of the flow path and plasma extractor by the others [28].
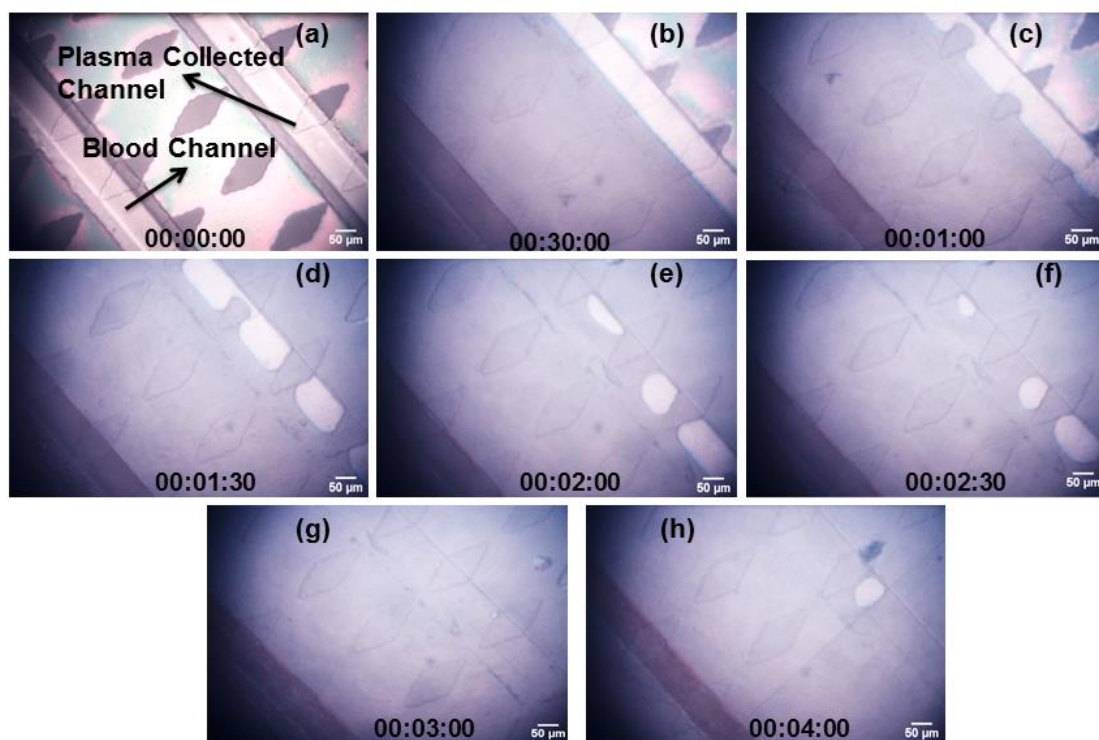
Figure 25. Blood plasma separation procedure in the Microdevice

To prove the high throughput capability of the presented microdevice, another collected channel was designed and embedded at a further distance (1mm) on the other side of the main

blood flow. Besides the filling of the second collected channel that open the possibility of multifunctional blood analysis microsystem, the volume of extracted plasma was increased to 0.1 µL from 5 µL drop of whole fresh blood with the same separation efficiency (more than 98%).

VIII.   CONCLUSIONS

This thesis has described the design, test and validation of self-driven microfluidic chip for the plasma separation from whole human blood.

Following the human whole blood rheology, a literature survey of the recent developments of cell separation technique was carried out and presented.

The research steps to make the microdevice can be classified in three categories: material, design and validation of the microdevice which is associated with fabrication procedure.

In the first step, Polydimethylsiloxane (PDMS) as a soft polymer was chosen to build the microfluidic device. Indeed, its low cost, ease of fabrication, permeability and optical transparency made PDMS the best material for microfluidic applications but PDMS is highly hydrophobic. Therefore the first step toward making the intended microdevice which is accomplished in paper I, was the use of different percentages of nonionic surfactants (Tween 20, Brij 35, and Triton X-100) mixed with precured PDMS to evaluate the possibility for using modified PDMS in disposable capillary driven microfluidic devices. The wettability of this modified PDMS was analyzed using short-term measurements of dynamic contact angle of a water droplet, and the stability of the hydrophilic surface was evaluated through long-term measurements of the static contact angle. According to the results, all the surfactants showed significant decrease of the contact angle during 600 s and the hydrophobic recovery of surfactant-added samples were tested for 2 months and the stability of the samples contact angle after 2 months was similar to the one achieved at beginning. These results provided desirable mixture compositions for building capillary driven devices in many biological and bioengineering applications without the need of tedious pre-processing techniques.

In the second step, a diamond microchannel integrated micropillar pump (dMIMP) with a resistance flow 35.5% lower than a circular based micropillar pump (cMIMP) was developed via the optimization of the fluid-dynamic behavior of different pillar shapes in low aspect ratio (H/D ranged from 0.06 to 0.2) integrated pillar micro-channel. For this purpose, the pressure drop and flow resistance of a laminar flow through low aspect ratio MIMP with different shapes and geometrical parameters were experimentally, numerically and analytically determined. The numerical model showed good agreement with experimental data for all the fabricated samples. The obtained results indicated that while the maximum flow resistance was achieved in elongated pillar MIMPs, the pine pillar MIMPs presented comparable resistance flow to diamond pillar MIMPs being in both cases the minimum value
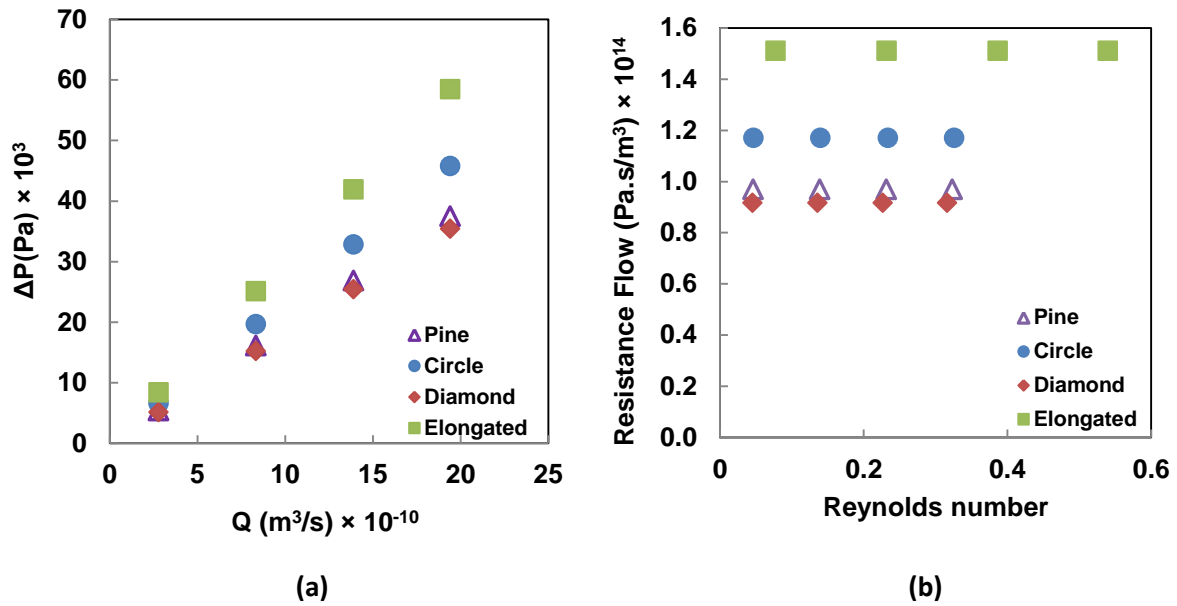
of all considered shapes. In addition, although porosity could be a determinant parameter to predict the resistance flow of MIMP, other geometrical parameters like, side distance between pillars or pillar shape, played a major role in this scenario.

To characterize the micro capillary MIMP pump design, a novel fabrication technique based on the prevention of PDMS deformation was developed. A photo-sensible thiolene resin (Norland Optical Adhesive 63 -NOA 63) was used to create a rigid coating layer over the stiff PDMS micropillar array, which significantly reduced the pressure-induced shape changes. This method used the exact same soft lithography manufacturing equipment. The verification of the presented technique in paper II was investigated experimentally and numerically and the manufactured samples showed a deformation 70% lower than PDMS conventional samples.

This micro capillary MIMP pump design which is accomplished in paper III is a key component of many micro-total analysis systems especially in the presented blood plasma separation microdevice.

Finally, in the last step (paper IV) a novel self-driven high throughput blood plasma separation microfluidic chip which with just single drop of blood ($\sim$ 5µL) could successfully separate 0.1 µL plasma from whole blood without the need of external forces with high efficiency (more than 90%) and reasonable time (3 to 5 minutes) is presented. The potential of the presented self-driven microdevice to integrate with an electrochemical sensor make a promise to manufacture a point-of-care blood analysis in the very near future.

IX. FUTURE WORKS

In this study, a passive high throughput blood plasma separation microdevice using a neat microfabrication technique is presented. The microdevice performance has shown this device produces more than 0.1µL plasma from 5µL of whole human fresh blood. The extracted plasma is collected in two separated 10µm depth microchannels.

The miniaturization of this strategic preliminary step would be the first phase towards the realization of single use, self-blood test and it is expected to help to produce a practical lab-on-a-chip system. The applications for separated plasma from whole blood are numerous and can be summarized in table 2. Additionally, the capability of the presented design to extract plasma in separated collected channels pave the path to accomplish different blood analysis simultaneously and as a consequence produce a multifunctional blood analysis point of care device.

Table 2.Summary of the blood plasma separation applications [29]

Clinical context	Parameter in plasma
Cancer	MicroRNA
Prenatal diagnosis	Cell-free fetal DNA
Myeloma	Plasma viscosity
Transplantation	Levels of donor cfDNA in host plasma

Hence, the next step to achieve this goal would be design a reaction chamber along the plasma collected channel to mix the separated blood plasma with the required reaction for a specific blood analysis. This step can be a supplement of the separation process and could be focused to study the mixing procedure of the reaction and blood plasma in terms of mixing time and sensitivity for a detecting device. Clearly, the precision of the detector as a measuring device is another issue which can be studied in the optofluidics field.

On the other hand, the presented microdevice design could be utilized to detect and isolate different kind of cell such as intact Circulating Tumour Cells (CTCs) or cancer cells from small amounts of blood in the exploratory stages of research.

X. REFERENCES

[1] Kost, Gerald J., *Principles & Practice of Point-of-Care Testing*, Philadelphia: Lippincott Williams & Wilkins, 2002.

[2] Kokoris M., Nabavi M., Lancaster C., Clemmens J., Maloney P., Capadanno J., Gerdes J., Battrell CF., "*Rare cancer cell analyzer for whole blood applications: automated nucleic acid purification in a microfluidic disposable card*," Methods, vol. 37, pp. 114-119, 2005.

[3] Magalie Faivre, Manouk Abkarian, Kimberly Bickraj, Howard A. Stone, "*Geometrical focusing of cells in a microfluidic device: An approach to separate blood plasma*", Biorheology, vol. 43, pp. 147-159, 2006.

[4] Nicole Pamme, Andreas Manz, "*On-Chip Free-Flow Magnetophoresis: Continuous Flow Separation of Magnetic Particles and Agglomerates*", Analytical Chemistry, vol. 76, pp. 7250-7256, 2004.

[5] David W. Inglis, R. Riehn and R. H. Austin, J. C. Sturm, "*Continuous microfluidic immunomagnetic cell separation*", Applied Physics Letters, vol. 85, pp. 5093-5096, 2004.

[6] Furlani, E. P., "*Continuous Magnetophoretic Separation of Blood Cells from Plasma at the Microscale*", Journal of Physics. D:Applied Physics, vol. 40, pp. 1313-1319, 2007.

[7] Beebe, Jaisree Moorthy and David J., "*In situ fabricated porous filters for microsystems*", Lab On A Chip, vol. 3, pp. 62-66, 2003.

[8] Pizziconi, Timothy A. Crowley and Vincent, "*Isolation of plasma from whole blood using planar microfilters for lab-on-a-chip applications*", Lab On A Chip, vol. 5, pp. 922-929, 2005.

[9] Aota A, Takahashi S, Mawatari K, Tanaka Y, Sugii Y, Kitamori T, "*Microchip-based plasma separation from whole blood via axial migration of blood cells*", Analytical Sciences, vol. 27, pp. 1173-1178, 2011.

[10] Angeles Ivón Rodríguez-Villarreal, Martin Arundell, Manuel, "*High flow rate microfluidic device for blood plasma separation using a range of temperatures*", Lab On A Chip, pp. 211-219, 2010.

[11] Santiago, Fabio Baldessari and Juan G, "*Electrophoresis in nanochannels: brief review and speculation"*, Journal of Nanobiotechnology, vol. 4(12), pp. 189-195, 2006.

[12] Pohl, H.A., *The behavior of neutral matter in non-uniform electric field*, Cambridge University Press, 1978.

[13] Cho, Sunghwan Chang and Young-Ho, "*A continuous size-dependent particle separator using a negative dielectrophoretic virtual pillar array*", Lab On A Chip, vol. 8, pp. 1930-1936, 2008.

[14] Pethig, A. Menachery and R., "*Controlling cell destruction using dielectrophoretic forces*", in *IEE Proceedings-Nanobiotechnology*, 2005.

[15] Lotien Richard Huang, Edward C. Cox, Robert H. Austin, James C. Sturm, "*Continuous Particle Separation Through Deterministic Lateral Displacement*", Science, vol. 304, pp. 987-990, 2004.

[16] John A. Davis, David W. Inglis, Keith J. Morton, David A. Lawrence, Lotien R. Huang, Stephen Y. Chou James C. Sturm, and Robert H. Austin, "*Deterministic hydrodynamics: Taking blood apart*", National Academy of Science, vol. 103, pp. 14779-84, 2006.

[17] Siyang Zheng, Yu-Chong Tai, Harvey Kasdan, "*A Micro Device for Separation of Erythrocytes and Leukocytes in Human Blood*", In Engineering in Medicine and Biology 27th Annual Conference (IEEE), Shanghai, China,, 2005.

[18] Sung Yang, a Akif Undar and Jeffrey D. Zahn, "*A microfluidic device for continuous, real time blood plasma separation*", Lab On A Chip, vol. 6, pp. 871-880, 2006.

[19] Faivre M, Abkarian M, Bickraj K, Stone HA., "*Geometrical focusing of cells in a microfluidic device: an approach to separate blood plasma*", Biorheology, pp. 147-159, 2006.

[20] Groisman, Virginia VanDelinder and Alex, "*Separation of Plasma from Whole Human Blood in a Continuous Cross-Flow in a Molded Microfluidic device*", Analytical Chemistry, vol. 78, pp. 3765-3771, 2006.

[21] Hinkle, Tyler Nathaniel, *Blood Model Plasma Separation in a Microfabricated PDMS Device Exploiting Capillary Action Driving Forces,* 2008.

[22] Yu Chang Kim, Seung-Hoon Kim, Duckjong Kim, Sang-Jin Park, Je-Kyun Park, "*Plasma extraction in a capillary-driven microfluidic device using surfactant-added poly(dimethylsiloxane)*", Sensors and Actuators B, vol. 145, pp. 861-865, 2010.

[23] H. Sakamoto, R. Hatsuda, K. Miyamura, S. Sugiyama, "*Plasma separation PMMA device driven by capillary force controlling surface wettability*", Micro & Nano Letters, vol. 7, no. 1, pp. 64-67, 2012.

[24] Hojjat Madadi, Jasmina Casals-Terré "*a self driven microfluidc device for separation liquid from a liquid including deformable particles*". 2013.

[25] Byung-Ho Jo, Linda M. Van Lerberghe, Kathleen M. Motsegood, and David J. Beebe, "*Three-Dimensional Micro-Channel Fabrication in Polydimethylsiloxane (PDMS) Elastomer*", Journal Of Microelectromechanical Systems, vol. 9, no. 1, pp. 76-81, 2000.

[26] Thomas Gervais, Jamil El-Ali, Axel Gu¨nther and Klavs F. Jensen, "*Flow-induced deformation of shallow microfluidic channels*", Lab On A Chip, p. 500–507, 2006.

[27] Brian S. Hardy, Kawika Uechi, Janet Zhen and H. Pirouz Kavehpour, "*The deformation of flexible PDMS microchannels under a pressure driven flow*", Lab On A Chip, vol. 9, p. 935–938, 2009.

[28] Duckjong Kim, Jae Young Yun, Sang-Jin Park, Seung S. Lee, "*Effect of microstructure on blood cell clogging in blood separators based on capillary action*", Microsystem Technology, vol. 15, p. 227–233, 2009.

[29] M. Kersaudy-Kerhoas, *Design, test and biological validation of microfluidic systems for blood plasma separation,* Heriot-Watt University, 2010.

ATTENTION ¡

Pages 42 to 57 of the doctoral dissertation containing two papers are available on the editor's webs

Paper I

Hojjat Madadi, Jasmina Casals-Terré *Long-term behavior of nonionic surfactant-added PDMS for self-driven microchips*. Microsystem Technologies, Jan. 2013 (19) #1, p. 143-150 DOI 10.1007/s00542-012-1641-7
http://link.springer.com/article/10.1007%2Fs00542-012-1641-7

Paper II

Hojjat Madadi, Mahdi Mohammadi, Jasmina Casals Terré, Roberto Castilla López, *A novel fabrication technique to minimize PDMS-microchannels deformation under high-pressure operation* . Electrophoresis. 2013 Dec; 34(22-23) p. 3126-32
DOI: 10.1002/elps.201300340
http://onlinelibrary.wiley.com/doi/10.1002/elps.201300340/pdf

Paper III

View Letter

Close

Ref.: Ms. No. MANO-D-13-00173R2
High throughput microcapillary pump with efficient integrated low aspect ratio micropillars
Microfluidics and Nanofluidics

Dear Dr. CASALS-TERRÉ,

I am pleased to inform you that your work has now been accepted for publication in Microfluidics and Nanofluidics.

Thank you for submitting your work to this journal.

With kind regards

Roland Zengerle
Editor-in-Chief
Microfluidics and Nanofluidics

—

****

Close

High throughput microcapillary pump with efficient integrated low aspect ratio micropillars

Hojjat Madadi, J. Casals-Terré [*], R. Castilla López, M. Sureda Anfres

Technical University of Catalonia, Mechanical Engineering Department, Terrassa, Spain

Abstract

Prediction and reduction of pressure drop and resistance flow in micropillar arrays is important for the design of microfluidic circuits used in different lab-on-a-chip and biomedical applications. In this work, a diamond microchannel integrated micropillar pump (dMIMP) with a resistance flow 35.5% lower than a circular based micropillar pump (cMIMP) has been developed via the optimization of the fluid-dynamic behavior of different pillar shapes in a low aspect ratio (H/D ranged from 0.06 to 0.2) integrated pillar micro-channel. The effect of different geometrical parameters (such as pillar shape, its distribution...) has been considered to minimize the micro-channel resistance flow. 6-µm depth polidimetilsiloxane (PDMS) channels have been fabricated using a modified soft lithography process, which prevents the PDMS deformation under high-pressure operation. Flow through the fabricated samples has been numerically solved and experimentally measured, with an agreement higher than 90%. The results have been used to validate the derived analytical formulation to determine the flow resistance in this type of channels, a fast approach to obtain the resistance flow in the design stage of microdevices. The analysis of the results indicates that although porosity can be a determinant parameter to predict the resistance flow of MIMP, other geometrical parameters like, side distance between pillars or pillar shape, play a major role in this scenario. Finally, a high throughput optimized diamond MIMP pump has been designed, tested and validated as a capillary pump, showing that it can provide a flow rate 73% higher than a circular MIMP pump.

Keywords

Microchannel integrated micropillars (MIMP), Microcapillar pump, Resistance flow and pressure drop

[*] Corresponding Author: Address: Microsystem Laboratory, Department of Mechanical Engineering, Technical University of Catalonia, Terrassa 08222, spain E-mail. Jasmina.casals@upc.edu

I. INTRODUCTION

Microfluidic devices are a new and promising technology for lab-on-a-chip applications since they offer low sample consumption, high degree of portability, and the possibility of cheap mass production by the use of standard microfabrication processes.

Proper operation of passive microfluidics can be achieved by accurate control of liquid flow rate through microchannels, which is encoded in the design of the microfluidic device. Microchannels with integrated micropillars (which we called MIMP in this paper) present increased heat and mass transfer coefficients by a great surface-area-to-volume ratio which make them a novel design in a vast verity of applications such as, controlling surface wettability of Microsystems (Toru Yamada et al. 2011), micro-reactors (Roumanie et al. 2006), micro-total analysis system (µTAS) (Sunitha Nagrath et al. 2007). Furthermore, in the recent years, this microstructure has shown high potential in biological and life sciences to analyze cells, DNA, proteins and chemical reagents (Chun-Ping Jen et al. 2010; Yick Chuen Chan et al. 2007; John A. Davis et al. 2006; Alicia D. Powers et al. 2012).

Low aspect ratio MIMPs are valuable since they offer the possibility to work as micro-filters (Waghmare et al. 2008) or micro-pumps (Auro Ashish Saha et al. 2009; Martin Zimmermann et al. 2007).

In terms of MIMP applications, Yeom et al. (J Yeom et al. 2009) presented design rules to optimize micropillar array performance of a micro-preconcentrator, which is a component of a micro-gas chromatography system. They studied low Reynolds number gas flow across an array of silicon DRIE microcylinder pillars with diameters ranging from 200 µm to less than 10 µm in a 200-µm-depth microchannel. They point out that two key parameters in the performance of the micro-preconcentrator are: the ratio of the radius of each post to the half-spacing between two adjacent posts and the number of micropillars in a row.

Particularly, MIMP structure is a strong candidate for microcapillary pumps to transport a precise volume in Lab-on-a-Chip designs since pillar structures make a significant effect on the capillary flow by increasing the surface/volume ratio. When capillary action is used for micropumps, the material wetting property and the MIMP characteristic dimension play the major roles in the pumps performance. Even though MIMP microcapillary pumps do not require an external energy source for fluid transportation, interesting property in healthcare and drug discovery applications, there are few works that characterize the capillary pump performance through the study of the different pillar shapes and their characteristic

dimensions. Zimmermann et al. (Zimmermann et al. 2007) investigated experimentally the effect of capillary pumps design with various pillar shapes on the flow properties of autonomous capillary systems. The capillary pumps have characteristic dimensions of 15-250 µm. They found the smallest characteristic dimension of symmetric line pillars exhibits the maximum flow rate namely 3.7 nL s^{-1}, but they did not study the effect of all the geometrical parameters separately on the MIMP flow resistance and accordingly the pump performance.

Understanding the effect of geometrical parameters of microchannels with integrated micropillars (MIMP) is important to improve and optimize the design of all the aforementioned microfluidic devices, but in particular it is essential to maximize the throughput in microcapillary pumps. The steady state flow of an incompressible fluid into a microchannel is known as Poiseuille flow (Bruus 2007) where a constant pressure drop (ΔP) results in a constant flow rate (Q):

$$\Delta P = R_{hyd}\, Q \qquad\qquad\qquad\qquad\qquad (1)$$

where R_{hyd} is hydraulic resistance of the channel and Q the flow rate through the channel. Therefore minimizing R_{hyd} will increase the flow rate and the efficiency of the MIMP structure as a micropump.

The flow resistance in a rectangular channel without pillars (Rosenhead 1963), when a Newtonian fluid flows through it can be calculated as:

$$r = \frac{3\mu}{4a^3}\left(1 - \frac{192a}{\pi^5 b}\sum_{n=1,3,5}^{\infty}\frac{\tanh\left(\frac{n\pi b}{2a}\right)}{n^5}\right)^{-1} \qquad (2)$$

Where $r = R_{hyd} * b/L$, µ is the fluid viscosity, L is the microchannel length, a is the half depth of the microchannel and b is the half width of the microchannel. Besides the length and the width, a MIMP channel has several geometrical parameters that modify this flow resistance (SD, side distance between pillars, ...) see Figure 1b.

Transport properties of MIMP flow such as velocity field has been extensively studied (A. Bazylak et al. 2008; Debjyoti Sen et al. 2012; Junkyu Jung et al. 2012). In contrary, there are few experimental and numerical investigations that characterize the pressure drop and flow resistance in MIMP structures, key parameters to obtain a high throughput micro-capillary pump. Kosar et. al. (Ali Kosar et al. 2005) investigated the laminar flow across 100-µm long

pin fins of 50 and 100-µm hydraulic diameters in both: in-line and staggered configurations, which were created by DRIE (deep reactive ion etching) in silicon. In their arrangements the calculated pressure drop using numerical macro-scale tube banks formulas showed a significant deviation from the microscale measurements. Vanapalli et al. (2007) investigated the pressure drop of gas flows in a 250-µm-depth microchannel with various pillar arrays. These high aspect-ratio pillar structures were created using DRIE in silicon. On the contrary, their results for circular pillar cross-section agreed with macroscale correlations. Later, Sirvastava et al. (Nimisha Srivastava et al. 2010) presented a finite element simulation scaling analysis to obtain the resistance flow in limiting regime of microcylinder arrays. They found that pressure driven flow through pillars could be modeled as a function of height, pillar diameter and spacing between them. The obtained coefficient of penetrance with their analysis presented only a 10% disagreement compared to the wetting experiments where they assumed a constant contact angle in the microchannel.

Recently, Tamayol et al. (2012) extended the previous work with a theoretical analysis, which proposed an analytical expression to calculate the pressure drop in a square MIMP, based on the combination of Brinkman equation and existing models for permeability of regular arrays of cylinders. To verify this formula, they utilized the soft lithography to fabricate Polydimethylsiloxane (PDMS) 100-µm-depth MIMP channels with embedded 50-µm up to 400-µm-diameter micropillars. According to them, the most important parameters to study the porous-filling of microchannels are: the porous medium permeability and the channel depth. Moreover, Gunda and their colleagues (2012) investigated the pressure drop and resistance flow through microchannels with integrated micropillars both in square and staggered arrangements to study the validation of all the existing models for computing permeability of such porous structure. They used DRIE as a precise and accurate technique to fabricate 98.4-µm-depth Silicon microchannel with integrated 30-µm to 100-µm diameter micropillars. Their experimental results indicate that the square arrangements offer higher resistance to fluid flow in comparison to their staggered counterparts and the existing theoretical models fail to accurately represent the permeability of microchannel with integrated micropillars (MIMP) as structured porous media.

The aforementioned works provide valuable insight into the pressure drop and flow resistance in cylindered MIMP but there is a lack of study of the hydrodynamic effect of different MIMP shapes with low aspect ratio (H/D ranged from 0.06 to 0.2), which in microfluidics are very valuable as micro capillary pumps. On the other hand, most of the mentioned studies used silicon as a manufacturing material whereas most microfluidic applications use PDMS.

Despite its many outstanding characteristics, PDMS is a low Young modulus material that under pressure can suffer considerable deformations (Thomas Gervais et al. 2006). In this study to minimize the deformation effect and harden PDMS, a novel fabrication technique is introduced by utilizing a coating layer of thiolene resin.

This work proposes an optimized design of high throughput capillary pump, here referred to as dMIMP (diamond MIMP Pump). The dMIMP can be qualitatively considered as an evolution of the traditional cylindered MIMP micropumps (Tsutomu Horiuchi et al. 2012; A. Mathur et al. 2009; Lauri Sainiemi et al. 2008). Its main advantage with respect to the other proposed micro capillary pumps (David Juncker et al. 2002; Zimmermann et al. 2007; N. Scott Lynn et al. 2009), is an increase in flow rate for the same in plane and out of plane channel dimensions since it has a low flow resistance, resulting in higher pumping performance.

This paper is organized as follows: the MIMP channels and their fabrication procedure are described in Section II; the analysis of the fluid-dynamic characteristics of MIMP channels follows in Section III, with the description of the numerical model used and its experimental validation. In Section IV, the proposed optimized MIMP structure is applied as pumping element in a microfluidic circuit, experimentally tested and validated and finally the conclusion are presented in section V.

SECTION II:
II.A MIMP DESCRIPTION

Generally microfluidic circuits consist of two main parts: the pumping system (internal or external) and the circuit itself (chambers and fluidic resistance), see Fig 1a. In capillary driven circuits the pump plays a major role in the device performance. The MIMP capillary pump is an array of micropillars, which can be designed to program the flow rate of the liquid in the circuit. The efficiency of the MIMP capillary pump depends on the contact angles of the filling liquid with the microchannel wall that is an intrinsic property of the material and the characteristic dimensions of MIMP that directly relate to the MIMP flow resistance.

In spite of all the efforts done by the researchers to find an analytical formulation of the flow resistance through MIMP, there is not an accurate theoretical model for such complex microstructure. Hence, in this study we focus on finding an efficient geometrical design for the MIMPs between different pillar shapes (Circle, Diamond, Elongated and Pine) and also

geometrical parameters (Short and large diameter, Side distance and Forward distance between pillars see Fig.1b) to minimize the resistance flow and maximize the throughput of the MIMP structure as a microcapillary pump.
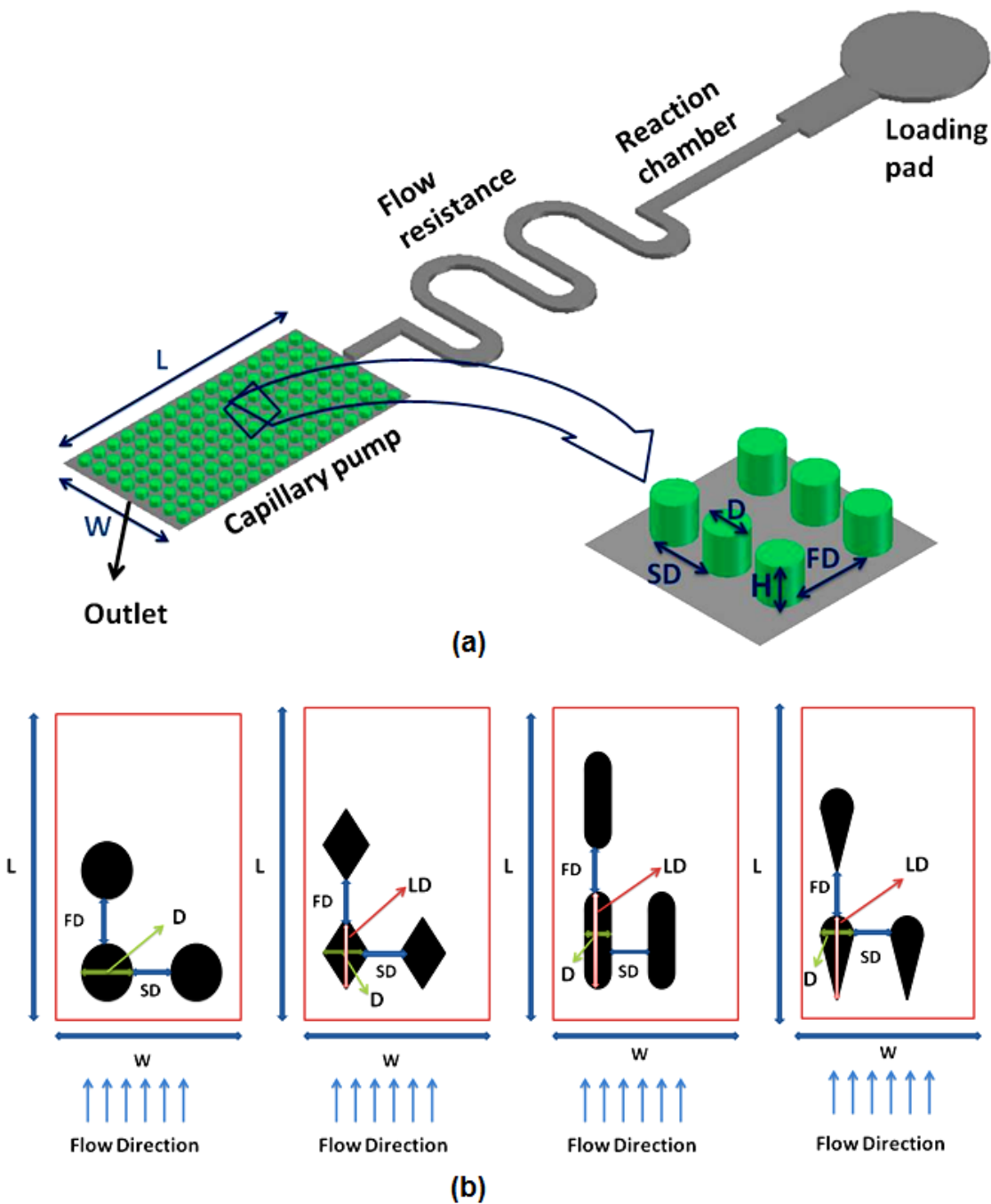
Figure 1. a) Schematics of a microfluidic circuit using a circular MIMP capillary pump b) The different pillar shapes (Circle, Diamond, Elongated, pine) and geometrical parameters (D: Diameter, LD: Large Diameter, SD: Side distance between pillars, FD: Forward distance between pillars) which can affect the flow resistance in MIMPs.

II.b FABRICATION PROCEDURE

The fabrication technology for the MIMP channels is a modified soft-lithography process, which withstands high pressures with low PDMS deformations. Fig. 2 summarizes the different steps of this technology.
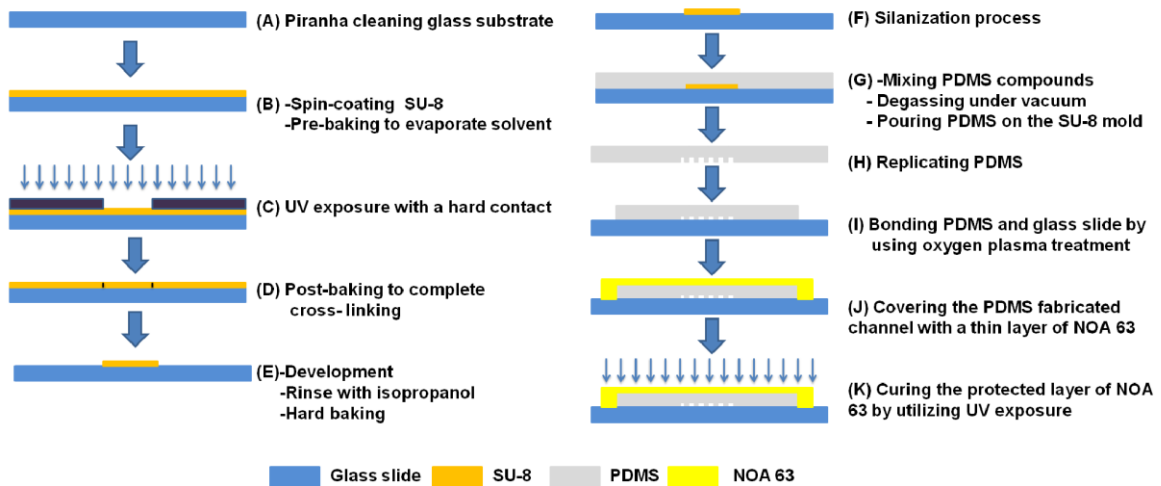
Figure 2. Microfabrication process steps (a)-(f) SU8 mold (g)-(k) Hardened PDMS microchannel integrated micropillar (MIMP) fabrication.

To overcome the PDMS deformation under high pressure operation, a novel technique is used which combines the use of stiff PDMS (10:2, the ratio between polymer base and cross linking agent) and a thin cover layer of thiolene resin (Norland Optical Adhesive 63) on the fabricated PDMS microchannel, see steps J and K in figure 2. More details about the fabrication process are referred in (Hojjat Madadi et al. 2013). Figure 3 shows a sample of the fabricated MIMP structures using this fabrication methodology.
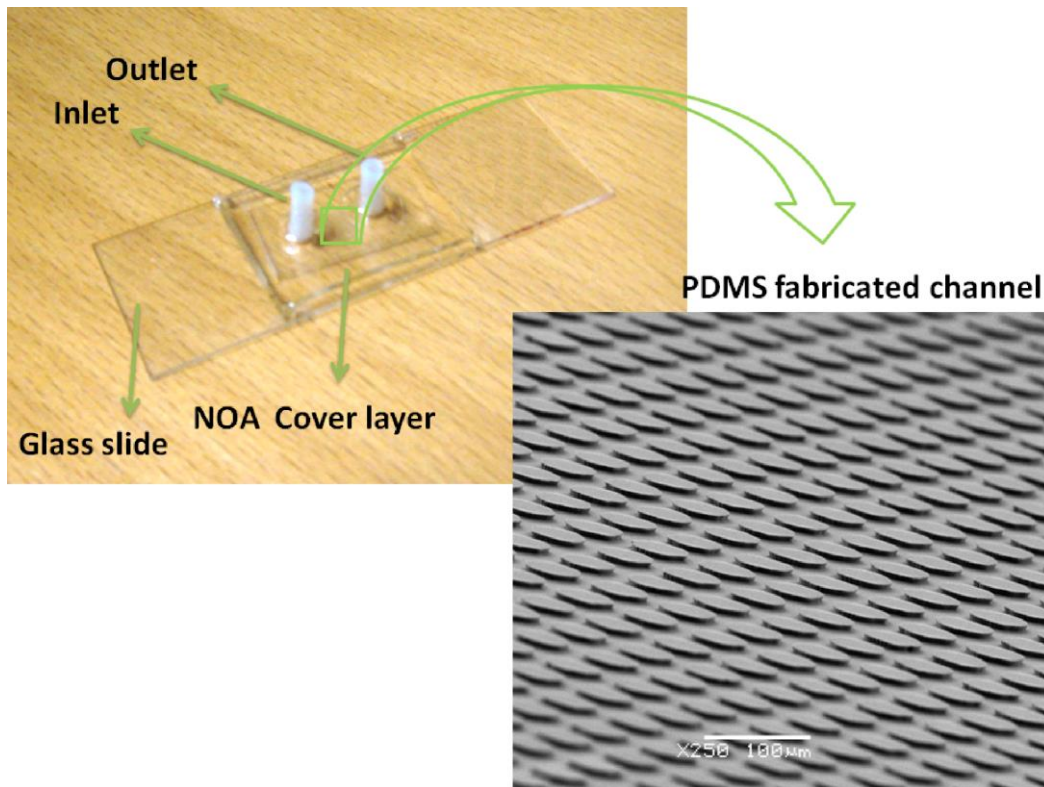
Figure 3. Optical image of a packaged MIMP and SEM details of the integrated micropillars.

SECTION III: MIMP FLUID DYNAMICS ANALYSIS

In order to maximize the MIMP capillary pump efficiency in the capillary driven microfluidics applications where the pressure difference is mainly intrinsic to the material, the flow resistance should be minimized through the design. The fluidic behavior of all the pillars in the array is considered to be the same. Therefore, the core of the microflow is the analysis of one pillar pressure drop, which is directly related to the flow resistance through a unit cell of this channel by assuming steady state flow of an incompressible fluid into the microchannel. The analytical and numerical analyses of the resistance flow in MIMPs structures are presented in the following sections.

III.A ANALYTICAL FLUIDIC RESISTANCE FOR DIFFERENT PILLAR-SHAPES

The steady state flow of incompressible fluid is considered into a unit cell of height (H=2a)
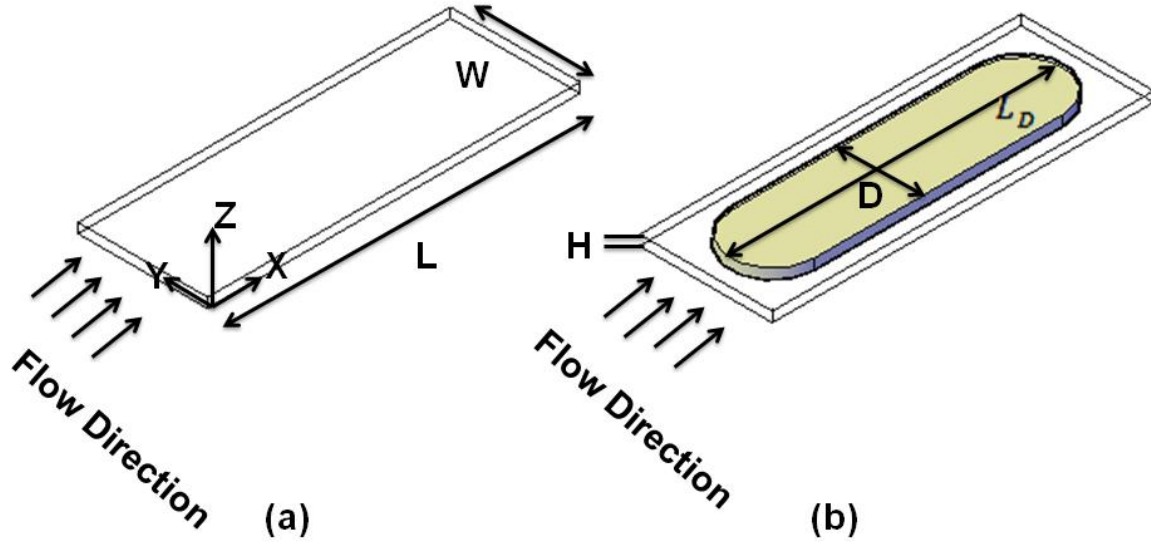
Figure 4. Considered rectangular unit cell a) without pillar b) with pillar

and width (W=2b) as it is shown in Fig.4a. For low aspect ratio microchannels W>>H with an imposed volumetric flow rate of an incompressible fluid, equation (1) can be simplified to:

$$\Delta p_0 = \frac{12 v L \dot{m}}{W H^3} \tag{3}$$

where v is the dynamic viscosity, $\dot{m}$ is the mass flux, L is the length and W is the width of the unit cell. This pressure drop is due to the viscous friction on the top and bottom walls of the unit cell:

$$F_w = \Delta p_0 H W = \frac{12 v \dot{m} L}{H^2} \tag{4}$$

In order to consider the effect of the pillar arrays in the pressure drop, the change in the unit cell pressure distribution is obtained when a pillar is added in the middle of the unit cell (See Fig.4b). As a first approximation, this obstacle does not affect to the flow in any other way than deviating the streamlines. It can be shown that, the friction viscous force on the walls remains unperturbed if it is assumed a uniform distribution of x velocity in the y direction, and parabolic profile in the z direction but the pressure distribution on the cell will produce a pressure force on the pillar:

$$F_{p0} = \Delta p_0 \frac{L_D}{L} H D = \frac{12 v \dot{m} L_D D}{W H^2} \tag{5}$$

where $D \times H$ is the cross-section of the pillar and L_D is the length of the pillar in the flow direction (See Fig.4b).

Due to the low aspect ratio of the channels the friction force in the pillar can be neglected compared to the friction force on the top and the bottom walls of the cell. The total pressure drop in the unit cell can then be written as:

9

$$F_w + F_{p0} = \Delta p_1 HW \tag{6}$$

$$\Delta p_1 = \frac{F_w + F_{p0}}{HW} = \frac{12 \nu L \dot{m}}{H^3 W}\left(1 + \frac{L_D}{L}\frac{D}{W}\right) \tag{7}$$

Since the pressure drop has changed in the unit cell, the pressure force on the pillar has also changed:

$$F_{p1} = \Delta p_1 L_D DHD \tag{8}$$

and, consequently, the total force and the pressure drop in the cell is now:

$$\Delta p_2 = \frac{F_w + F_{p1}}{HW} = \frac{12 \nu L \dot{m}}{H^3 W}\left(1 + \left(1 + \frac{L_D}{L}\frac{D}{W}\right)\frac{L_D}{L}\frac{D}{W}\right) \tag{9}$$

If equation (9) is iteratively expanded, a geometric series will be obtained:

$$\Delta p_n = \frac{12 \nu L \dot{m}}{H^3 W}\sum_{i=0}^{n} \alpha^i \tag{10}$$

where $\alpha = \frac{L_D}{L}\frac{D}{W}$. This geometric series converges if $\alpha < 1$, and the total pressure drop in a low aspect ratio unit cell with an integrated pillar can be written as:

$$\Delta p_\infty = \frac{12 \nu L \dot{m}}{H^3 W}\frac{1}{1 - \alpha} \tag{11}$$

And from equation (2) the specific theoretical resistance can be calculated as:

$$r_{th} = \frac{\Delta p_\infty}{Q}\frac{W}{L} = \frac{12\mu}{H^3}\frac{LW}{LW - L_D D} \tag{12}$$

Following this method, the theoretical resistance of pillar shapes shown in Figure 1b can be expressed in terms of the porosity, which is defined as a fraction of the free spaces volume between pillars over the total volume of MIMP, which is between 0-1. In the presented model, because of the z-direction symmetry, the porosity is the ratio between surfaces. As it is shown in figure 4, the total surface is LW. So, the porosity is:

$$\varepsilon = \frac{LW - S_S}{LW} \tag{13}$$

where S_S is the solid surface which depends on the pillar shape. For a cylinder pillar shape:

$$S_S = \frac{\pi D^2}{4} \tag{14}$$

also in this case, $L_D = D$ that leads to eq.15. In the next expressions, the only change is in the S_S calculation for the different pillar shapes. The final expressions for the flow resistance in function of the porosity are in the following:

For circle pillar shape:
$$r_{th} = \frac{12\mu}{H^3} \frac{1}{1-\frac{4}{\pi}(1-\varepsilon)}$$
(15)

For diamond pillar shape:
$$r_{th} = \frac{12\mu}{H^3} \left(\frac{1}{2\varepsilon-1}\right)$$
(16)

For elongated pillar shape:
$$r_{th} = \frac{12\mu}{H^3} \frac{1-\left(1-\frac{\pi}{4}\right)\frac{D}{L_D}}{\varepsilon-\left(1-\frac{\pi}{4}\right)\frac{D}{L_D}}$$
(17)

For pine pillar shape:
$$r_{th} = \frac{12\mu}{H^3} \frac{\left(\frac{\pi}{4}-\frac{1}{2}\right)\frac{D}{L_D}+1}{2\varepsilon+\left(\frac{\pi}{4}-\frac{1}{2}\right)\frac{D}{L_D}-1}$$
(18)

where μ is the fluid viscosity, H is the height of microchannel, ε is the porosity, D and L_D are the short and large pillar diameters in the flow direction (See Fig1b and 4b).

III.B NUMERICAL MODELLING OF MIMP UNIT CELL

Due to the assumptions in the analytically approach to obtain the resistance flow through a unit cell, e.g. neglecting friction force on the pillar, the reliability of the analytical model is decreased for low porosity MIMPs. In this case, the numerical analysis is a key tool for the resistance flow calculation through MIMPs. On this basis, the flow through MIMPs is solved numerically for different pillar shapes and different pillar arrangements (see Figure 1b).
Ansys Fluent 12.0.1 software, which is based on finite volume method, was used to perform the numerical simulations. The flow is assumed to be fully developed with constant properties, which enabled us modeling the half of unit cell, see Figure 5, by imposing periodic boundary condition to calculate the pressure gradient in the whole MIMP.
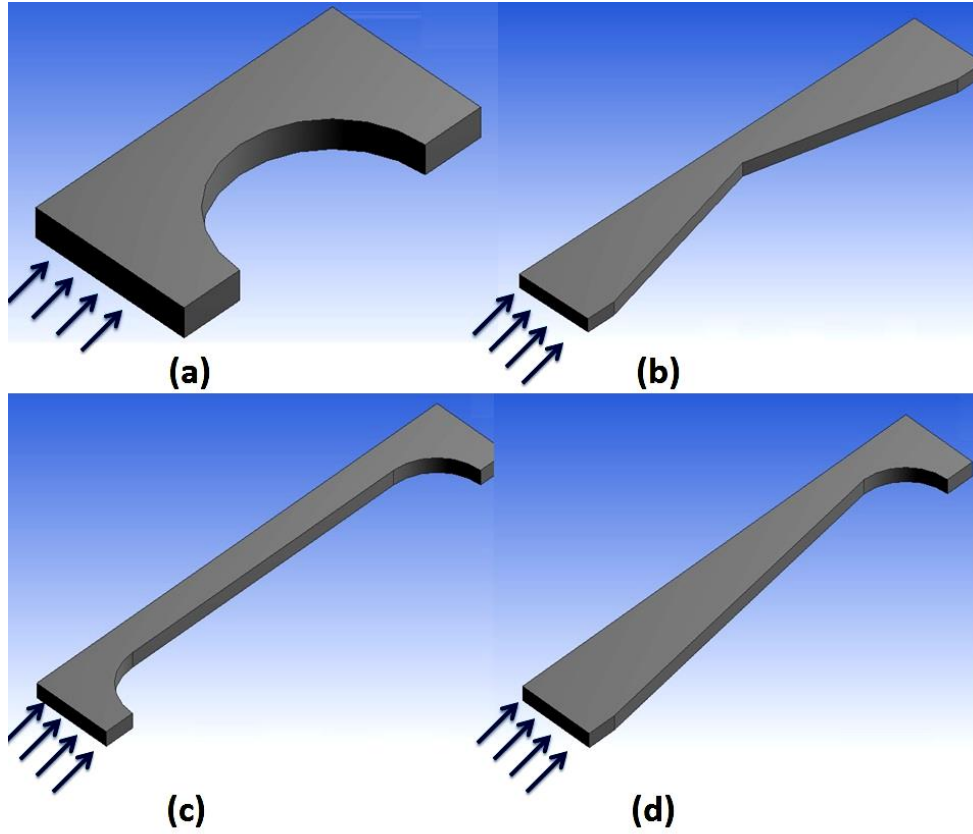
Figure 5. Numerical modeled half of unit cells: a) circle shape b) diamond shape c) elongated shape d) pine shape

The second order upwind scheme was selected to discretize the governing equation and SIMPLE algorithm was applied for pressure-velocity coupling (Ansys, Inc. 2009). The periodic boundary condition was imposed on the inlet and outlet faces while the symmetry boundary condition was applied on the considered unit cell side walls. Actually, the pressure cannot be periodic, since there will be a pressure drop between the inlet and outlet. Hence, the pressure drop is periodic, and Ansys Fluent calculates the pressure gradient as a superposition of a linearly-varying pressure and a periodic one.

$$\nabla p(\vec{r}) = \beta \frac{\vec{L}}{|\vec{L}|} + \nabla \widetilde{p}(\vec{r}) \tag{19}$$

where the value of β is calculated for each flow rate by the code with an iterative procedure and the distribution of the periodic pressure component p̃ by solving the Navier-Stokes equations. The numerical values of the flow resistance are calculated with β and equations (1) and (2). The simulated mass flow rate is selected between 0.1-0.7 mL/h, to be of a similar range to the ones used in the operation of passive microfluidics circuits. Grid independency

12

of the predicted pressure drop was checked in the range of 10000 to 500000 to ensure that the solutions were independent of the computational grids and finally the optimum number of cell was 124000, see Figure 6.
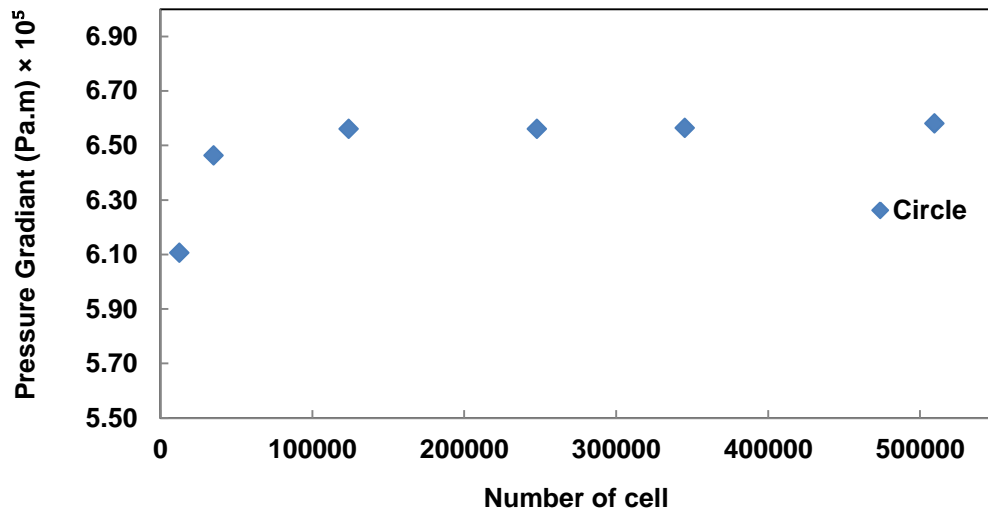
Figure 6. Pressure gradient values versus number of elements

An example of the numerical grid produced by Ansys Fluent 12.0.1 and the velocity contour of the considered geometry with different pillar shapes by using the numerical model are shown in Fig.7.

(a)   (b)
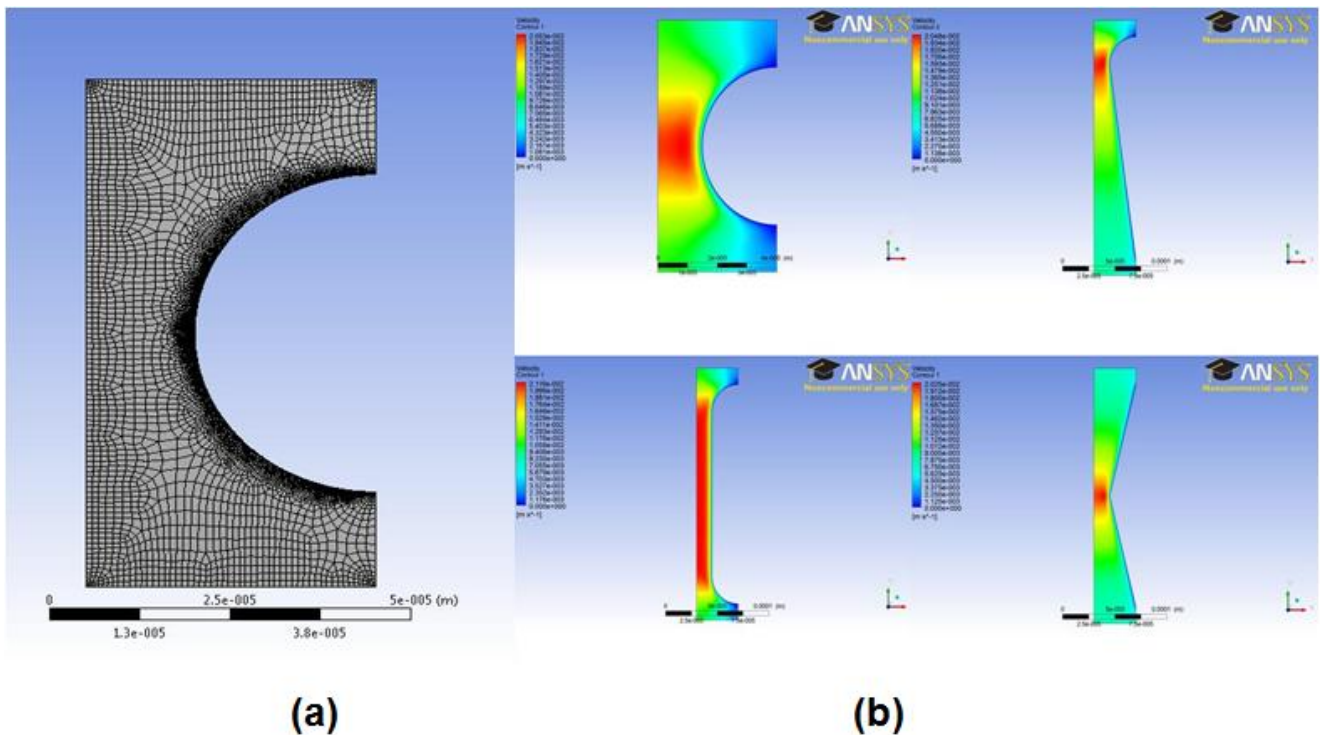
Figure 7. a) The produced numerical grid of considered unit cell b) The velocity contour of different pillar shape

III.C MODEL VALIDATION

The proposed microfabrication process that uses a thiolene resin to harden the PDMS MIMP channels opens the possibility to implement MIMP pumps and the whole microfludic system in PDMS with a behavior similar to glass fabricated devices. Hence, the testing of the packaged MIMP pumps have been conducted using distilled water.

The testing setup is shown in Fig. 8. The MIMP circuit is placed on a flat substrate. The experiment is carried out for each selected pillar shape design to validate the numerical model. The fluid is moved thanks to the syringe pump (Graseby 3200, Smiths medical, USA) which is used to provide and control the desired flow rate of distilled water at the MIMP circuit inlet. During the operation, the MIMP inlet is connected to the syringe pump while the outlet is kept open to the atmosphere. The total pressure drop during the experiments is measured using a pressure transducer, ΔP total. This pressure can be divided in:

$$\Delta P_{total} = \Delta P_I + \Delta P_{en} + \Delta P_{FD} + \Delta P_{minor} + \Delta P_{ev} \qquad (20)$$

Where ΔP_I is the pressure drop in the tube between the pressure transducer and the MIMP inlet, ΔP_{en} is the pressure drop in the entrance region of the MIMP where the fully-developed flow is not achieved, ΔP_{FD} is the pressure drop in the fully-developed flow region of the MIMP, ΔP_{minor} is the pressure drop due to the minor losses of bends in the inlet and outlet of the MIMP and ΔP_{ev} is the pressure drop related to electro-viscous effect (Mohsen Akbari 2009).
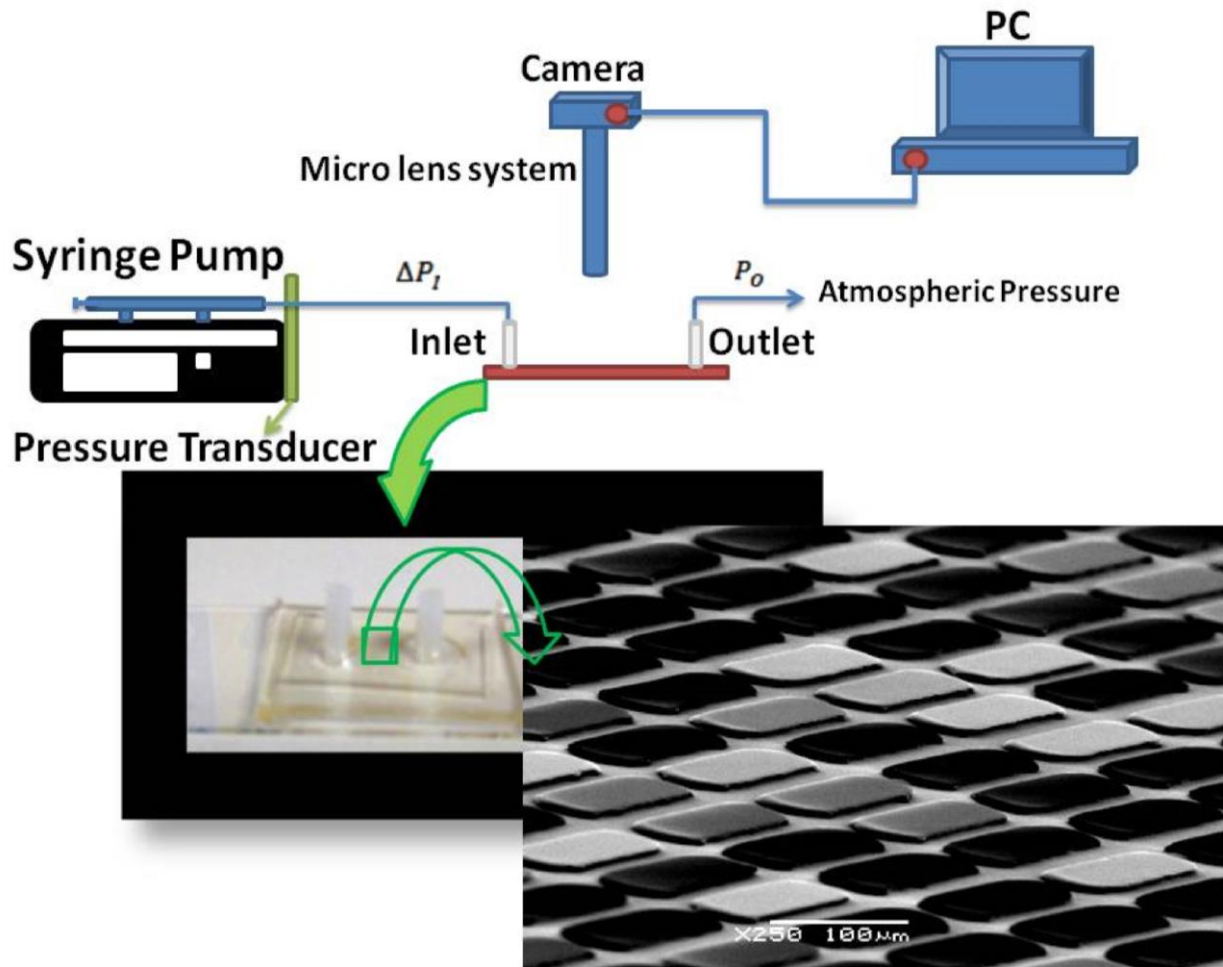
Figure 8. Schematic of the experimental setup for pressure drop measurement in the fabricated samples.

The connecting tube pressure drop ΔP_I includes the losses due to all fittings and the capillary tube from the transducer to the MIMP inlet. This pressure drop was measured directly at each flow rate when the end of the tubing was kept at the atmospheric pressure. To avoid the effects of the hydrostatic pressure, the tubing level was identical in all the connected MIMP. Akbari et al. (Mohsen Akbari 2009) showed that the pressure drop due to the minor losses of bends port and electro-viscous effects ΔP_{minor} and ΔP_{ev} are less than 1% of the pressure drop in the fully-developed region ΔP_{FD}, therefore they were neglected. The pressure drop in the developing region ΔP_{en} of most microchannel cases is negligible since the viscous boundary layer grows faster in microchannels than in macroscales. Additionally, it is reported that the fully developed condition in parallel cylinders systems is achieved in the first three rows (Kirsch et al. 1967). Therefore, the measured pressure drop in the MIMP is related to the

15

pressure drop in the fully developed region of the MIMP by considering ΔP_l as the connecting tube pressure drop.

The geometrical parameters of the manufactured devices have been measured using SEM image analysis and listed in Table.1. Figure 9 shows different pillar shape MIMPs SEM images and a close up view of the dimensions of the manufactured devices. Actually, in the fabrication process the intended structures were patterned through a high-resolution printed photo mask which did not have enough resolution to make straight lines in diamond and pine sides. Because of this reason, you can see some indentations in the diamond and pine shapes which are inevitable in the photolithography process.
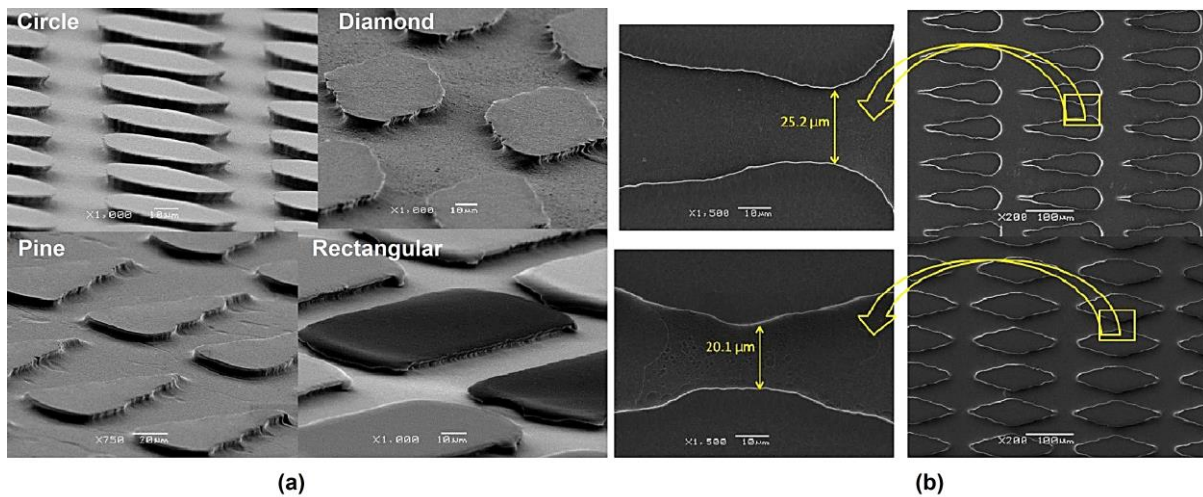
Figure 9. (a) SEM image of micropillars with different pillar shapes (b) An example of the measurement process for different geometrical dimension by using SEM image

Table 1. Average dimensions (μm) of the MIMP fabricated samples

Sample	D	SD	FD	LD
Circle A	52	28	32	52
Circle B	98	27	31	98
Diamond A	54	20	42	193
Diamond B	95	19	40	194
Elongated A	53	20	21	202
Elongated B	104	19	20	201
Pine A	54	23	62	206
Pine B	103	25	60	205

Fig. 10 (a-b) shows the resistance flow versus the volumetric flow rate for two different arrangements of circular pillars using the proposed analytical formulation in this paper and compared to the numerical and experimental values and the presented results by Tamayol (2012).
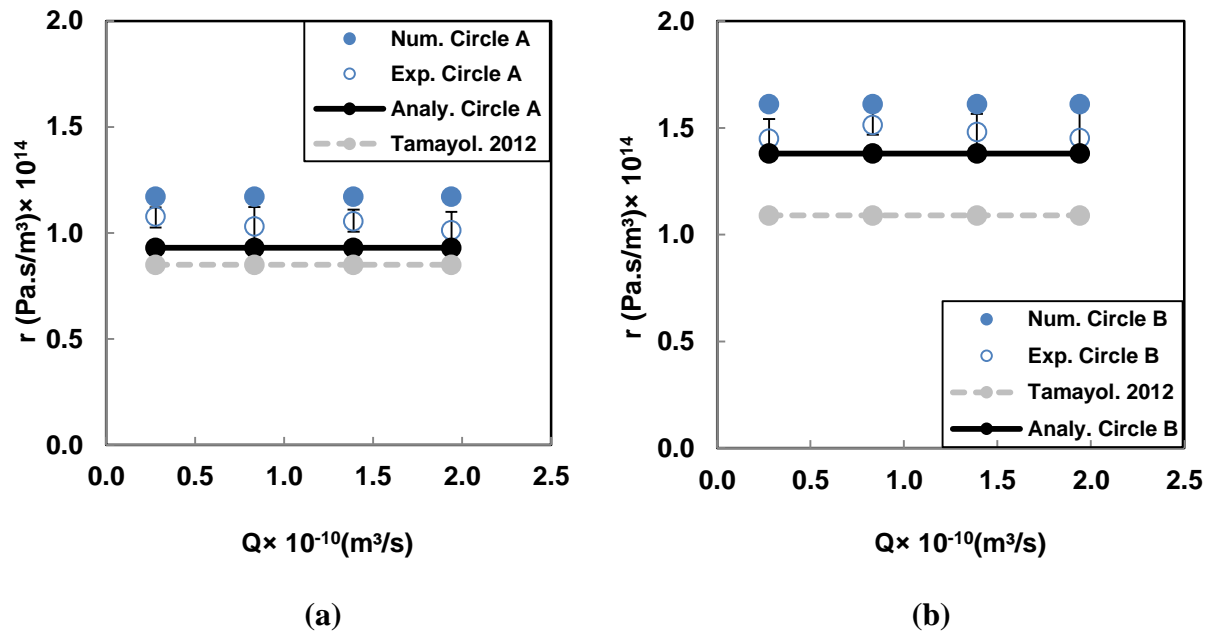
Figure 10. Comparison of the resistance flow versus flow rate in a) Case A and b) Case B for the circular pillar shape

The analytical model shows a reasonable agreement with experimental and numerical data in both cases (see Table 2) while the Tamayol's results show certain variation due to the fact that the considered pillars have low aspect ratio. Figs. 11 (a-d) shows the obtained analytical, numerical and experimental values of resistance flow versus the volumetric flow rate for different pillar shapes.
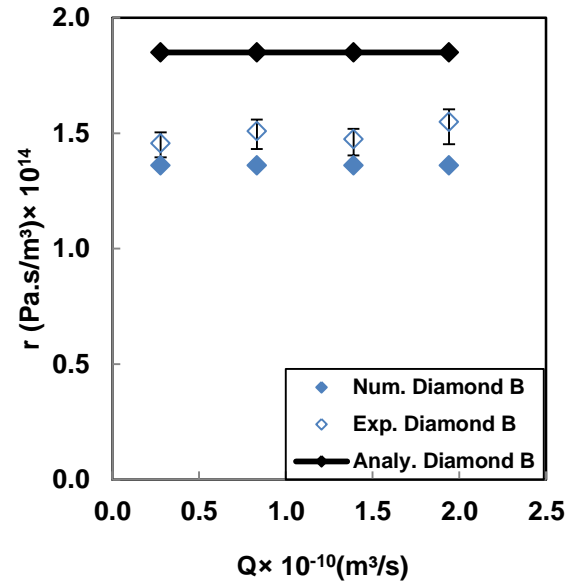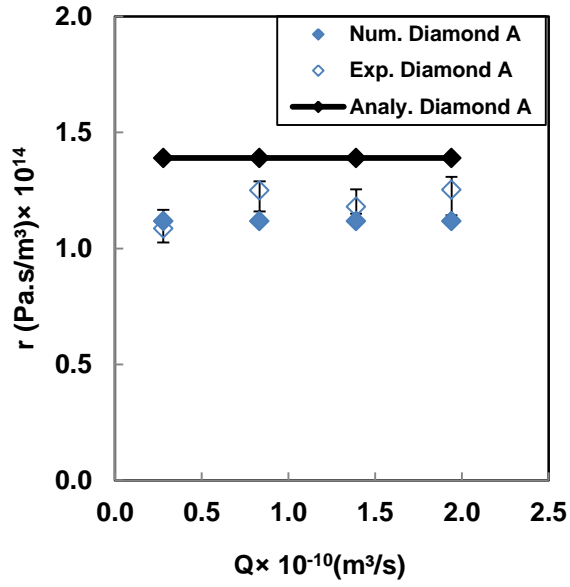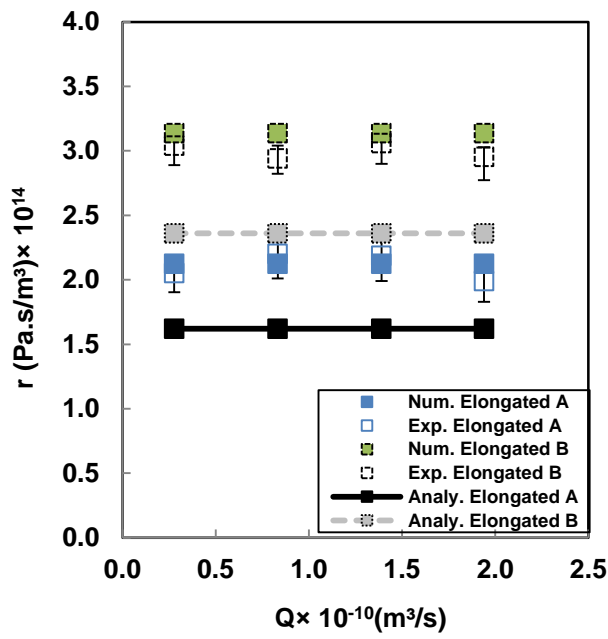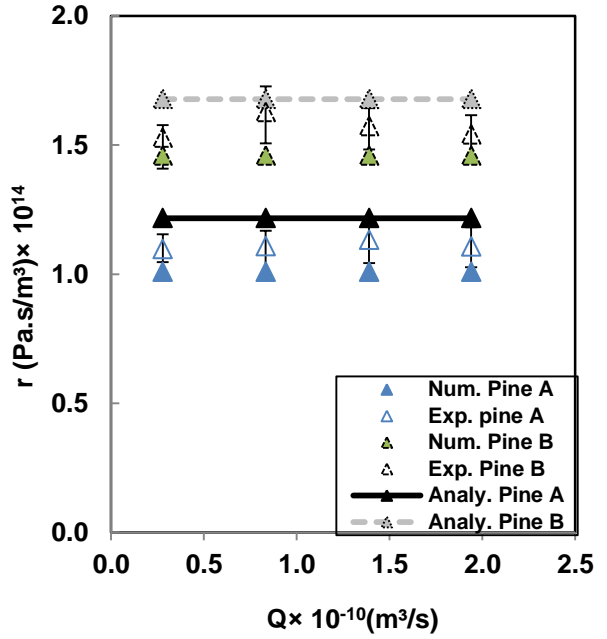
Figure 11. Comparison between numerical, analytical and experimental resistance flow versus flow rate in Case A and B for the different pillar shapes: a) Diamond A b) Diamond B c) Elongated d) Pine shape model

Table 2. The deviation between the calculated numerical and analytical resistance flow from measured experimental resistance flow

Sample	Porosity	Experimental Resistance flow $\times 10^{14}$	Numerical Resistance flow $\times 10^{14}$	Deviation (%)	Analytical Resistance flow $\times 10^{14}$	Deviation (%)
Circle A	0.68	1.04	1.17	-12.50	0.93	10.58
Circle B	0.53	1.47	1.61	-9.52	1.38	6.12
Diamond A	0.70	1.19	1.12	5.88	1.39	-16.81
Diamond B	0.65	1.50	1.36	9.33	1.68	-12.00
Elongated A	0.38	2.11	2.12	-0.47	1.62	23.22
Elongated B	0.32	3.00	3.14	-4.67	2.36	21.33
Pine A	0.71	1.11	1.01	9.01	1.22	-9.91
Pine B	0.64	1.57	1.46	7.01	1.68	-7.01

The flow resistance remains almost constant versus all the tested flow rates as it is shown in figures 10 and 11. In general for all the pillar shapes, the MIMPs with larger diameters (case B) offer higher resistance to flow than case A. Due to the assumptions done to derive the analytical formula, the low porosity arrangements present less accuracy, see elongated shape in Table 2. The deviation of the experimental data from the analytical and numerical results can be due to the uncertainty of the fabrication process that affect the microchannel depth, which has an important impact in the flow resistance (Ali Tamayol 2012) or the fact that the numerical model assumes rigid walls while the proposed fabrication technique tends to minimize the deformation but not eliminate it completely.

III.D NUMERICAL MIMP MODEL ANALYSIS

Table 3.Geometrical parameters of different considered models (all the dimensions are in microns).

	Pillar dimensions				Channel dimensions			Channel characteristics		
	Elongated shape									
Sample	D	SD	FD	LD	W	L	H	N.R	N.C	Porosity
Elongated	50	30	30	200	4960	9890	6	62	43	0.49
Elongated D	**100**	30	30	200	4940	9890	6	38	43	0.40
Elongated SD	50	**60**	30	200	4950	9890	6	45	43	0.63
Elongated FD	50	30	**60**	200	4960	9880	6	62	38	0.55
Elongated LD	50	30	30	**400**	4960	9890	6	62	23	0.43
	Diamond shape									
Sample	D	SD	FD	LD	W	L	H	N.R	N.C	Porosity
Diamond	50	30	30	200	4960	9890	6	62	43	0.73
Diamond D	**100**	30	30	200	4940	9890	6	38	43	0.67
Diamond SD	50	**60**	30	200	4950	9890	6	45	43	0.80
Diamond FD	50	30	**60**	200	4960	9880	6	62	38	0.76
Diamond LD	50	30	30	**400**	4960	9890	6	62	23	0.71
	Circle shape									
Sample	D	SD	FD	LD	W	L	H	N.R	N.C	Porosity
Circle	50	30	30	50	4960	10000	6	62	125	0.69
Circle D	**100**	30	30	100	4940	9880	6	38	76	0.54
Circle SD	50	**60**	30	50	4950	10000	6	45	125	0.78
Circle FD	50	30	**60**	50	4960	9900	6	62	90	0.78
	Pine shape									
Sample	D	SD	FD	LD	W	L	H	N.R	N.C	Porosity
Pine	50	30	30	200	4960	9890	6	62	43	0.71
Pine D	**100**	30	30	200	4940	9890	6	38	43	0.62
Pine SD	50	**60**	30	200	4950	9890	6	45	43	0.79
Pine FD	50	30	**60**	200	4960	9880	6	62	38	0.74
Pine LD	50	30	30	**400**	4960	9890	6	62	23	0.70

In order to minimize the MIMP pump resistance flow, the effect of the different geometrical parameters are analyzed using the different MIMP arrangements summarized in Table 3. The micropillars are arranged inside a 4940 to 4960-µm width and 9880 to 10000-µm length in a 6-µm depth microchannel. In table 3 the dimensions of the simulated samples are summarized in µm. H is the depth of the microchannel or height of the micropillar, SD and FD are the side distance and forward distance between pillars (See Fig.1b), N.R and N.C are the number of micropillar rows and columns integrated in the microchannel. In Table 3, the first sample for every pillar shape is considered as the base and the others correspond to the

parameter increment towards the first one. For example, Elongated FD shows the elongated pillar shape with twice increment in the forward distance towards Elongated (the first one).

In order to investigate the effect of geometrical parameters, the variation of resistance flow according to the dimensionless value SD/D and FD/D is depicted in Fig. 12(a-d) while the influence of the short and large diameter variation of different pillar shapes on the changing resistance flow is shown in Figure 13(a-b). The analysis of the resistance flow based on the parameters changes is discussed for every pillar shape in the following section.
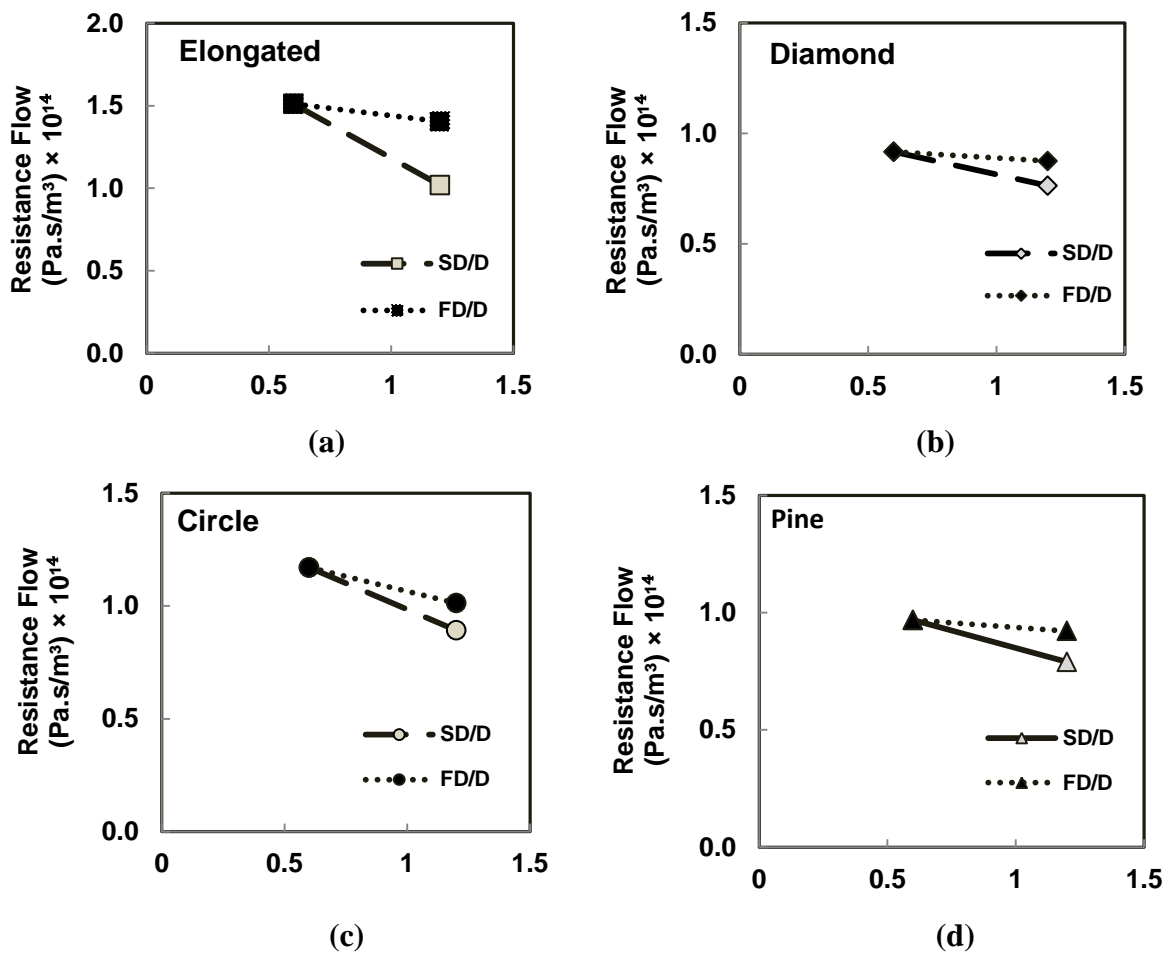
Figure 12. Comparison of the MIMP resistance flow evolution to the change of side distance and forward distance between pillars for a) Elongated b) Diamond c) Circle and d) Pine pillar shapes.
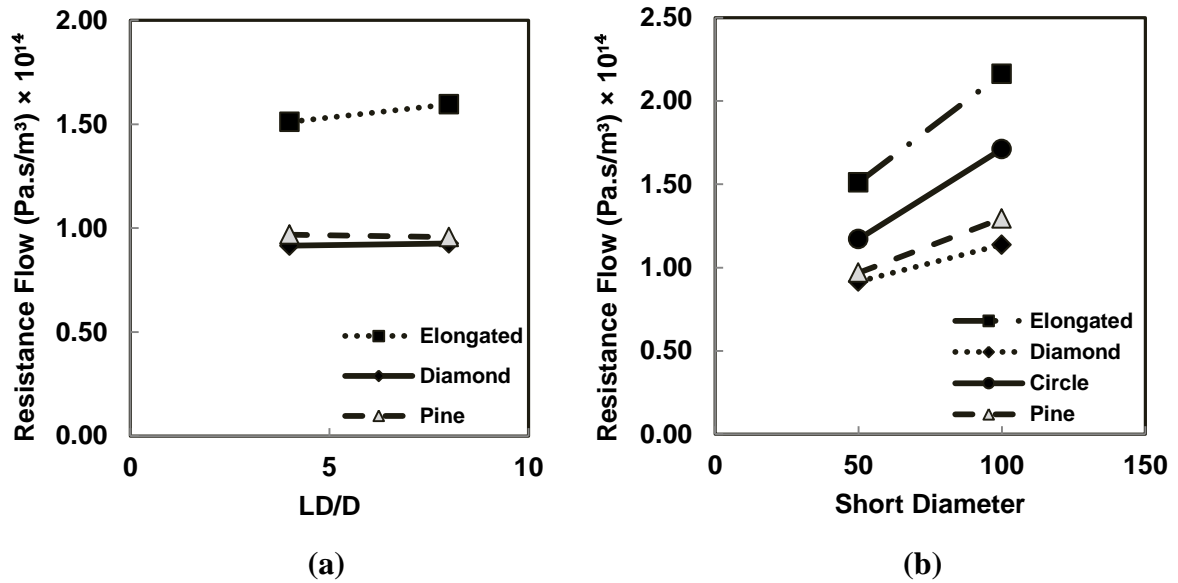
Figure 13. Comparison of the MIMP resistance flow evolution to the change of a) large and b) short diameter for different pillar shapes

Circular pillar shape

Fig. 13b shows that the flow resistance increases with the pillar diameter whereas, a reduction in the resistance flow is achieved when forward distance and side distance between circular pillars are increased (See Fig12c). But increasing SD, side distance has a much larger effect (more than 24%) on the flow resistance reduction than increasing FD, forward distance (around 14%).

Diamond Pillar shape

According to the results, a 20% flow resistance enhancement is achieved when increasing two times the diamond pillar short diameter (See Fig. 13b). But the change is insignificant for the same increment of diamond pillar large diameter (See Fig. 13a). Besides, a side distance (SD) increment generates a flow resistance reduction 12% more than the same increment in forward distance between diamonds pillars shape (See Fig.12b).

Elongated pillar shape

The variations of resistance flow based on the increment of forward distance and large diameter are insignificant in comparison to the other parameters (See Fig. 12a and Fig.13).

Fig.13b shows that the elongated shape with two times increment in short diameter generates a 30% increase in the resistance flow. In terms of side distance increment between pillars, it is also interesting to note that among all the pillar shapes, the maximum reduction of the resistance flow occurs for MIMPs with elongated pillar shape which is more than 32% (See Fig.12a).

Pine pillar shape

According to Fig. 13b, a 25% flow resistance increment is generated by an increase of two times of the pine pillar short diameter. In the case of side distance and forward distance increase, the resistance flow behavior is quite similar to the diamond pillar shape, hence two times increase of the side distance and forward distance leads to a flow resistance decrease around 18% and 5%, respectively (See Fig.12d).

Comparison between different pillar shapes

(a)   (b)

Figure 14. Variation of a) Pressure drop versus flow rate b) Flow resistance versus the Reynolds number

Although the MIMP with elongated pillar shapes can be used to control the progression of a liquid along different directions of the capillary pump, Figure 14 shows that this shape

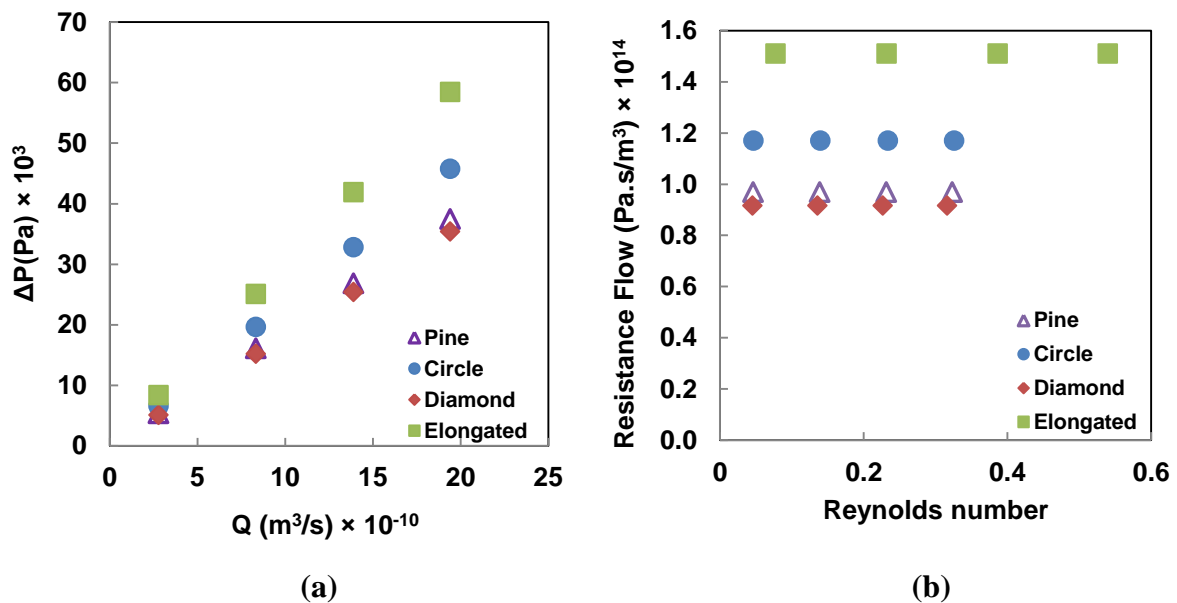generates the maximum flow resistance while MIMP with diamond pillar shape presents the minimum flow resistance which leads to achieve the highest flow rate in microcapillary pumps. For further investigating the effect of micropillar arrangement on the flow resistance of the MIMP, the variation of the analytical and numerical predicted flow resistance according to the porosity is shown in Fig.15 and summarized in Table.4. In general, both numerical and analytical results show that the pressure drop is higher for the denser configuration in agreement with Kumar and Tamayol (Naga Siva Kumar Gunda et al 2012; Ali Tamayol et al. 2012).

Table 4. The predicted analytical and numerical resistance flow according to the porosity

Sample	Circle			Diamond		
	Porosity	R Analytical. (Pa.s/m³)	R Numerical (Pa.s/m³)	Porosity	R Analytical (Pa.s/m³)	R Numurical (Pa.s/m³)
Base	0.69	9.12×10^{13}	1.17×10^{14}	0.73	1.22×10^{14}	9.16×10^{13}
D	0.54	1.36×10^{14}	1.71×10^{14}	0.67	1.68×10^{14}	1.14×10^{14}
SD	0.78	7.76×10^{13}	8.92×10^{13}	0.80	9.19×10^{13}	7.62×10^{13}
FD	0.78	7.76×10^{13}	1.01×10^{14}	0.76	1.07×10^{14}	8.74×10^{13}
LD				0.71	1.33×10^{14}	9.26×10^{13}

Sample	Elongated			Pine		
	Porosity	R Analytical. (Pa.s/m³)	R Numerical (Pa.s/m³)	Porosity	R Analytical. (Pa.s/m³)	R Numerical (Pa.s/m³)
Base	0.49	1.22×10^{14}	1.51×10^{14}	0.71	1.22×10^{14}	9.68×10^{13}
D	0.40	1.68×10^{14}	2.16×10^{14}	0.62	1.68×10^{14}	1.30×10^{14}
SD	0.63	9.19×10^{13}	1.02×10^{14}	0.79	9.19×10^{13}	7.90×10^{13}
FD	0.55	1.07×10^{14}	1.40×10^{14}	0.74	1.07×10^{14}	9.21×10^{13}
LD	0.43	1.33×10^{14}	1.60×10^{14}	0.70	1.33×10^{14}	9.57×10^{13}
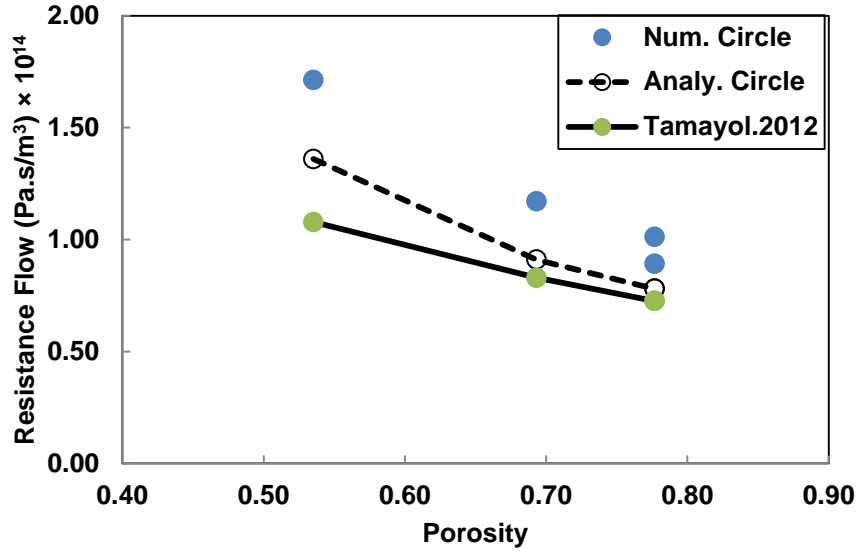
(a)
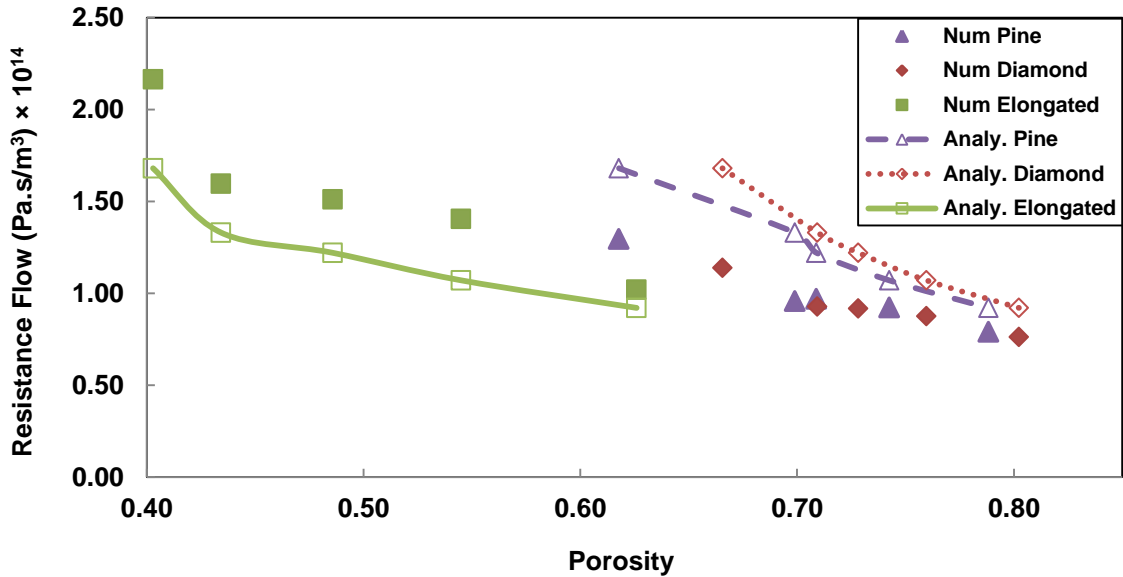
(b)

Figure 15. Variation of the predicted analytical and numerical resistance flow with the porosity for a) Circle pillar shape b) all the other considered arrangements

Fig.15b shows that the trends of the numerical results were well predicted by the theoretical results. The deviation of the analytical results from the numerical results is mostly caused by the assumptions done to derive theoretical formulation such as neglecting the friction force in the pillar. On the other hand, this deviation decreases to less than 15% when the porosity is increased for all the pillar shapes, which is associated to the mentioned assumption.

Figure 15a and Table 4 show that both theoretical methods (Tamayol 2012 and present) fail to distinguish between Circle SD and Circle FD, two different arrangements that change the side distance and forward distance between circular pillar shapes.

It can be highlighted that the circular pillar shape with wider side distance (Circle SD) offers lower flow resistance in comparison to the circular arrangements with the same increment in forward distance (Circle FD) while both arrangements have the same porosity (0.78). Moreover, Figure 15 shows that the resistance flow in MIMP with Diamond LD pillar shape reduced more than 4% in comparison to MIMP with Pine pillar shape, even though they have the same porosity. It can be finally concluded that, although porosity can be a determinant parameter to predict the resistance flow of MIMPs, other geometrical parameter like side distance can play a major role in this scenario.

IV. FLUIDIC CAPILLARY PUMP CHARACTERIZATION

According to the results summarized in Table 4, diamond MIMP provides the lowest flow resistance and therefore it offers the best pumping performance. In order to investigate the effect of hydrodynamic pillar shape and MIMP geometry on the capillary pumping performance, three different PDMS MIMP including pump 1 with circular pillar shape, pump 2 with diamond pillar arrangement and pump 3 with Diamond SD pillar arrangement have been fabricated.

The capillary pressure inside the MIMP is due to the interaction between the surface tension of the liquid and the surface geometry of the microstructure and therefore is directly related to contact angle and MIMP geometry. In order to investigate the influence of MIMP geometry optimization in the pumping performance, the tests were done in the channels with the same wetting properties to deactivate the contact angle effect. In other words, the samples are tested simultaneously 4 minutes after PDMS oxygen plasma treatment.

The diamond and circle design shapes where chosen to show the effect of hydrodynamic pillar shape and Diamond SD was chosen to demonstrate the influence of geometrical parameter on the flow resistance of the microcapillary pump. The samples were fabricated following the steps A to I in Figure 2.

Fig.16 shows a picture of the fabricated PDMS MIMP capillary pumps. A 10-µL drop of deionized water mixed with ink is placed at the inlet of the fabricated device. Capillary pressure spontaneously draws the liquid into the MIMP pump. Table 5 summarizes the flow

rates measured for the different samples. The flow rate is determined multiplying the microchannel cross sectional area by the fluid velocity, which is calculated based on the required time to fill a capillary pump completely. The achieved flow rate for the optimized diamond MIMP pump is 73% higher than the non-optimized or the cylindrical MIMP and one order of magnitude higher than the obtained flow rate in the best pillar arrangements of Zimmermann et al. work (2007). Notice that by decreasing the resistance flow about 36% from pump 1 (Circle) to pump 3 (Diamond SD), the flow rate has increased more than 73%. In the supplementary material there is a video clip of the performance of the optimized diamond MIMP pump in comparison to the elongated MIMP pump.

Table 5. Average measured flow rates for three different fabricated samples

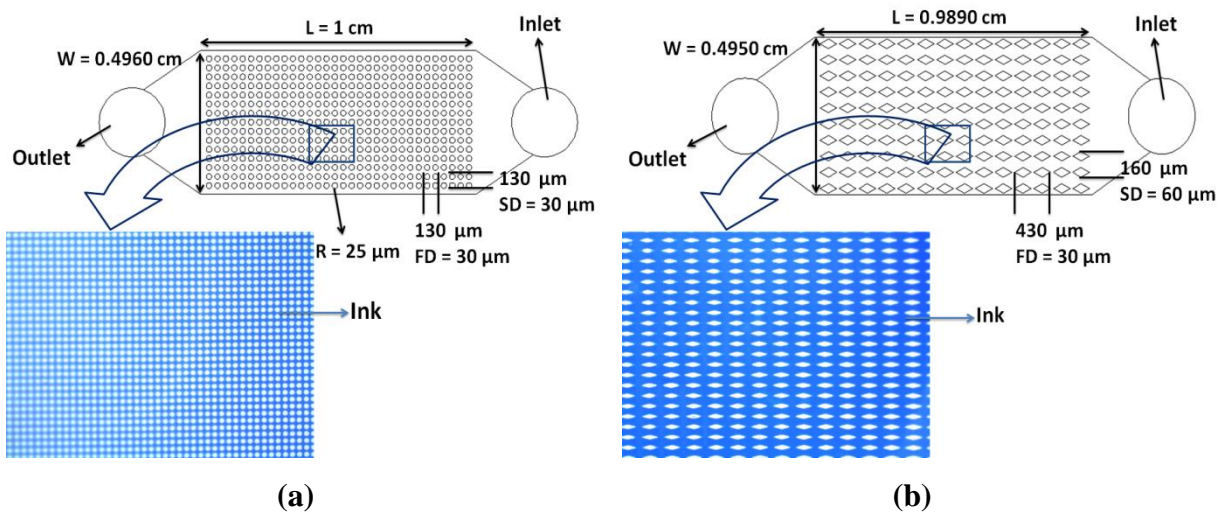| Sample	Resistance flow (Pa.s/m³)	Filling time (s)	Flow rate (μL/min)
Pump1 (Circle)	2.36×10^{14}	12.61 ± 2	1.416
Pump2 (Diamond)	1.83×10^{14}	9.12 ± 2	1.938
Pump3 (Diamond SD)	1.52×10^{14}	7.20 ± 2	2.448

(a)   (b)

Figure 16. The ink filled PDMS MIMP capillary pump with a) Circle b) Diamond SD, pillars arrangement

V. Conclusions

The performance of a micro capillary MIMP pump, which is a key component of many micro-total analysis systems, has been optimized through the analysis of fluid-dynamic behavior of the embedded pillars in the microchannel. A diamond microchannel integrated micropillar (MIMP) pump with high throughput and pumping performance was developed. For this purpose, the pressure drop and flow resistance of a laminar flow through low aspect ratio MIMP with different shapes and geometrical parameters were experimentally, numerically and analytically determined. The numerical model shows good agreement with experimental data for all the fabricated samples. Different PDMS MIMPs were fabricated using modified soft lithography technique to withstand against PDMS deformation. The obtained results indicate that while the maximum flow resistance is achieved in elongated pillar MIMPs, the pine pillar MIMPs present comparable resistance flow to diamond pillar MIMPs being in both cases the minimum value of all considered shapes.

In terms of geometrical parameters, pillar diameter in the flow direction and side distance between two adjacent pillars are the most effective design parameters to control the pressure drop of MIMPs. This analysis can be a useful tool for designing lab-on-a-chip devices in which an appropriate MIMP design is desired to achieve an accurate flow rate for different applications.

References

Akbari M, Sinton D, Bahrami M (2009) Pressure Drop in Rectangular Microchannels as Compared With Theory Based on Arbitrary Cross Section. J. Fluids Eng. 131(4): 041202.

Armani D, Liu C, Aluru N (1998) Re-Configurable fluid circuits by PDMS elastomer micromachining. Proc. 12th Inter. Conf. MEMS. Orland, FL 222-227.

Bazylak A, Berejnov V et al (2008) A microfluidic pore network approach to investigate water transport in fuel cell porous transport layers. Proc. ASME Confere. ICNMM2008 Darmstadt, Germany 62349: 1-6.

Bruus Henrik (2007) Theoretical Microfluidics, Oxford Master Series in Physics : Oxford University Press, New York.

Chan YC, Lee YK and Zohar Y (2007) Pillar size effect on DNA electrophoresis in microchips with sub-micron pillar arrays. Proc. IEEE MEMS Confere. Kobe, Japan.

Choi KM, Rogers JA (2003) A Photocurable Poly(dimethylsiloxane) Chemistry Designed for Soft Lithographic Molding and Printing in the Nanometer Regime. J. AM. CHEM. SOC. 125:4060-4061.

Davis JA, Inglis DW, Morton KJ et al (2006) Deterministic hydrodynamics: Taking blood apart. PNAS. 103(40):14779–14784.

Gervais T, El-Ali J, Gunther A, Jensen KF (2006) Flow-induced deformation of shallow microfluidic channels. Lab Chip. 6:500–507.

Gunda NSK, Bera B, Karadimitriou NK, Mitra SK and Hassanizadeh SM (2011) Reservoir-on-a-Chip (ROC): A new paradigm in reservoir engineering. Lab Chip 11:3785–3792.

Gunda NSK, Joseph J, Tamayol A, Akbari M, Mitra SK (2013) Measurement of pressure drop and flow resistance in microchannels with integrated micropillars. Microfluid. Nanofluid. 14:711–721.

Horiuchi T, Hayashi K, Seyama M et al (2012) Cooperative Suction by Vertical Capillary Array Pump for Controlling Flow Profiles of Microfluidic Sensor Chips. Sensors. 12:14053-14067.

Inc. ANSYS (2009) Fluent 12.0 User's Guide.

Inglis DW (2010) A method for reducing pressure-induced deformation in silicone microfluidics. Biomicrofluidics. 4(2):9700-9709.

Jen CP, Huang CT, Shih HY (2010) Hydrodynamic separation of cells utilizing insulator-based dielectrophoresis. Microsyst. Technol. 16:1097–1104.

Juncker D, Schmid H, Drechsler U et al (2002) Autonomous Microfluidic Capillary System. Anal. Chem. 74: 6139-6144.

Jung J, Kuo C-J, Peles Y, Amitay M (2012) The flow field around a micropillar confined in a microchannel. Int. J. Heat Fluid Flow 36:118–132.

Kirsch AA, Fuchs NA (1967) Studies on Fibrous Aerosol Filters—II. Pressure Drops in Systems of Parallel Cylinders. Ann. Occup. Hyg. 10(1): 23-30.

Kosar A, Mishra C, Peles Y (2005) Laminar Flow Across a Bank of Low Aspect Ratio Micro Pin Fins. J. Fluids Eng. 127: 419-430.

Lynn NS, Dandy DS (2009) Passive microfluidic pumping using coupled capillary/evaporation effects. Lab Chip 9:3422-3429.

Madadi H, Casals-Terre J (2013) Long-term behavior of nonionic surfactant-added PDMS for self-driven microchips. Microsyst. Technol. 19:143-150.

Madadi H, Mohammadi M, Casals-Terré J, López RC (2013) A novel fabrication technique for reduce PDMS deforamtion under high pressure operation in microfluidics chip. Electrrophoresis doi:10.1002/elps.201300340.

Mathur A, Roy SS, Tweedie M (2009) Characterisation of PMMA microfluidic channels and devices fabricated by hot embossing and sealed by direct bonding. Curr. Appl Phys. 9:1199–1202.

Nagrath S, Sequist LV, Maheswaran S et al (2007) Isolation of rare circulating tumour cells in cancer patients by microchip technology. Nature. 450(7173):1235-1239.

Odom TW, Love JC, Wolfe DB, Paul KE, Whitesides GM (2002) Improved Pattern Transfer in Soft Lithography Using Composite Stamps. Langmuir 18:5314-5320.

Powers AD, Liu B, Lee AG and Palecek SP (2012) Macroporous hydrogel micropillars for quantifying Met kinase activity in cancer cell lysates. Analyst. 137: 4052–4061.

Rosenhead Louis (1963) Laminar boundary layers, Dover Pubns, New York.

Roumanie M, Pijolat C, Meille V et al (2006) Deposition of Pt-catalyst in a micro-channel of a silicon reactor:Application to gas micro-TAS working at high temperature. Sens. Actuators, B 118:297–304.

Saha AA, Mitra SK, Tweedie M, Roy S, McLaughlin J (2009) Experimental and numerical investigation of capillary flow in SU8 and PDMS microchannels with integrated pillars. Microfluid Nanofluid. 7:451–465.

Sainiemi L, Nissila T, Jokinen V et al (2008) Fabrication and fluidic characterization of silicon micropillar array electrospray ionization chip. Sens. Actuators, B 132:380–387.

Sen D, Nobes DS, Mitra SK (2012) Optical measurement of pore scale velocity field inside microporous media. Microfluid Nanofluid. 12: 189–200.

Srivastava N, Din C et al (2010) A unified scaling model for flow through a lattice of microfabricated posts. Lab Chip 10:1148–1152.

Tamayol A, Gunda NSK, Akbari M, Mitra SK, Bahrami M (2012) Creeping flow through microchannels with integrated micro-pillars. Proc. ASME Confere. ICNMM2012 Rio Grande, Puerto Rico 731991-731997.

Tamayol A, Khosla A, Gray BL, Bahrami M (2012) Creeping flow through ordered arrays of micro-cylinders embedded in a rectangular minichannel. Inter. J. Heat Mass Transfer 55: 3900–3908.

Tan SH, Nguyen NT, Chua YC, Kang TG (2010) Oxygen plasma treatment for reducing hydrophobicity of a sealed polydimethylsiloxane microchannel. Biomicrofluidics 4(3): 032204.

Vanapalli S, Brake HJMt, Jansen HV et al (2007) Pressure drop of laminar gas flow in a microchannel containing various pillar matrices. J. Micromech. Microeng. 17:1381-1386.

Waghmare PR, Mithra SK, Mather A, McLaughlin J (2008) Modeling, fabrication and simulation of microfilters. Proc. Inter. Conf. Heat Transfer Fluid Flow Microscale (ECI), Whistler, Canada.

Whitesides GM, Ostuni E, Takayama S, Jiang X and Ingber DE (2001) Soft lithography in biology and biochemistry. Annu. Rev. Biomed. Eng. 3: 335-373.

Yamada T, Hong C, Gregory OJ, Faghri M (2011) Experimental investigations of liquid flow in rib-patterned microchannels with different surface wettability. Microfluid Nanofluid. 11:45-55.

Yeom J, Agonafer DD, Han JH and Shannon MA (2009) Low Reynolds number flow across an array of cylindrical microposts in a microchannel and figure-of-merit analysis of micropost-filled microreactors. J. Micromech. Microeng. 19(6):065025.

Zhou J, Ellis AV, Voelcker NH (2010) Recent developments in PDMS surface modification for microfluidic devices. Electrophoresis 31: 2-16.

Zhou J, Khodakov DA, Ellis AV, Voelcker NH (2012) Surface modification for PDMS-based microfluidic devices. Electrophoresis. 33:89-104.

Zimmermann M, Schmid H, Hunziker P, Delamarche E (2007) Capillary pumps for autonomous capillary systems. Lab Chip. 7:119-125.

Paper IV

Self-driven Highly Efficient Blood Plasma Separator with Multiple Reaction Chambers

Hojjat Madadi and Jasmina Casals-Terré [a)]

Technical University of Catalonia, Mechanical Engineering Department, Terrassa, Spain

ABSTRACT

Nowadays, there is a growing need for lab-on-a-chip devices especially in clinical analysis and diagnostics. First step, in most blood tests is plasma extraction from whole blood. This paper presents a novel high throughput blood plasma separation microfluidic chip which with just single drop of blood ($\sim$5µL) can separate (more than 0.1µL) plasma from whole blood without the need of external forces with high efficiency (more than 98%) and reasonable time (3 to 5 minutes). This would be the first step towards the realization of single use, self-blood test which now takes multiple technicians' hours to do. Polydimethylsiloxane (PDMS) is used as base material to manufacture the microchip due to its biocompatibility and outstanding characteristics. PDMS has been modified with a strong nonionic surfactant (Silwet L-77) to achieve a hydrophilic behavior. The main advantage of this design compared to previous ones, besides the amount of extracted plasma (4% of the initial sample), is the fact that the plasma can be collected in one or more 10-µm-depth channels to facilitate the detection and readout of multiple blood assays. This high volume of extracted plasma is achieved thanks to a design that combines the maximum pumping efficiency without disturbing the red blood cells (RBCs) trajectory with different hydrodynamic principles that minimize the tendency of RBCs to enter in the plasma channel, such as constriction effect and symmetrical filtration mode.

[a)] Corresponding Author: Address: Microsystem Laboratory, Department of Mechanical Engineering, Technical University of Catalonia, Terrassa 08222, spain E-mail. Jasmina.casals@upc.edu

I.   INTRODUCTION

Many pathologies and physiological conditions can be diagnosed through the analysis of blood plasma which provides crucial information of various internal organs. In order to fulfill these analysis most researchers, scientist and doctors use centrifugation to separate plasma from whole blood. But this technique requires a laboratory. In order to minimize error, reduce the time from blood collection to the test and provide faster and yet less expensive and comprehensive results, "lab-on-a-chip" type of devices are an attractive tool for blood plasma separation and analysis. Although many researchers have developed plasma separation from whole blood utilizing different techniques in microtechnologies, the volume of extracted plasma to implement the test is still one barrier to achieve a reliable lab on a chip (LOC) blood test.

There are some reviews on the blood plasma separation methods[1,2,3] which can be divided into two main categories: passive and non-inertial. In non-inertial separation methods, the plasma is extracted using different external force fields such as electric field[4], magnetic field[5] and techniques such as cross flow filtration[6], deterministic lateral displacement[7], pinched flow fractionation[8], dielectrophoresis[9,10]or biomimetic separation methods[11]. Normally all these design principles require a pressure-driven source like a syringe pump to work, which it is not always available when thinking in a point of care device. Although many attempts have been done to improve the microfluidic devices for blood plasma separation, there are only few works carried out to design this device without externally applied forces.

In 2005, Crowley and Pizziconi reported a cross-flow plasma separation design from whole blood where flow was driven by capillary forces[12]. The generic microfilter design consisted of an input reservoir, a narrow filtration channel with a transverse flow microfilter, an outlet channel to collect filtered plasma, and a wider expanded channel connected in series to the filtration channel to increase significantly the duration of the capillary operation. The filter consisted in a series of rectangular shaped pores (200 μm wide, 0.5 μm high, and 50 μm long) placed on both sides of the filtration channel. The microfilter device was made out of silicon and glass wafers using photolithography and reactive ion etching. Besides the complexity of fabrication process, they could separate 14 to 45 nL of plasma (which is just 0.5% to 1.8% of the input volume) from 5 μL citrated bovine blood with an average flux between 35 to 175 μm s^{-1}. Later, Chang Kim and his colleagues[13] presented another design which used PDMS with nonioninc surfactant (Silwet L-77) as the base material. The plasma

extraction device was designed to have a main blood channel with a planner cross flow filter to extract plasma from whole blood. Although this microdevice confirmed the feasibility to manufacture a capillary microfluidic device in surfactant-added PDMS, the volume of the extracted plasma was very small in order of 20nL (0.4% of the input volume). Recently, Hiramoaki Sakamoto and their colleagues proposed a PMMA microfluidic device for blood plasma separation that it is driven just by capillary action[14]. The design of the presented device included an array of 2-μm-depth and 2-μm-wide PMMA channels. In this research, the embossed PMMA sample was bonded to another PMMA plate using the surface activation method to create a very firm bonding. They utilized hot embossing and thermal bonding to fabricate the microfluidic device. To improve the wettability of the PMMA, firstly they performed plasma irradiation to obtain polar functional groups containing oxygen onto the surface and then applied a Poly-L-Lysine coating which has active amino groups for promoting cell adhesion. They claimed that the fabricated PMMA microchannels filtered a drop of blood in about 3 min with an efficiency of almost 100% and volumes of about 150 nL of blood plasma were isolated during this time. In spite of the 6% in volume of plasma extraction from 5μL of blood, complexity of the fabrication process, instability of PMMA surface modification process and clogging in the entrance of microchannel array are challenges to be overcome to use this approach. Besides, the depth of the separated plasma channel (~2 μm) cannot be enough to use integrate this design in a bio-sensor chip that reads the results using optical methods.

In this work, a novel high throughput blood plasma separation microfluidic chip is designed and fabricated. Hydrodynamic behavior of red blood cells in the PDMS constriction channel and plasma extraction using a symmetric cross flow filtration MIMP channel are used to maximize the amount of extracted plasma. The presented microdevice has several advantages over the mentioned devices for blood plasma separation. This microdevice is self-driven which means that the capillary forces are sufficient to separate more than 0.1μL of blood plasma from 5μL drop of the real fresh blood. The microdevice is fabricated using PDMS and glass two common materials in the microfabrication processes. The combination of in plane blood transport and out of plane plasma filtration based on various hydrodynamic principles help to postpone the entrance clogging in the separation area and accordingly to increase the separation efficiency (more than 98%) and plasma extraction (more than 0.1μL).

This paper is organized as follows: design and principles of the self-driven microfluidic device, the theory of the capillary driven device and the fabrication procedure is described in

Section II; the proposed blood plasma separation microfluidic device is experimentally tested and validated in section III and finally the conclusions are presented in section IV.

II. EXPERIMENTAL

A. DESIGN AND PRINCIPLE OF THE SELF DRIVEN MICROFLUIDC DEVICE

For the design of a high throuput self-driven blood plasma separation microfluidic device several aspects such as separation science, fluid dynamics and blood rheology should be addressed.
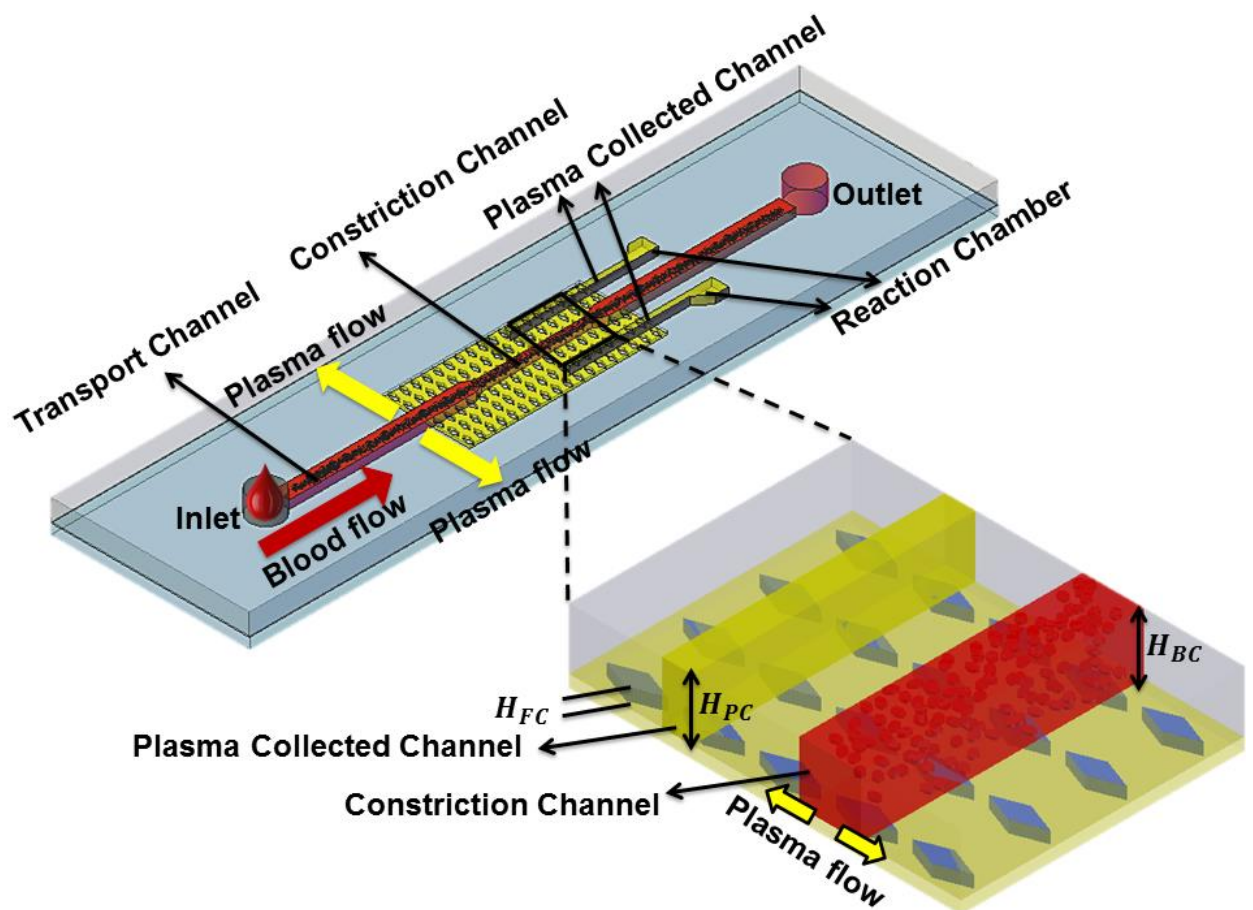

Figure 1. Schematic diagram of the blood plasma separation microdevice

Figure 1 shows a schematic view of the microfluidic device, which is manufactured in two parts. The top part comprises a main channel (height, 10μm) (called transport channel for delivering the blood drop sample), which includes one constriction at a branch point where the flow is divided between the high RBCs concentration blood that flows through the transport channel and the plasma flow, flows through the down part. This extracted blood plasma through the MIMP filtration channel is collected to one or more channels (height, 10μm) located (500 microns apart from the transport channel) in the top part allowing multiple blood assays.

The red blood cell clogging is an inevitable and major issue in filtration, which can be modulated by increasing the shear rate on the trapped cells that can sweep them away from the entrance of the filtration channel.
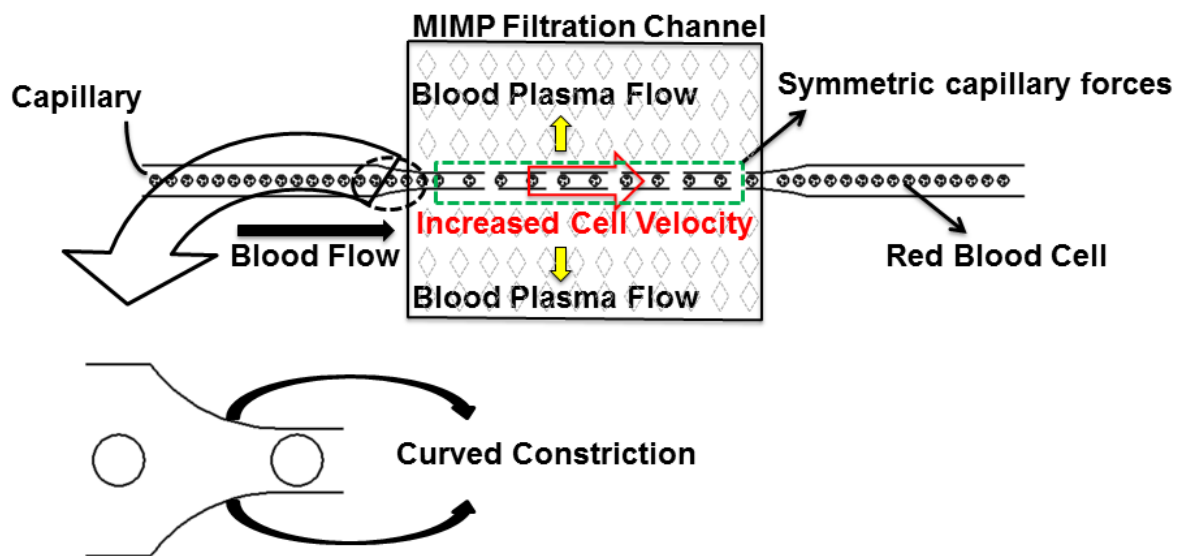

Figure 2. Detail of the transport channel constriction where RBCs increased velocity helps to reduce the accumulation in the filtration area entrance.

For this purpose a constriction has been designed in the middle of the transport channel reduces RBCS accumulation in the entrance of the separation area and therefore delays the clogging of the separation area entrance, see Figure 2. Moreover, the constriction in the entrance and exit of the transportation channel uses a smooth design to reduce the cell

damage risk. Specifically in case of RBCS, hemolysis could appear if a sudden stress is applied.

Additionally regardless the red blood cells interaction, the extraction of blood plasma from whole blood in the transport channel is done through a symmetric filtration channel which ends up counteracting the cross capillary forces in opposite direction, resulting in an indivertible red blood cell movement and consequently a clogging reduction in the separation channel entrance, see the yellow arrows indicating the capillary force direction in Figure 2.

Due to the delayed accumulation of RBCs in the filtration area entrance, two different transport channel designs are implemented, see Figure 3. In design A the blood flow in the transport channel is perpendicular to the blood plasma flow while in design B both flows are parallel. Design B tries to maximize the first instance filling rate, before the entrance clogging takes place.
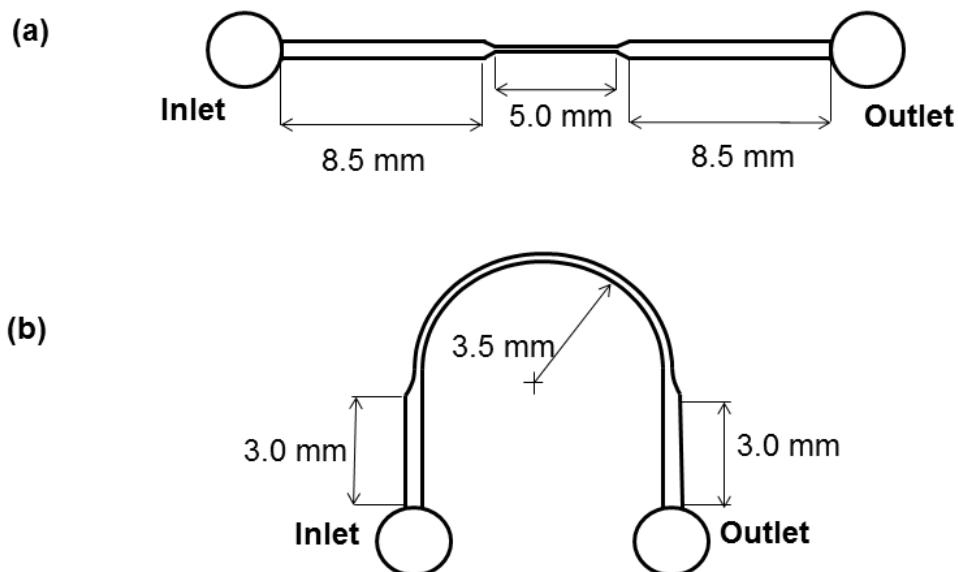

Figure 3. . Layouts of the two proposed transport microchannel designs: a) Straight transport channel in which the plasma flow and primary main channel flow directions are perpendicular b) Curved transport channel which the plasma flow and primary main channel flow directions are parallel

The microdevice down part (called MIMP filtration channel) includes an arrangement of diamond microposts (to decrease the flow resistance as well as increase the capillary force) which not only filtratie but also pave the path for collecting the separated plasma in the top part using multiple collected channels, since there is a distributed area filled with plasma.

6

Because of the deformability of human red blood cells, the down part depth of the device H_{FC}, is designed to be less than 2 μm to successfully filter the red blood cells (1.5 μm). The two top and down parts of the microdevice are manufactured separately and then joined to extract the blood plasma from the whole blood.

The fluidic behavior of the whole device can be analyzed using an equivalent electrical network (Figure 4):
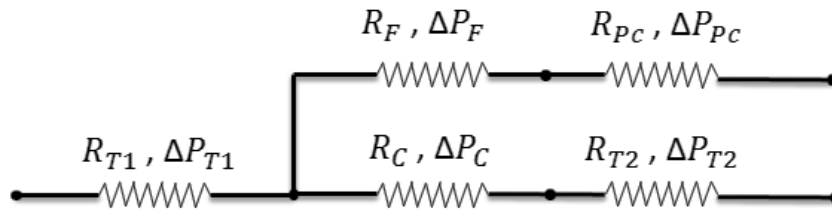

Figure 4. The equivalent electrical network of the microdevice

Where R_{T1} and ΔP_{T1} are the flow resistance and pressure drop of the first part of the transported channel (before constriction channel), R_C and ΔP_C are the flow resistance and pressure drop of the constriction channel, R_{T2} and ΔP_{T2} are the flow resistance and pressure drop of the second part of the transported channel (After constriction channel), R_F and ΔP_F are the flow resistance and pressure drop of the MIMP filtration channel and R_{PC} and ΔP_{PC} are the flow resistance and pressure drop of the plasma collected channel respectively.

Once the hydrophilicity of the material is fixed (surface tension), the capillary pressure ΔP for each of the rectangular microchannels can be calculated using the Young-Laplace equation:

$$\Delta P_i = \sigma \cos\theta \left(\frac{1}{h} + \frac{1}{w} \right)$$

(1)

where σ is the surface tension, θ is the contact angle, h is the half height and w is the half width of the microchannel respectively.

Therefore, since the flow rate Q of a liquid in a capillary microchannel depends on the viscosity of the liquid, the capillary pressure and the microchannel flow resistance:

$$Q = \frac{1}{\mu} \frac{\Delta P}{R}$$

(2)

where ΔP is the pressure difference between inside and in front of the liquid (eq. 1), μ is the viscosity of the liquid and R is the microchannel flow resistance.

The minimization of the MIMP channel flow resistance R_F will increase the plasma flow rate in the MIMP filtration channel. According to Madadi et al. [15] the diamond post shape with increased side distance between pillars is the most efficient design for minimizing the MIMP channel flow resistance and it can be calculated through:

$$R_F = \frac{12\mu L}{wH^3} \left(\frac{1}{2\epsilon - 1} \right)$$

(3)

where μ is the fluid viscosity, L is the length of microchannel, w is the half depth of microchannel, H is the height of microchannel and ϵ is the porosity. Since the fluid and the height of the channel are fixed, we have maximized the porosity to achieve a manufacturable device. Figure 5 shows the dimensions of the selected MIMP filtration channel.
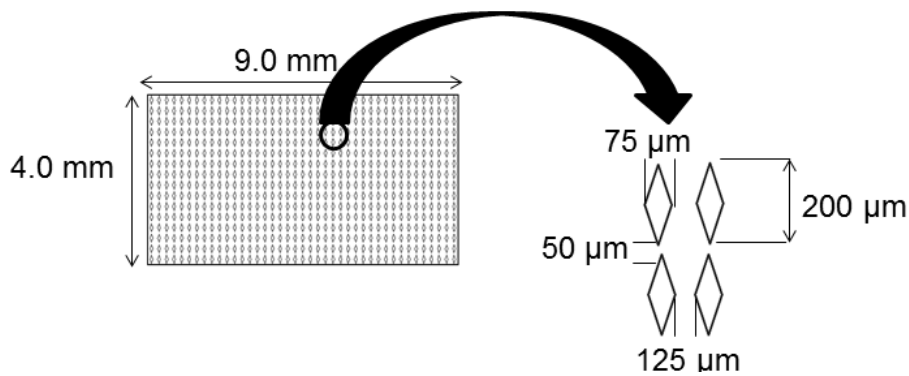

Figure 5. Diamond shaped post array in the filtration area

B. FABRICATION PROCEDURE

As mentioned before the microfluidic device is manufactured in two main parts: The top part and the bottom part, which are fabricated using different manufacturing processes.

a) Top part manufacturing process

Polydimethylsiloxane (PDMS) a common material in microfluidics chips was utilized for manufacturing the microdevice top part. In spite of all favorable physical and chemical properties, the hydrophobic surface of PDMS is a handicap when pumping aqueous solutions through microchannels using only capillary forces. There are several techniques to achieve a hydrophilic behavior of PDMS[16,17], but the use of surfactants added to PDMS provides a novel method to overcome hydrophobicity and to control the hydrophobic recovery over a long period of time[18]. Despite the different types of surfactants available, Silwet L-77 was chosen to be added to PDMS in terms of efficiency, clearance and duration of the hydrophilic behavior[19]. Prior to the use of PDMS a mold was created.

SU-8, a negative tone photo-epoxy was employed to create a master mold. SU-8 (GM 1060, Gersteltec Sarl., Switzerland) was chosen since it can be used in thin films between 6 to 50 micrometers. The prepared designed mask was printed in high-resolution film. Microscopy glass slides 75×25 mm were utilized as substrates which were firstly cleaned by Piranha cleaning process (3:1 of $H_2SO_4 : H_2O_2$) and preheated on the hotplate at 200°C for 30 minutes to ensure that the glass slide dried completely. After cooling the substrate, a 10-µm layer of the photoresist (SU-8) was spin coated at 2555 RPM during 40 s on the top of glass slide. After 5 minutes relaxation time, the coated substrate was soft-baked in two steps: 5 minutes at 65 °C and 30 minutes at 95 °C and cooled down to the room temperature. The structures were patterned through the high-resolution printed photo mask by using 6 s UV exposure lamp. The coated substrate was post-exposure baked in two steps: 5 minute at 65 °C and 20 minutes at 95 °C which leads to achieve fully cross-linking. After 10 minutes delay time, the structure was cleared through the development process in PGMEA (Propylene glycol methyl ether acetate) for 1 minute and 30 s and used as mold.

To make PDMS microchannel, Dow Corning Sylgard 184 silicone elastomer and curing agent was thoroughly mixed 10:1 in weight. Then, the intended concentration of the surfactant (1% of Silwet L-77) was added to the PDMS mixture. For getting uniform distribution of the surfactant, the mixture was blended and then degassed in a vacuum chamber for 1 h to get rid of trapped air bubbles in the sample. In order to ensure the easy peel-off of the channels once cured, the mold was silanized. After, the mixture was poured on the SU-8 master mold and finally, it was cured. The curing process of surfactant-added PDMS is depended to the type of surfactant and its concentration. There is not any reliable

data for curing time of the applied surfactants (Silwet L-77). DSC (differential scanning calorimetry) technique was utilized to discover the appropriate curing time of the modified PDMS. DSC is one the most common technique for measuring the thermal events such as physical transition (melting or crystallization point) and chemical reactions. Conventional DSC employs linear temperature program what means that heat or cool the sample at linear rate (dynamic scan) or holds the sample in constant temperature (isothermal scan).
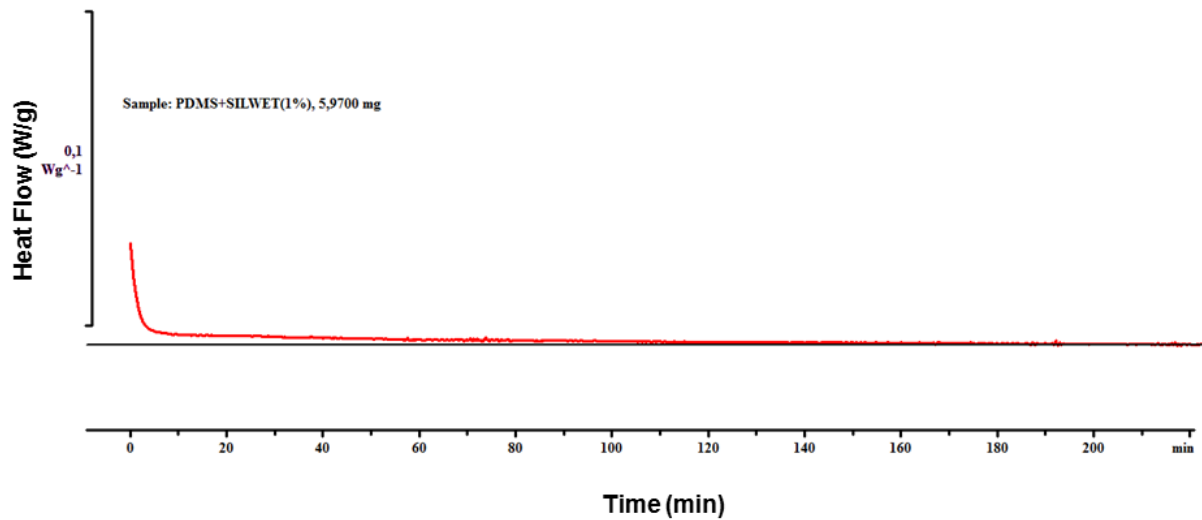

Figure 6. The isothermal scan of the DSC (differential scanning calorimetry)

The Figure 6 displays that the curing reaction of Modified PDMS with 1% of Silwet L-77 is completed after 3hours (180min). Therefore 150ºC were chosen as curing temperature for 3 hours. In the last step, the microchannel inlet and outlet were punched.

b) **Down part manufacturing process**

The MIMP filtration channel was fabricated on a glass substrate using both photolithography and wet chemical methods. Fig.7 illustrates the fabrication steps of the MIMP filtration channel. S1818 is a positive photoresist which can be employed as the etching mask in the wet chemical methods. In fact, in the fabrication process the intended structures were patterned through the high resolution printed photo mask which did not have enough resolution to make straight lines in diamond sides. Therefore, some indentations are shown in the diamond sides, which are inevitable in the photolithography process.

Figure 7. MIMP filtration channel manufacturing steps.
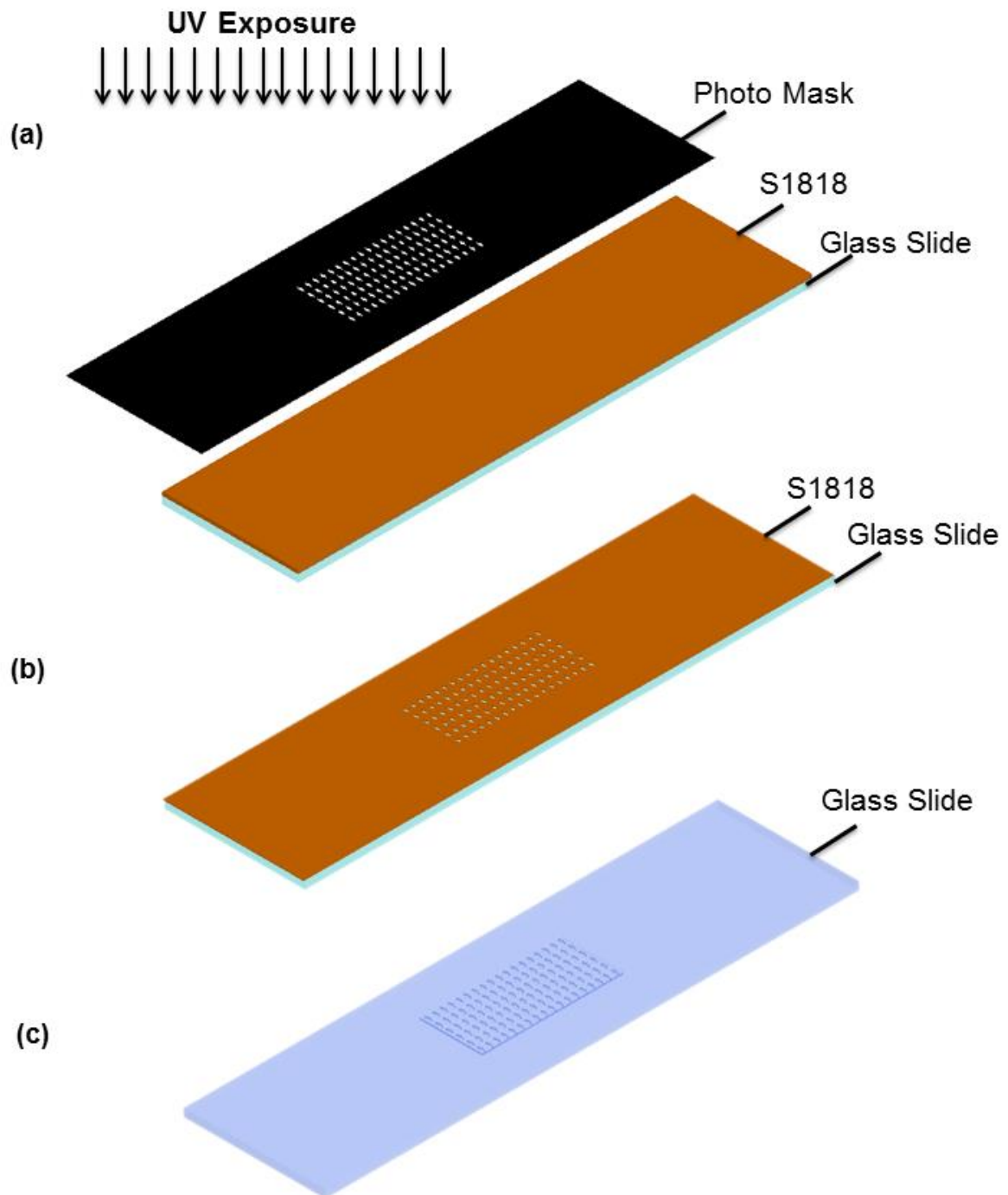
Microscopy glass slides 75×25 mm were firstly cleaned by Piranha cleaning process (3:1 of $H_2SO_4 : H_2O_2$) and preheated on the hotplate at 200°C for 30 minutes to ensure that the glass slide dried completely. After cooling the substrate, S1818 (G2, Dow, Denmark) was spin coated at 2000 RPM during 30 s on the top of glass slide and soft baked at 120 °C for 1 minute.

The MIMP structure was patterned through the high-resolution printed photo mask by using 5 s UV exposure lamp (Fig.7 Step a).
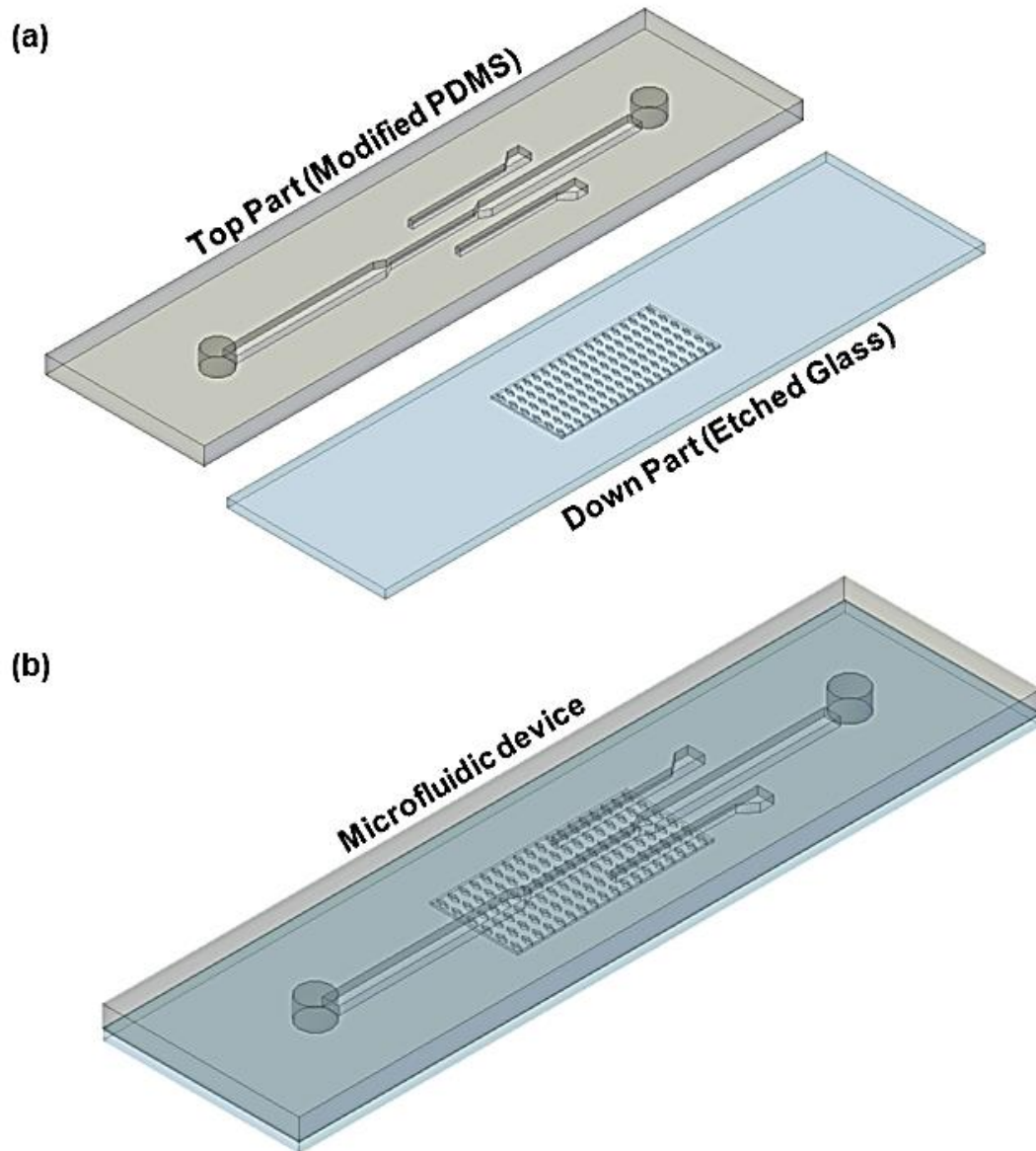

Figure 8. The microdevice top and down parts a) before and b) after plasma bonding

Then the MIMP structure was cleared through the development process in MF-24A (Microposit MF-24, Dow, Denmark) for 52 s and used as a mask for etching process (Fig.7 Step b). The top and down parts of the final microfluidic device after fabrication process are shown in Fig.8.

In etching process, the glass substrate was immersed in a buffer oxide etchant (BOE 6:1) at room temperature. Figure 9 shows measurements of the fabricated MIMP channel before (a) and after (b) etching process using scanning confocal microscope (Sensofar Plu neox, Sensofar -Tech, Terrassa, Spain).
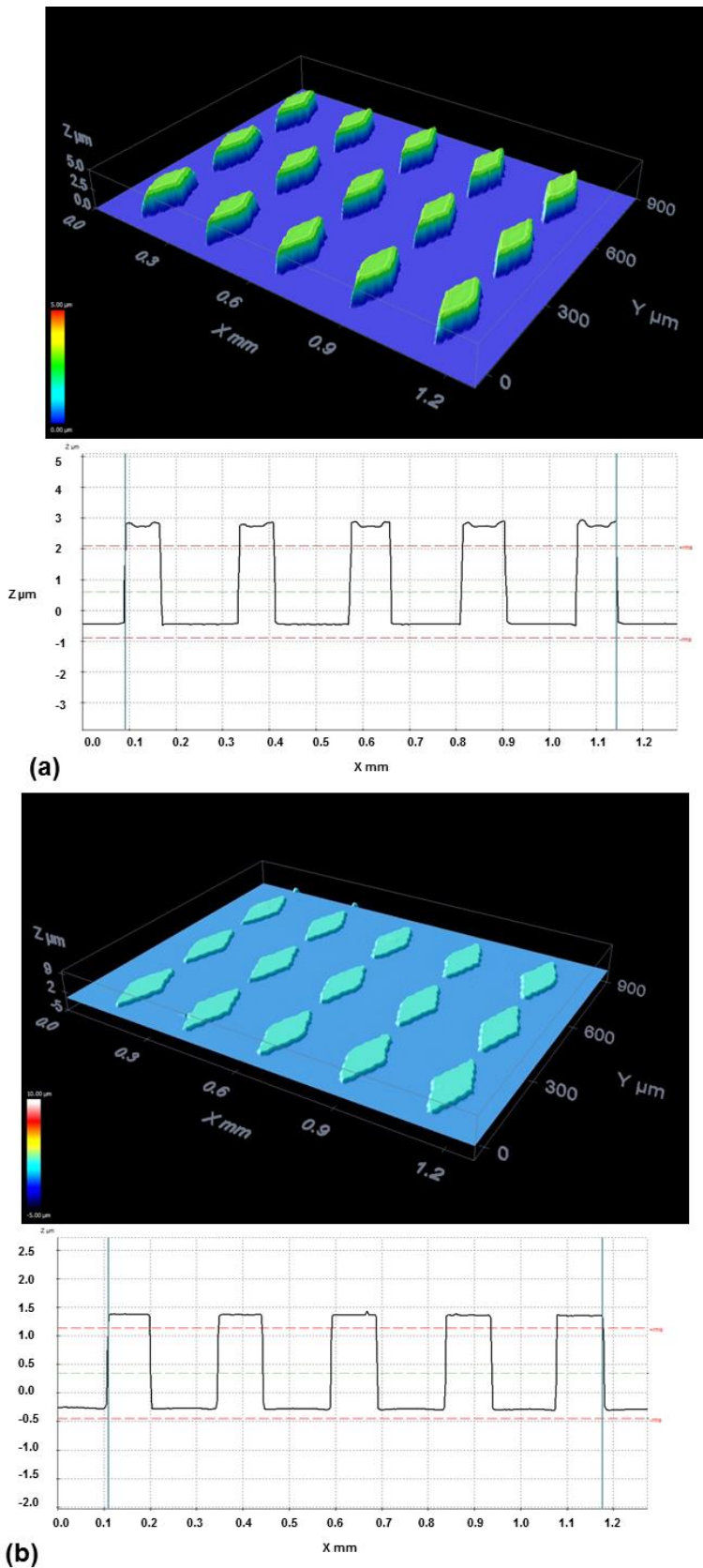
Figure 9. MIMP filtration channel dimension a) before b) after etching process

The MIMP channel depth of etching mask (after photolithographyranges between 3.16 to 3.18 µm to achieve a depth of the etched glass MIMP channel of 1.5 µm. Since the depth of

the MIMP channel is a key parameter in RBCs filtration and the microdevice efficiency, the relationship between etching time and depth was analyzed. Figure 10 summarizes the linear relationship between the filtration MIMP channel depth and etching time, showing an average etching rate of 0.6 µm/min.
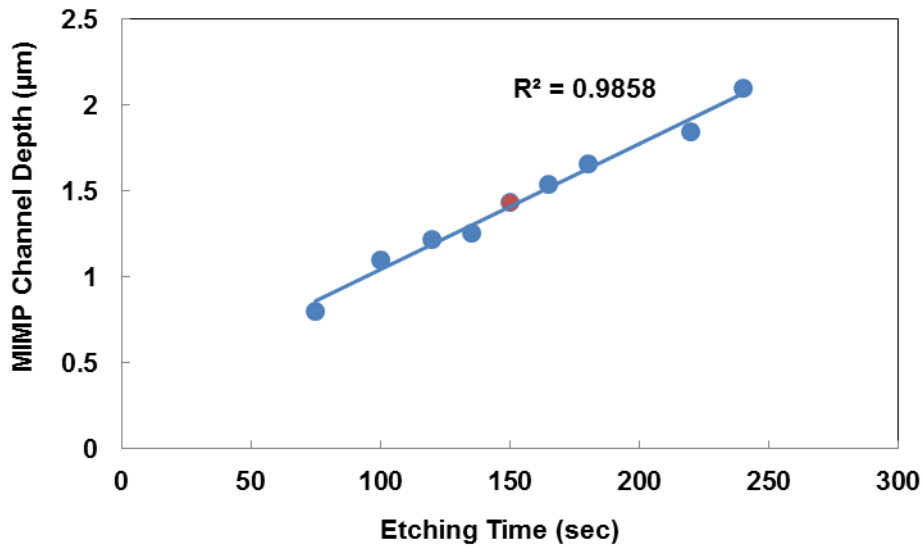
Figure 10. Depth of the filtration MIMP channel versus etching time

Following, the remaining photoresist from the etched glass were removed using an Acetone solution and in the last step the etched glass rinsed with DI water for some minutes.

c) Microdevice assembly

The main PDMS microchannel (Top Part) and the etched glass MIMP filtration channel (Bottom part) were bonded via an oxygen plasma treatment. Oxygen at 200 Torr was introduced in the oxygen plasma chamber (Gambetti) and the plasma was run for 30 seconds. The oxygen plasma parameters were chosen to achieve the maximum bond strength[20].Fig.11 shows photograph of the completed blood plasma separation microfluidic device.

Figure 11. Photograph of a) PDMS part (up part), b) glass part (down part) and c) final microdevice
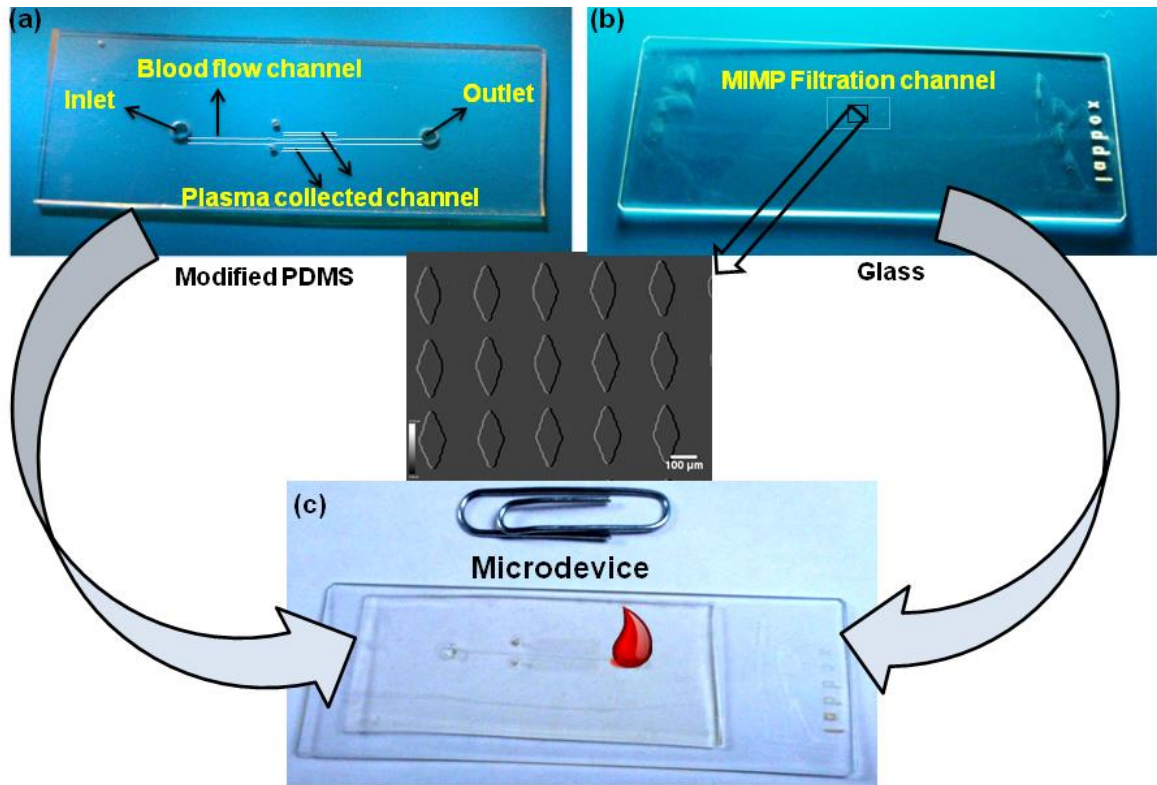
III. RESULTS AND DISCUSSION

Fresh blood collected from a healthy adult was used in the experiments. In order to record images and movies of the blood plasma separation process and analyze the results, a digital camera (Tucsen ISH500, 5.0 M pixel,) was connected to a microinspection lens system Optem zoom 125C (with a broad 12.5:1 zoom range) and a 20X objective.

In order to study the effect of PDMS main channel geometry on the blood plasma separation two different channel geometries were considered: A) Straight Transport Channel, B) Curved Transport Chanel.

A 5-µL drop of fresh whole blood was introduced into the inlet port of the transport channel. The blood sample was drawn into the microdevice only by capillary forces due to the hydrophilicity of modified PDMS with surfactant (Silwet L-77). Fig 12 illustrates the filtration performance for the separation plasma from whole blood in a Curved Transport Channel.
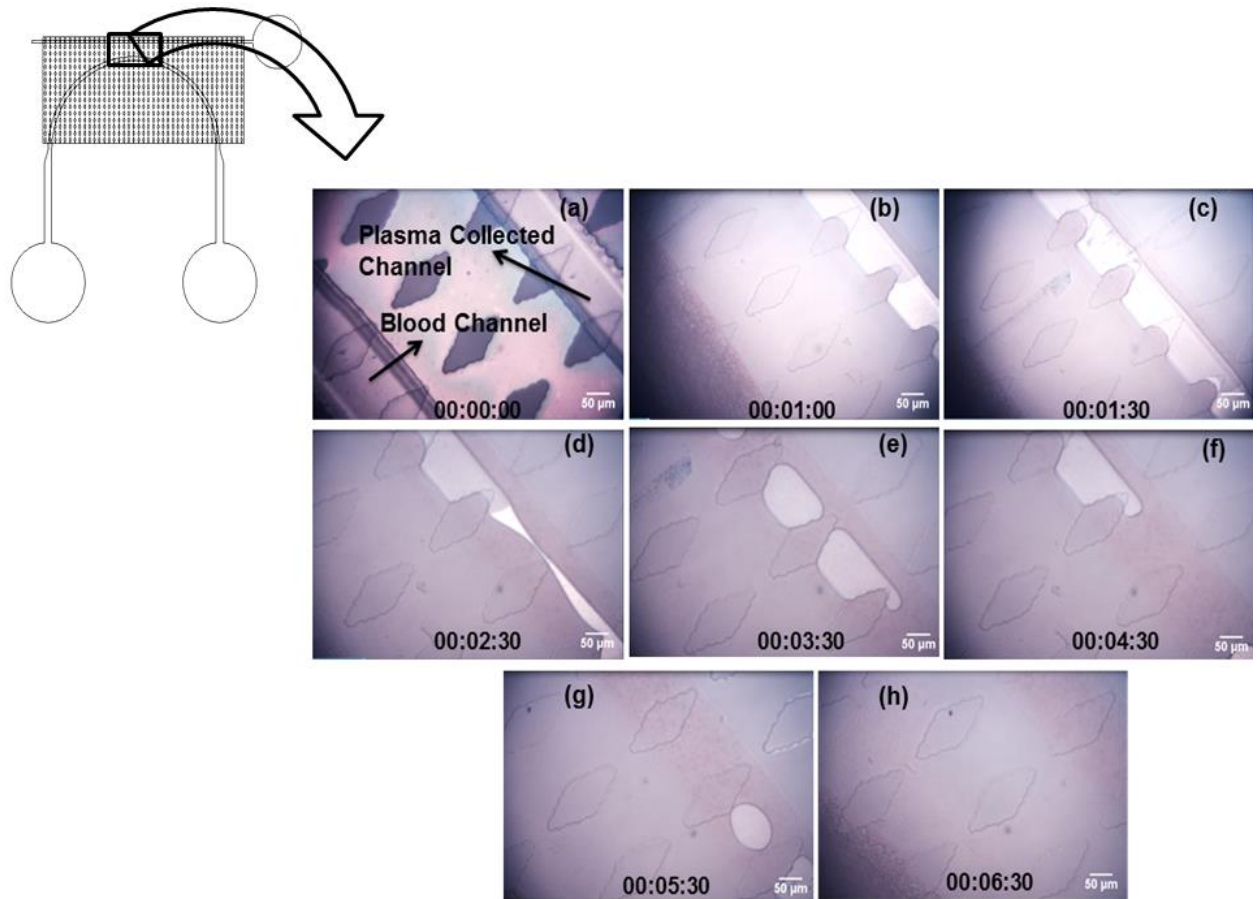
Figure 12. Blood plasma separation process using the curved main channel geometry

When the separation process starts, since the MIMP filtration channel depth is less than 1.5 μm, RBCs do not penetrate into the plasma channel but the flow velocity of the blood in the transport channel is slowed down which leads to the accumulation of cells in the entrance of separation area. In the curved transport channel design even though the constriction in the transport channel generates a local flow acceleration, the centrifugal force due to the curvature and the nonsymmetrical arrangement of the separation zone results in precocious RBCs entrance clogging of the separation zone. When using curved transport channel, 0.07μL of blood plasma were extracted from 5μL fresh blood drop (extracting 2.8% of blood plasma from the input volume). The separation MIMP channel was filled in the first minute, see Figure 12 b (since the plasma flow direction is parallel to the blood plasma flow in transport channel). But the collected channel was filled after 5 to 7 minutes, see Figure 12 g and h. Figures 12b and 12c show that the collected channel was filled firstly by the top surface of the pillars in collected channel due to the higher capillary force compared to the other zones. Figure 13 shows the collected channel once filled compared to the transport channel.
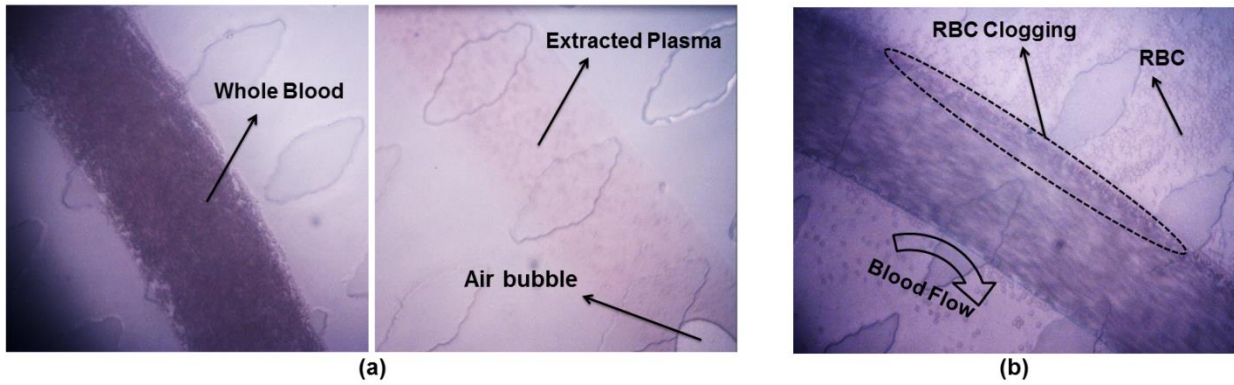
Figure 13.a)A comparsion between RBCs concentration in the main blood channel and the plasma collected channel b)The effect of the curved geometry and resulting centrifugal force on the RBCs

The separation efficiency was defined as:

$$\eta = \frac{C_M - C_P}{C_M} \times 100$$

(4)

Where, C_M is the number of RBC in the main channel and C_P is the number of RBC in the collected channel. Analyzing Figure 13 the separation efficiency of the blood plasma from whole blood in the curved transport channel topology is around 80 to 85%, using image processing. Although the curved transport channel fills the separation MIMP channel quickly (less than 1 minute), the centrifugal force on the RBCs attributed to this geometry and the nonsymmetrical capillary forces generate accumulation of RBCs in the entrance of MIMP filtration channel and secondly drive them into the MIMP channel and thereby in the collected channel (See Fig 13b).

A video clip of the performance of the blood plasma separation microdevice using curved channel is shown in the supplementary material.

In order to increase the separation efficiency and avoid the effect of the centrifugal force owing to the curvature, the straight transport channel was tested, see Figure 14. The mechanism of separation is similar to the curved transport channel which is explained earlier. The only difference in this design is related to the direction of the blood flow which is perpendicular to the plasma extracted channel flow and the capillary forces that are applied on both sides of the RBCs flowing in the transport channel, resulting in an unappreciable applied force. Fig. 14 shows
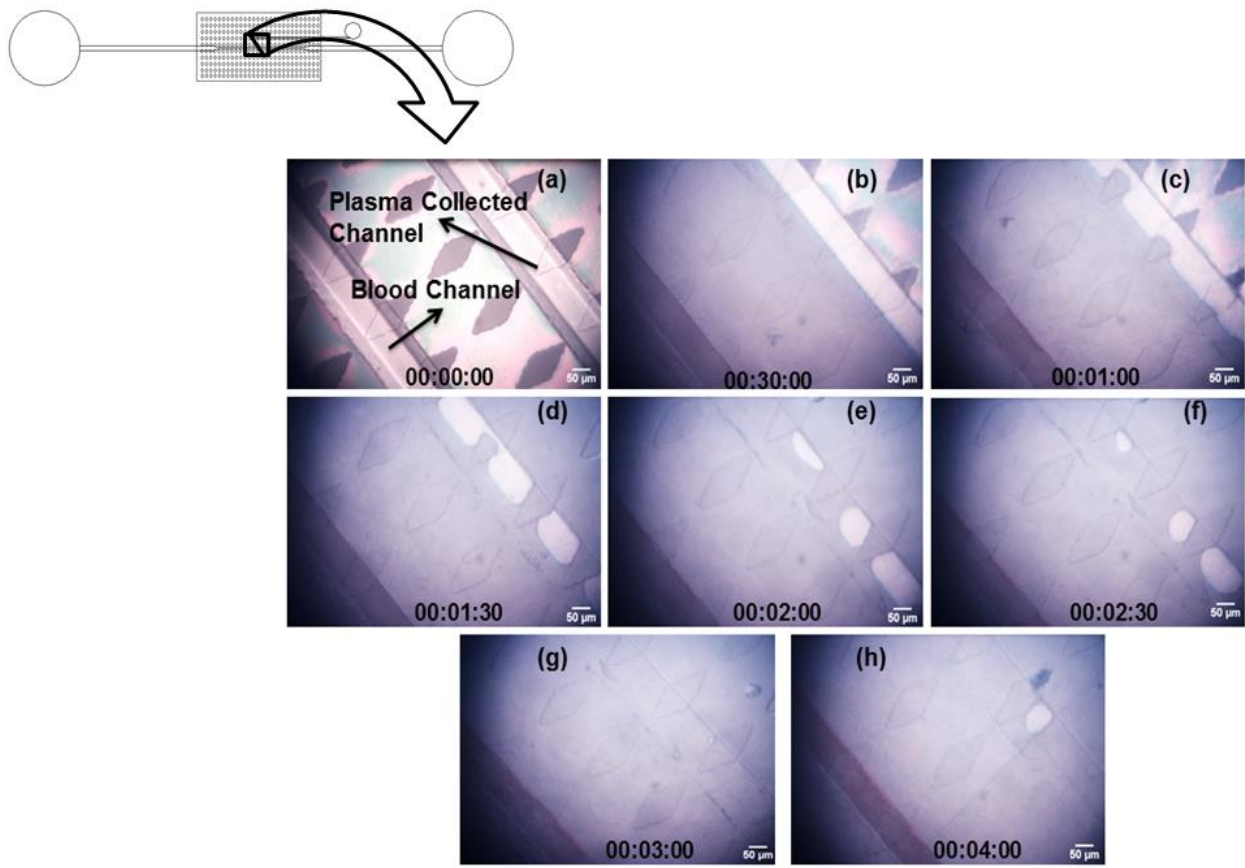
Figure 14.Blood plasma separation process using the straight main channel geometry

micrographs of the microdevice performance. Because of the clogging delay due to the elimination of curvature centrifugal force, 0.09 µL of blood plasma was successfully separated from 5 µL of whole fresh blood (extracting 3.6% of blood plasma from the input volume). According to the results the plasma collected channel was filled in 3 to 5 minutes with a separation efficiency of more than 98%. Therefore validating that perpendicular plasma flow decreases the time needed to fill the collected channel[21].A video clip of the performance of the blood plasma separation microdevice using straight channel is shown in the supplementary material

For further investigation about the capability of the presented microdevice to perform simultaneously different assays on the same blood sample, another collected channel was added at the other side of the main blood flow (1 mm apart). Besides the filling of this second plasma collected channel, which opens the possibility to perform multifunctional blood analysis, the volume of extracted plasma was increased up to 0.1 µL (4% of the input volume) from 5 µL drop of whole fresh blood with the same separation efficiency (more than 98%). Since the presented blood plasma separation device is driven just by capillary forces,

no hemolysis has been observed. The result of this experiment is shown as a video clip in the supplementary material.

IV.   CONCLUSION

This research work presents the development of a novel high throughput blood plasma separation microfluidic chip which with just single drop of blood (~ 5μL) can separate plasma from whole blood without the need of external forces with high efficiency (more than 90%) and reasonable time (3 to 5 minutes). The high strong capillary force is achieved due to the hydrophilicity of modified PDMS with nonionic surfactant Silwet L-77. Experiments were carried out for both curved and straight main channel; it was found that in the curved channel the plasma flowed quickly in the plasma extracted MIMP channel in the first minute while the centrifugal force due to the curvature geometry make a precocious RBC clogging and reduction the plasma purity in the collected channel. In the other hand using the straight channel, 0.1 µL of blood plasma was successfully separated and collected in 10-µm-depth channels from 5 µL of whole fresh blood between 3 to 5 minutes with separation efficiency more than 98%. The long term hydrophilicity of the employed material and the achieved plasma volume (0.1 µL) in 10 µm-depth collected channels of the presented self-driven microdevice paves the path to integrate with portable medical point-of-care-testing (POCT) for doing different blood analysis.

V.   REFERENCES

[1]E. Sollier, H. Rostaing, P. Pouteau, Y. Fouillet, J. Achard, Sens. Actuators B 141, 617-624(2009).
[2]N. Pamme, Lab Chip 7, 1644–1659(2007).
[3]S. Mukherjee, T. G. Kang, Y. Chen, S. Kim, Crit. Rev. Biomed. Eng. 37(6), 517-529(2009).
[4]J. G. Kralj, M. T. Lis, M. A. Schmidt, K. F. Jensen, Anal Chem. 78, 5019-5025(2006).
[5]E. Furlani, J. Phys. D: Appl. Phys. 40(5), 1313(2007).
[6]A. Aota, S. Takashi, K. Mawatari, Y. Tanaka, Y. Sugii, T. Kitamori, Anal Sci. 27(12), 1173-1178(2011).
[7]L. R. Huang, E. C. Cox, R. H. Austin, J. C. Sturm, Science 304(5673), 987-990(2004).

[8]A. I. Rodriguez-Villarreal, M. Arundell, M. Carmona, J. Samitier, Lab Chip 10(2), 211-219(2010).

[9]S. Chang, Y. H. Cho, Lab Chip 8(11), 1930-1936(2008).

[10]S. H. Liao, C. Y. Chang, H. C. Chang, Biomicrofluidics 7(2), 024110(2013).

[11]S. Yang, A. Undar, J. D. Zahn, Lab Chip 6(7), 871–880(2006).

[12]T. A. Crowley, V. Pizziconi, Lab Chip 5(9), 922–929(2005).

[13]Y. C. Kim, S. H. Kim, D. Kim, S. J. Park, J. K. Park, Sens. Actuators B 145, 861-868(2010).

[14]H. Sakamoto, R. Hatsuda, K. Miyamura, S. Sugiyama, Micro & Nano Letters 7(1), 64-67(2012).

[15]H. Madadi, J. Casals-Terre, R. C. Lopez, M. S. Anfrez, High throughput microcapillary pump with efficient integrated low aspect ratio micropillars, Microfluid Nanofluidics, In press (2013).

[16]J. Zhou, A. V. Ellis, N. H. Voelcker, Electrophoresis 31(1), 2–16(2010).

[17]J. Zhou, D. A. Khodakov, A. V. Ellis, N. H. Voelcker, Electrophoresis 33(1), 89–104(2012).

[18]H. Madadi, J. Casals-Terre, Microsyst. Technol. 19(1), 143–150(2013).

[19]H. T. Kim, J. K. Kim, O. C. Jeong, Jpn. J. Appl. Phys. 50, 06GL04(2011).

[20]S. Bhattacharya, A. Datta, J. M. Berg, S. Gangopadhyay, J. Microelectromech. Syst. 14(3), 590-597(2005).

[21]D. Kim, J. Y. Yun, S. J. Park, S. S. Lee, Microsyst. Technol. 15(2), 227–233(2009).

Patent

Justificante de presentación electrónica de solicitud de patente

Este documento es un justificante de que se ha recibido una solicitud española de patente por vía electrónica, utilizando la conexión segura de la O.E.P.M. Asimismo, se le ha asignado de forma automática un número de solicitud y una fecha de recepción, conforme al artículo 14.3 del Reglamento para la ejecución de la Ley 11/1986, de 20 de marzo, de Patentes. La fecha de presentación de la solicitud de acuerdo con el art. 22 de la Ley de Patentes, le será comunicada posteriormente.

Número de solicitud:	P201331666
Fecha de recepción:	15 noviembre 2013, 12:59 (CET)
Oficina receptora:	OEPM Madrid
Su referencia:	SepLiquid
Solicitante:	UNIVERSITAT POLITÈCNICA DE CATALUNYA
Número de solicitantes:	1
País:	ES
Título:	DISPOSITIVO MICROFLUÍDICO PARA LA SEPARACIÓN DE LÍQUIDO DEL MISMO LÍQUIDO CONTENIENDO PARTICULAS DEFORMABLES SIN FUENTES DE ENERGÍA EXTERNAS
Documentos enviados:	Descripcion.pdf (11 p.) Reivindicaciones.pdf (2 p.) Resumen.pdf (1 p.) Dibujos.pdf (7 p.) OLF-ARCHIVE.zip package-data.xml es-request.xml application-body.xml es-fee-sheet.xml feesheet.pdf request.pdf
Enviados por:	CN=CPISR-1 C JAVIER GIL MUR,serialNumber=43394027L,T=-Vicerector de Política Científica,givenName=JAVIER,SN=GIL MUR,OU=Vegeu https://www.catcert.cat/verCPISR-1CarrecUR (c)03,OU=Serveis Públics de Certificació CPISR-1 amb càrrec,OU=Ciencia dels Materials i Eng. Metal.lúrgica,O=Universitat Politècnica de Catalunya,C=ES
Fecha y hora de recepción:	15 noviembre 2013, 12:59 (CET)
Codificación del envío:	CD:5F:5E:61:66:2F:AE:31:58:09:A9:FF:81:65:66:5F:2D:5E:38:AB

A SELF DRIVEN MICROFLUIDIC DEVICE FOR SEPERATING LIQUID FROM A LIQUID INCLUDING DEFORMABLE PARTICLES

Hojjat Madadi, Jasmina Casals Terré

Technical University of Catalonia, Mechanical Engineering Department, Terrassa, Spain

Address: Microsystem Laboratory, Department of Mechanical Engineering, Technical University of Catalonia, Terrassa 08222, spain. E-mail. Jasmina.casals@upc.edu

ABSTRACT

A self-driven microfluidic device that separates liquid from a particle-containing fluid is introduced. The microfluidic device comprises at least one transport channel (1) which utilizes various fluid hydrodynamic principles to increase the device throughput; at least one separating area (2) which, adjoined at the bottom of the transport channels, diverts a part of the liquid that flows through the transport channel to at least one collected channel (3) or reaction chamber. The separating area (2) can include at least one arrangement of different post shapes to amplify the throughput during the same time. The collected channel (3) has a depth and a width adaptable depending on the test needs. Specifically, the invention provides a high throughput filter that can separate plasma from whole blood which is utilized for blood analysis in lab-on-a-chip systems.

FIELD OF THE INVENTION

The present innovation relates to a microfluidic device for separating particles from a liquid in which the particles are suspended, and more specifically, for the separation of plasma from whole blood for blood analysis on a self-driven microchip.

BACKGROUND ART

Nowadays, considerable progress has been made in the field of microfluidics especially for chemical, biological and biomedical applications. Actually, Point-of-care products show the greatest potential for this technology. The majority of attempts done by researchers in these years are focused to develop a point-of-care microchip for blood plasma separation, although there are many challenges such as obtaining high efficiency without clogging or hemolysis (the rupture or destruction of red blood cells) in this approach. The use of microfluidics not only increases convenience, but also expedites results of the test. Traditional blood samples sit for hours or even days before the measurement process are completed, allowing plenty of time for them to degrade. The new diagnostics should also be more accurate, since the blood will be fresh and since the test is done after the extraction the manipulation errors are minimized and the results are obtained faster.

Blood is used in many clinical trials to detect a broad range of illnesses. But previously the different elements of blood need to be separated from plasma (serum and fibrin): erythrocytes (red blood cells-RBC), leukocytes (white blood cells-WBC) and thrombocytes (platelets). Normal blood constituents are 45% RBC, 1% WBC, 0.5% platelets and the rest is plasma. RBC is disk-shaped with a diameter of 8 microns and a height of 2 microns and it is easily deformable. WBCs have a diameter between 8 and 12 μm and they are responsible to avoid infections and diseases. The other main blood components are platelets which aggregate to form clots. All these particles are suspended in the plasma, which is 90% water and is yellow colored. Besides water, plasma also contains small particles (between 1 and 3 microns in diameter) that are mainly, serum albumin, clotting factors, hormones, carbon dioxide, proteins, electrolytes and immunoglobin.

Currently the separation of plasma from blood requires a complex laboratory centrifuge and a relatively large volume of blood or sedimentation but this procedure is very time consuming.

In order to minimize errors, reduce the time from blood collection and provide faster and yet less expensive and comprehensive results, "lab-on-a-chip" type of devices are attractive for blood plasma separation and analysis. Many researchers have been developed plasma separation from whole blood by utilizing different technique in microtechnologies. Plasma has been extracted by various methods such as cross flow filtration, deterministic lateral displacement, pinched flow fractionation, dielectrophoretic techniques, biomimetic separation methods but these devices need a pressure-driven source like a syringe pump which is not

comfortable for patients as a point of care device. In spite of all the attempts done by researchers to design a self-driven microdevice for blood plasma separation, the volume of extracted plasma due to clogging in the entrance of the plasma channel is still minimum and sometimes not enough to implement some type of tests. Accordingly, providing a novel design and fabrication procedure for a cost effective and high throughput blood plasma separation microfluidic device would be desirable.

Ralf-Peter Peters et al. U.S. Patent Application Publication No. US 2004/0232074, discloses a microstructured separating device to isolate blood plasma from the cellular components contained in the blood. The microstructure included: one straight transport channel for displacing the whole blood in a given transport direction, one separating-area at a branch point of the transport channel which is adjoined by a perpendicular channel of different height wherein blood plasma is separated from the whole blood. Besides, the separating area has a microstructure which retains the larger particles and slows down the smaller particles in the separating area. If this filtration area has a height higher than the particle to be filtered or the deformable cells can   enter the separation area, the quality of the filtered liquid is not 100% free of particles and the filtration is achieved due to the chromatographic effect in which the liquid is transported more rapidly through the separation area than the particles. But if the filtration area has a height smaller than the minimum size of particle to be filtered since there is no mechanism to prevent entrance clogging, the bigger particle will close the entrance of separation area resulting in a limitation of the filtrated liquid amount. The high concentration of particles in blood (45% hematocrit) causes that the separation with chromatographic effect is very unlikely to happen and if there is separation the amount of plasma without particles will not be sufficient to implement most of the blood test (i.e. coagulation). Besides, the proposed design is based on different channel heights in just a single part and a flat cover, which may involve complex fabrication procedure. In addition, the red blood cells clotting time has not been taken into consideration to dimension the collecting channel for the filling time of the proposed collecting chamber.

Jee-Hoon SEO et al., International Patent NO. WO 2005/095954, discloses a filter design placed in a microchannel on an integrated chip to effectively separate and extract red blood cells without the need of filter membranes or other devices. The filter comprises: a substrate including a microchannel formed thereon, the microchannel including one inlet and at least two outlets with a given angle to each other; and a plurality of rectangular structures formed in the main microchannel at a given angle to the inlet of the microchannel. The rectangular

structures allow the whole blood in the microchannel to be separated into the red blood cell flow and the blood plasma flow by the interval between and arrangement of the rectangular structures. Although the mentioned invention provided a new design to separate plasma from whole blood, the efficiency of separated plasma from the whole blood is an issue due to the waiver of red blood cells deformability and thickness (~ 2 μm) which can cross the distance between the designed rectangular (8-10 μm) and go through the plasma outlet.

The goal of the present invention is to create a microfluidic chip that can be part of point of care devices that with just a single drop of blood can separate plasma from whole blood without the need of external forces with high efficiency and reasonable time (minutes at most). This would be the first step towards the realization of single use, self-blood test, which now takes multiple technicians' hours to do.

Another key aspect compared to previous patents it that the volume of liquid at the outlet is maximized. This is thanks to the fact that the present invention considers the red blood cells rheological behavior in the transport channel and delays till the collection chamber is filled the clogging of the separation area. This delay is achieved acting on two points: first, the collecting channel is filled faster since the separation area is designed based on a high efficiency capillary pump and the appropriate hydrophilic behavior of all the involved surfaces and secondly minimizing the concentration of red blood cells at the entrance of the separation area, which instead of being placed on one side of transport channel such as in patent No. US 2004/0232074, is symmetrically placed on both side of the transport channel, causing a counteract of the cross capillary forces on RBCS, resulting indivertible to red blood cell movement and consequently the clogging reduction and plasma throughput increment and third, if needed electrodes can be placed in the inlet and the outlet to apply AC electrophoretic forces on RBCs forcing them to move away from the entrance of the separation area.

Another goal of the present invention is to present a device that can be mass-produced using different types of manufacturing process. In particular for blood plasma separation, to provide a cost effective microfluidic separation device which can be manufactured in a very simple process and thus apply to biosensor system to analyze the separated blood plasma in a short period of time. Therefore, the device is thought in two parts, which nowadays facilitates its fabrication.

SUMMARY OF THE INVENTION

This invention provides a self-driven microfluidic device **100** for particle separation from a liquid in which the particles are suspended by out-of-plane filtration. The microfluidic device is composed of two parts: top part (101) which comprises at least one transport channel (1) that utilizes various hydrodynamics principles to make a high throughput separation microdevice (100) and the bottom part (102) contains at least one separating area (2) which filters the particles and pumps the desired fluid to the collected channel and at least one collected channel (3) with a depth adaptable depending on the test needs, which collects the filter liquid from the separation area and can have or not electrodes to electrically prevent the RBCS to enter the separation zone. The separating area can include an arrangement of different post shapes to amplify the throughput during the same time and covers the transport channel or not.

The invention has a main channel (for transmission of the supplied, particle-included liquid), which includes at least one constriction (1b) at a branch point of the transport channel where a separation area is connected by an out-of-plane side channel, which the goal flow is diverted. The constriction (1b) increases the particle local velocity to avoid the clogging of the filtration channel and therefore increases the separation efficiency.

In another arrangement of the invention, the main channel after separation area is extended by a micropump which consists of parallel microchannels or a collection of microposts. In this version, the induced shear force on the particles by the promoting flow relay the effect of constriction to avoid the clogging of the filtration channel for a high throughput separation microdevice.

The microdevice has several advantages over the previous devices for separating particles from a liquid in which the particles are suspended. This microdevice is self-driven which means that the capillary forces are sufficient to transport the liquid in the main microchannel. The capillary force inside the microchannel is derived by the material hydrophilicity which can be achieved via different surface modifications (hydrophilic coating or plasma treatment) for hydrophobic material such as PDMS or using hydrophilic materials. If a hydrophobic material such as Polydimethylsiloxane (PDMS) is utilized as base material to manufacture the microdevice, a nonionic surfactant can be applied to overcome the hydrophobicity for creating a self-driven microdevice.

Since the clogging is prevented, the microstructure height in the separation area is less than the height of the main channel and clearly less than the diameter of desired particle to separate, therefore the quality of the filtered liquid is improved over other previous designs where this height was higher than characteristic size of the particles to be filtered. When the blood plasma separation is considered, the deformability of red blood cells restricts the microstructure height between 0.5 to 2 microns. The microdevice design can have one or more separating areas which can be located one after the other.

Furthermore, the separation microdevice has a collected channel which joins the output of the separation areas. In the case of blood plasma separation, the reagents can be located in this collected chamber and once the separated plasma enters the collected channel can react with reagents to pursue the blood analysis. The collected channel can be divided in several ones to pursue one or more test at the same time. Moreover, the separated liquid in the collecting channel can be removed from it by means of a pump or a syringe.

This separation microdevice can be used to separate very small particles from a particle-containing liquid by utilizing microscale amount of sample.

BRIEF DESCRIPTION OF THE DRAWINGS

Embodiments for the invented separating microdevice are detailed using the drawings.

FIG 1A shows an overhead view of a version of the separating microdevice as claimed in the invention.

FIG 1B shows a cross section through the microdevice filtration area

FIG 2 is a schematic illustration of the increment of particles velocity in a constricted channel to avoid particles clogging of the filtration region and the damage risk reduction of biocells due to the smooth transmission flow across the curvature

FIG 3 shows an overhead view of another version of the separating microdevice using a curved transport channel

FIG 4 shows an overhead view of another version of the separating microdevice using curved main transport channel and changing the separating direction

FIG 5 shows an overhead view of a modified version of the invention by promoting flow via parallel channels

FIG 6 shows an overhead view of a modified version of the invention which promotes flow via micropillar array capillary pump

FIG 7 shows an overhead view of the invention with three separation areas

FIG 8 shows an overhead view of the invention with three separation areas with reduced capillary length after every separation area

FIG 9 shows an overhead view of the invention with six separation areas to increase the throughput of the device

DETAILED DESCRIPTION

FIG 1A illustrates a first version of the microfluidic device which has a straight transport channel (1) with an inlet port (11) and outlet port (12), a primary main flow channel (1a) is linked through a constriction channel (1c) that at certain point (1b) has a transition of smaller width (1c) and then it goes back to its normal width (1e) through another transition (1d). These two transitions (1b) and (1d) can be straight or curved as shown in Fig. 2 to reduce the damage risk of biocells by smooth reduction of the flow from 1a to 1c or 1c to 1e. Specifically for the blood cells, hemolysis (the rupturing of red blood cells) increases due to the induced stress in the bumpy constriction. During most of its length, the constriction channel (1c) is covered by a separating area (2) which is machined in another part (101). In the case of blood, the blood plasma which is to be separated flows through this separating area (2) while it is connected to a collecting channel (3) for purposes of blood analysis. The filtered liquid or plasma is collected from the separation area by a collection channel (3) that is connected to the environment via a removal port (31). A syringe pump can be connected to the removal port (31) in order to remove the separated blood plasma from the collecting channel (3) if needed. In the up part (101) if needed, electrodes 4 and 5 can be placed to

apply alternatively electric forces on the particles to prevent the entrance clogging of the separation area.

FIG 1B shows a cross section of the separating device in which the transport channel (1) and collected channel (3) are machined in part (102). The separation area can include an arrangement of microposts (2) and is machined in part (101). The height H_2 is fixed by the size of particle to be filtered, while the height of (102) is fixed by the required test.

In the separating area 2 capillary forces are greater than in the constriction channel 1c such that the flow velocity of the blood sample in the transport channel 1 is slowed down relative to the flow velocity of blood plasma in the separating area 2 thereby the clogging of separating area 2 may happen by the cellular components of the blood which collect in the entry opening of the separating area 2. To solve the clogging problem, the constriction channel 1c is designed to increase the local flow velocity of red blood cells in the separating area accordingly impede the red blood cells clogging in the entrance of separating area. FIG 2a illustrates the hydrodynamics principles used to avoid clogging at the entrance of the separation area. The constriction in the channel width reduces the particle clogging by an increasing on the particles local velocity. In particular for blood plasma separation, the blood cells tend to migrate toward the center of the vessels and leave the region adjacent to the vessel wall which is known as plasma skimming. Additionally, when a blood vessel branches in two, blood cells tend to move in the branch having the higher velocity and leave the branch having lower flow velocity, as a result leaving the latter branch with enriched plasma which is known as bifurcation effect. Beside these two phenomena, the plasma skimming and the bifurcation effect, the constriction geometry is introduced in the invention to impede blood cells clogging in the entrance of separated area.

Figure 2b, illustrates the fact that the extraction of blood plasma is increased using a symmetric filtration channel design which causes to counteract the cross capillary forces in opposite direction, resulting in an indivertible red blood cell resulting force and consequently the clogging reduction and plasma throughput increment.

FIG 3 illustrates another version of microfluidic device in which the direction of the main flow channel 1a is parallel to the flow in the separation area 2 to increase the microdevice throughput. This has been achieved building the transport channel with a curved shape. The blood plasma flows through the separation area faster than the first version of microdevice because the flow direction is the same that in the separation area but the filling time of the

collected channel will increase because of the red blood cell clogging in the entrance of separation area due to the applied centrifugal force on the red blood cell, that will accumulate at the entrance of the separation area. To avoid clogging electrodes 4 and 5 can be used.

FIG 4 illustrates a modified version of the mentioned microdevice in FIG 3. In this case the transport channel is also curved, but the collected channel is placed below the inlet and outlet. Then the centrifugal force acting on the RBCs move them away from the separation area. The blood plasma flows through the separation area slower than the version of microdevice in FIG 3 because of the blood flow direction is opposite to the desired plasma flow.

Another hydrodynamic effect to delay the clogging in the separation relays on increasing the shear forces acting upon the particles and therefore promoting the flow by increasing the capillary length of the microdevice.

FIG 5 and FIG 6 show another version of the separating microfluidic device where the final main channel 1e is extended via a collection of parallel microchannels 41 in FIG 5 or via a collection of circle microposts 51 in FIG6. In the both designs FIG 5 and FIG 6, the particles are driven away from the entrance of separation area (2) by the induced shear force due to the generated capillary force of the micropump (41 or 51). In this modified version of separating microdevice, the induced shear force on the particles by the promoting flow relay the effect of constriction to prevent the clogging passage opening in the separating border entrance for a high throughput separating microdevice.

FIG 7 shows a three-stage microfluidic separating device which includes three separated areas 2, 21, 22 to increase the separation efficiency. In FIG 7 the supplied sample in inlet port 11 flows through a primary main channel 1a which is connected to a constriction channel 1c by smooth transmission through a curved constriction 1b. The entered sample in the constriction 1c is bifurcated into separating area 2 and a transport channel 15 which is designed to increase the induced shear force on the particles before attaining to the next separating area 21. The three separating areas 2, 21, 22 are connected to a collection channel 3 which is utilized to collect blood plasma for blood analysis in the case of blood sample. The separation occurs while the transport channel it is not completely filled, because once filled the blood flow velocity is so slow that RBCs tend to clog the entrance in the separation area. In FIG 7 a final main channel 25 has been added to the end of the transport channel to

increase the resistance flow and therefore the time to completely fill it. Finally, the final main channel 25 is connected to an outlet port 12 where the concentrated liquid sample is collected.

FIG 8 shows another three-stage microfluidic separating device with three separated areas 2, 21, 22 while the primary main channel 1a length is reduced to optimize the working time of the microfluidic device besides the reduction of the transport channel 15 length after every separation area in order to maximize the efficiency of the separating microdevice.

FIG 9 shows a six-stage microfluidic separating device which includes six separated areas 2. In this design, the supplied sample in an inlet port 11 flows through a primary main channel 1a which is connected to a constriction channel 1c by smooth transmission through a curved constriction 1d. The entered sample in the constriction 1c is furcated into separating area 2 and a transport channel 15 and after three-stage separation in the first separation part 200; the liquid sample is transmitted to the second separation part 300 by a transported channel 35. Two parallel collected channels 3 are designed for every separation part to increase the capability of the separating microfluidic device. In the case of blood plasma separation, these two distinct collected channels make a possibility for doing two different blood analyses simultaneously in the same device.

What is claimed is:

1. A self-driven microfluidic separation device for separating particles from a liquid in which the particles are suspended and in particularly for blood plasma separation, comprising the following:

   a) At least one transport channel (1) divided in three regions: 1a and 1e of width w_1 and 1c of width w_2, where $w_2 < w_1$. These three regions are connected through a constriction (which can be curved or not see Fig.2) to transport the liquid from an inlet port (11) to an outlet port (12) and avoid clogging in the separation area due to the increased velocity in the constriction.

   b) At least one out of plane separation area (2), which is adjoined at the constriction channel (1c) as a branch point of the transport channel to divert a desired partial flow, which is simmetrically placed at both sides the transport channel.

   c) At least one collected channel (3) that can include an outlet (31) or a reaction chamber.

   d) The microfluidic device (100) is machined in two parts. Part 101 contains the separation area or filter with height less than the size of particle to be separated and 102 contains the transport channel and the collected channel and test chambers with the adaptable height to the required test.

   e) Both parts are manufactured using appropriate hydrophilic material or treated to achieve hydrophilic behavior for hydrophobic material.

2. The microfluidic separation device of claim 1, wherein at least one micropump including parallel channels (41) or a collection of microposts (51) is connected to the final flow channel (1e) to promote flow.

3. The microfluidic separation device of claim, wherein at least two electrodes 4 and 5 are placed in the inlet and outlet to apply alternatively electric electrophoretic forces on the particles.

4. The microfluidic device of claim 1 and 2 and 3, where the transports channel 1 is curved as in figure 3 and the separation area can be simmetrically placed or not.

5. The microfluidic device of claim 1 and 2, where the transports channel 1 is curved as in figure 4 and the separation area can be simmetrically placed or not.
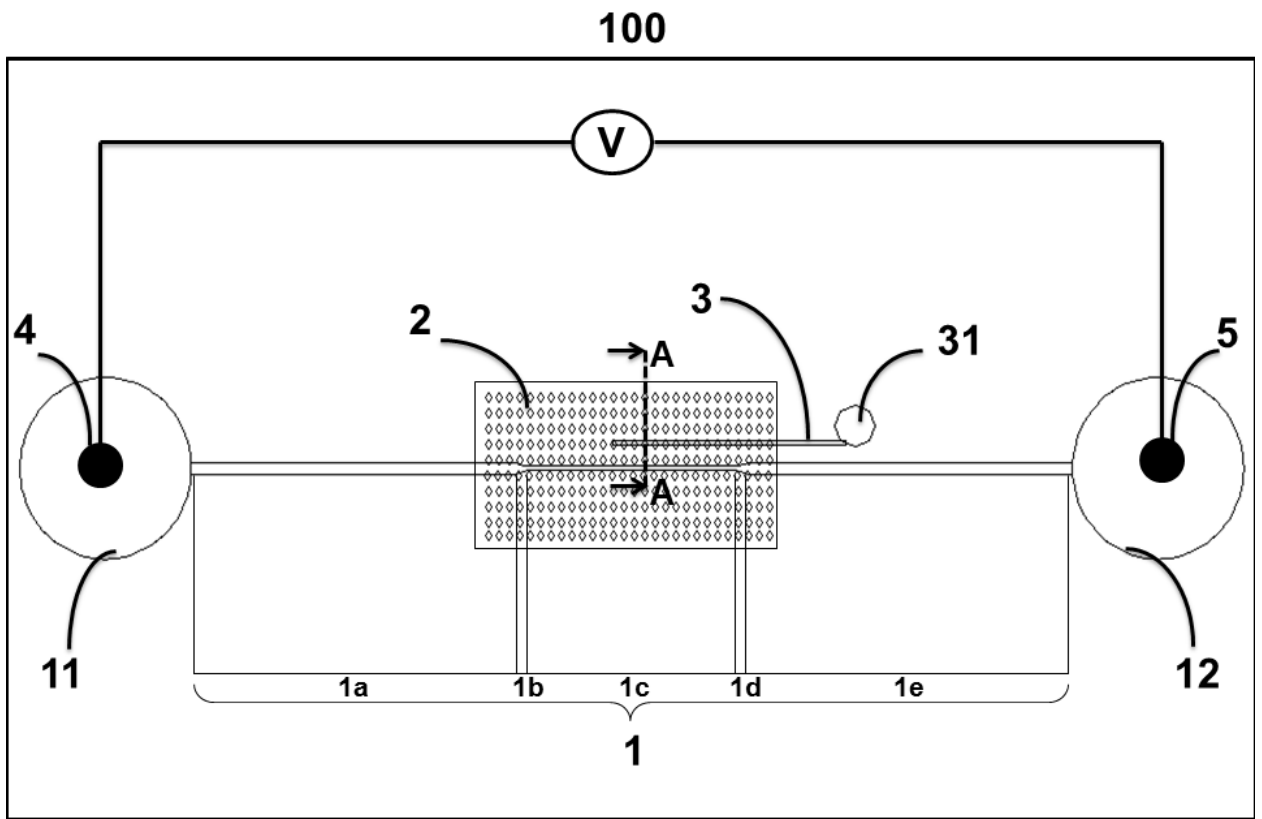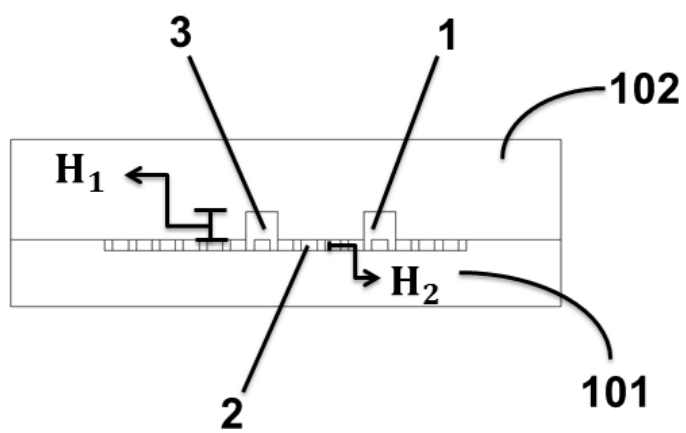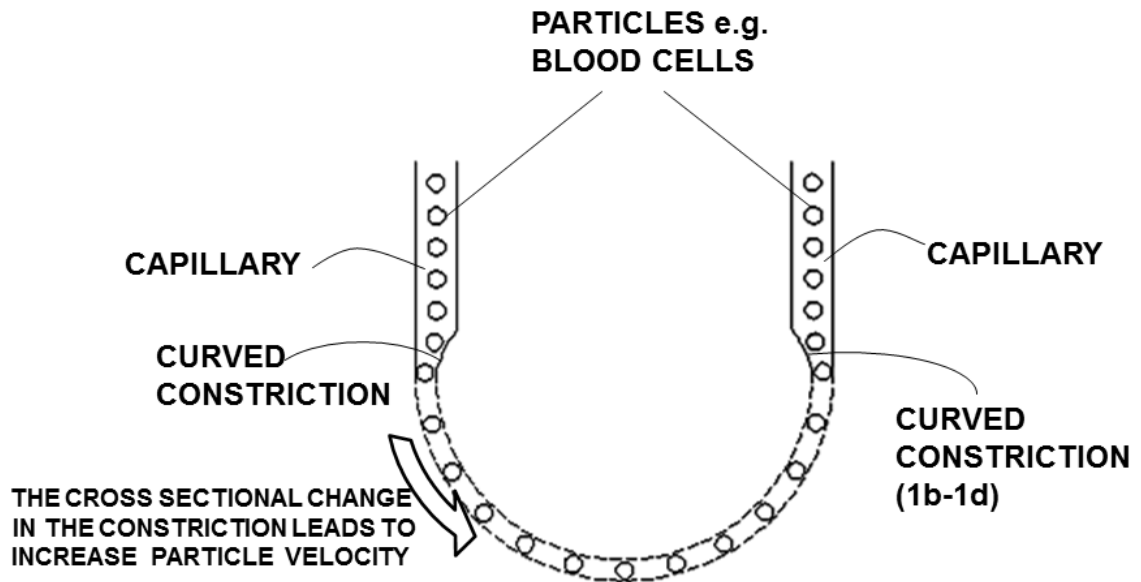
FIG. 1A

FIG. 1B

PARTICLES e.g.
BLOOD CELLS

CAPILLARY

CAPILLARY

CURVED
CONSTRICTION

CURVED
CONSTRICTION
(1b-1d)

THE CROSS SECTIONAL CHANGE
IN THE CONSTRICTION LEADS TO
INCREASE PARTICLE VELOCITY

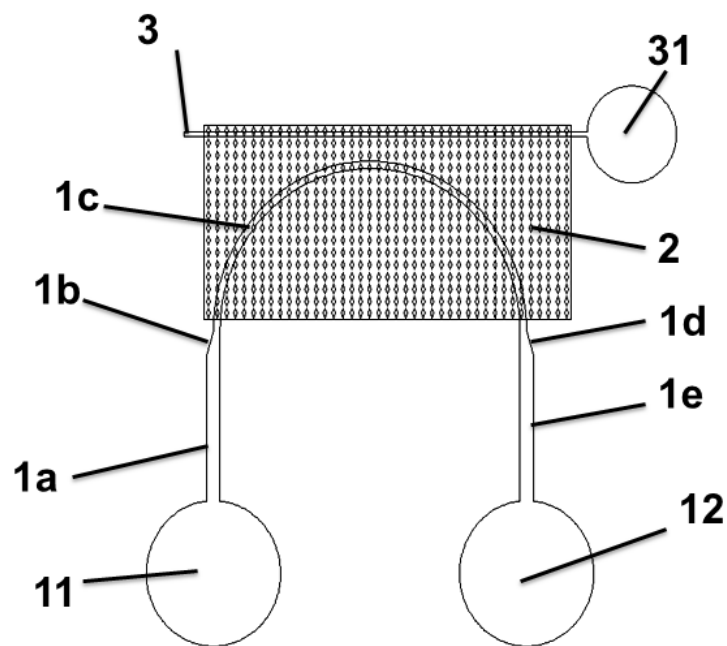REDUCE DAMAGE RISK OF CELLS DUE TO
THE SMOOTH TRANSMISSION FLOW
ACROSS THE CURVATURE
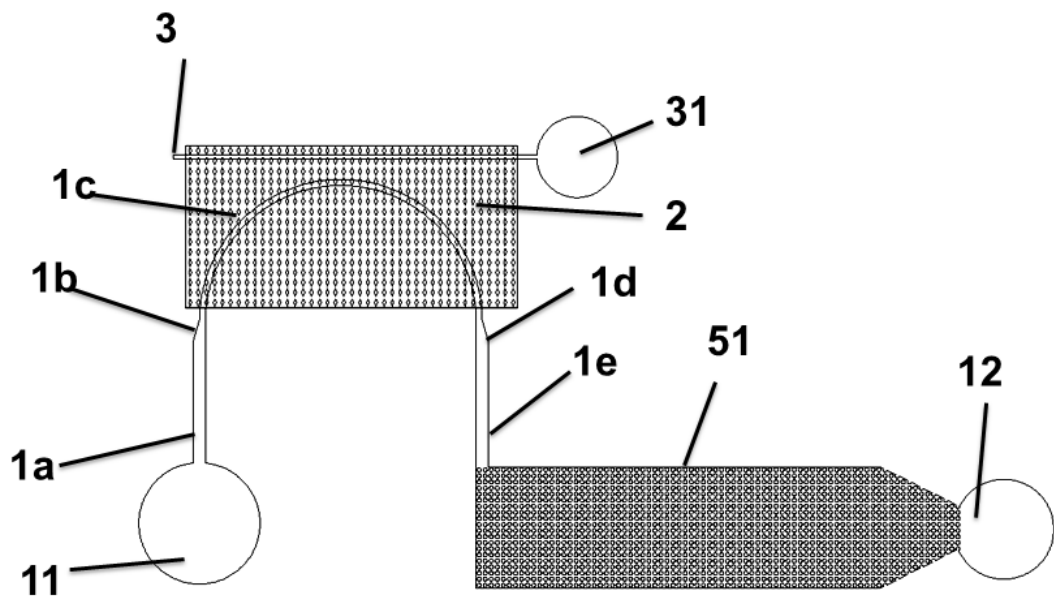
FIG. 2

FIG. 3

FIG. 4

FIG. 5

FIG. 6

FIG. 7

16

FIG. 8

17

FIG. 9

18